Publications

2012

Effects of Activated Carbon Surface Chemistry Modification on the Adsorption of Mercury from Aqueous Solution

Emily K. Faulconer
Embry-Riddle Aeronautical University, faulcone@erau.edu

EFFECTS OF ACTIVATED CARBON SURFACE CHEMISTRY MODIFICATION ON
THE ADSORPTION OF MERCURY FROM AQUEOUS SOLUTION

By

EMILY KAYE FAULCONER

A DISSERTATION PRESENTED TO THE GRADUATE SCHOOL
OF THE UNIVERSITY OF FLORIDA IN PARTIAL FULFILLMENT
OF THE REQUIREMENTS FOR THE DEGREE OF
DOCTOR OF PHILOSOPHY

UNIVERSITY OF FLORIDA

2012

To my mother and father

ACKNOWLEDGMENTS

4

TABLE OF CONTENTS

6

LIST OF TABLES

LIST OF FIGURES

Abstract of Dissertation Presented to the Graduate School
of the University of Florida in Partial Fulfillment of the
Requirements for the Degree of Doctor of Philosophy

EFFECTS OF ACTIVATED CARBON SURFACE CHEMISTRY MODIFICATION ON
THE ADSORPTION OF MERCURY FROM AQUEOUS SOLUTION

By

Emily Kaye Faulconer

May 2012

Chair: David Mazyck
Major: Environmental Engineering Sciences

Mercury (Hg), a naturally occurring element, is toxic and can lead to negative
health impacts for humans and ecosystems. Activated carbon adsorption is effective in
treating Hg-laden aqueous effluent for safe discharge. Two modifications of
commercially available activated carbon were investigated: iron impregnation to allow
for magnetic sorbent recapture and wet chemical oxidation to enhance aqueous Hg
capture. The modified carbons were characterized by nitrogen adsorption-desorption,
XRD, pH_{pzc}, vibrating sample magnetometry, elemental analysis, and total acidity
titration. The 3:1 C:Fe magnetic powdered activated carbon (MPAC) retained a high
surface area of 790 m^2/g and was 95% magnetically recoverable, with the iron present
primarily as maghemite. The characteristics of the surface oxygen modified carbons
varied based on the nature of the modifying reagent and its concentration.

The modified carbons were applied to trace level Hg solutions (100 µg/L). The 3:1
MPAC achieved the highest adsorption capacity, reaching 91% Hg removal with 2%
volatilized and 84% adsorbed. Adsorption occurs primarily as chemisorption, thus
allowing for non-hazardous residuals disposal until reaching a loading of greater than

11

800 µg Hg/ g MPAC. Surface area and point of zero charge were identified as primary variables influencing adsorption in this system.

Hg(II) adsorption was strongly correlated with oxygen content of the C(O)-modified activated carbons. Carbons with the highest oxygen content achieved the highest Hg(II) removal. Contrary to expectations, a strong correlation with oxygen content was not seen in Hg(0) adsorption. Rather, these data best fit a four variable model that identified surface area, pore volume, pH_{pzc}, and oxygen content, with the pH_{pzc} being the primary variable influencing results. Using the standardized EPA TCLP protocol, it was found that no carbons leached Hg at levels requiring disposal as a hazardous waste at the experimental loading rate. Kinetic models indicated both physisorption and chemisorption adsorption mechanisms.

Hg speciation and binding mechanisms was predicted using sorbent and matrix characteristics. The use of sequential chemical extraction to verify these operational binding mechanisms was unsuccessful due to extraction inefficiencies and phase transformation.

CHAPTER 1
INTRODUCTION

Problem Statement

Mercury (Hg) is a naturally occurring element found in air, water, and soil. The U.S. EPA lists Hg and Hg compounds as toxic pollutants under section 307(a) of the Clean Water Act. In aquatic ecosystems, inorganic mercury undergoes chemical and microbial transformation to methylmercury. Methylmercury is a serious environmental concern due to its high toxicity and ability to bioaccumulate and biomagnify [1].

Hg enters the environment from sources such as volcanoes or anthropogenically from sources such as the chlor-alkali industry, coal-fired power plants, battery manufacturing, metal mining, and the pharmaceutical industry. The toxic nature of Hg was fully realized in the late 1950's, when the industrial release of methylmercury into Minamata Bay resulted in Hg poisoning of the local population through consumption of contaminated fish and shellfish. Industrial Hg release continues today. The EPA's Toxics Release Inventory stated that the total disposal or release of Hg in the United States increased by 1.9 million pounds from 2006 to 2007, a 38% increase [1]. Current Hg discharge limits for industrial effluent vary by region [2].

As Hg regulations become increasingly strict, new effluent control technologies will be required to treat trace levels of aqueous Hg. The traditional technologies for aqueous Hg treatment, including precipitation and adsorption, have struggled to treat to ng/L effluent levels that are required to ensure the health of the environment and humans. Any residual Hg that remains in the wastewater upon discharge can persist in its dissolved or particulate form and may undergo transformation to methylmercury [3].

Thus, it is vital to control Hg discharges wherever possible in order to protect the health of humans and the environment.

Activated carbon, a high surface area sorbent, has been used for many applications in aqueous treatment. Recent research has focused on enhancing the effectiveness of activated carbon by modifying specific properties, chemically and physically. It is possible to tailor the surface chemistry of activated carbon to increase adsorption capacity and selectivity for Hg. Modification by iron impregnation can provide the carbon with magnetic properties, allowing for magnetic capture and thus easier residuals disposal. This study focuses on understanding the surface chemistry reactions between aqueous Hg and activated carbon, in order to develop a sorbent that can be applied to water with varying characteristics, is recoverable from aqueous solution, and can treat trace levels of Hg.

Hypotheses

1. The impregnation of activated carbon with ferrimagnetic iron oxides (magnetite and maghemite) would allow for magnetic separation and thus more responsible residuals disposal.

2. Iron impregnation would not significantly impact the adsorption capacity of the composite sorbent.

3. Matrix characteristics such as pH and pCl would influence Hg speciation and thus adsorption mechanisms.

4. Wet chemical oxidation of activated carbon would increase surface oxygen functionality; increased surface oxygen functionality would increase Hg adsorption capacity.

Objectives

1. Synthesize magnetic carbons that are at least 95% recoverable through magnetic separation.

2. Increase acidic C(O) on activated carbon surfaces with minimal pore degradation.

3. Characterize carbons with various techniques including nitrogen adsorption-desorption, point of zero charge, and total acidity.

4. Determine which experimental conditions yield the highest removal of aqueous Hg.

5. Predict the influence of matrix pH and pCl on Hg speciation; propose Hg adsorption mechanisms.

CHAPTER 2
LITERATURE REVIEW

Mercury

History

Mercury (Hg) has been used by humans throughout history for various purposes including mirror production and medicines, despite awareness of its poisonous properties. In 1527, Paracelsus wrote of the occupational disease "mercurialism" that appeared among workers in Idrija, Slowenia [3]. As mercury toxicity became better understood, its use in dental amalgams and pharmaceuticals diminished, with a few exceptions. Even with the current understanding of mercury toxicity, some cultures continue to use mercury for rituals as well as cosmetic and pharmaceutical purposes. Artisanal gold mining, which often uses elemental Hg-Au amalgamation for gold recovery, has been increasing over the past few decades, leading to a resurgence in mercury use.

Mercury Chemistry

Physical and chemical properties

The heavy metal mercury has an atomic number of 80, an atomic mass of 200.59, and a density of 13.55 g/cm^3. Mercury has an electron configuration of $[Xe]5s^2p^6d^{10}6s^2$, with the highest energy electron occupying a d-orbital. With a melting point of -39.8°C, Mercury is the only metal that is a liquid at standard temperature and pressure (STP). Mercury has three oxidation states, Hg(0) (elemental Hg), Hg(I) (mercurous Hg), and Hg(II) (mercuric Hg).

Mercury speciation

Three broad categories of Hg speciation are elemental (Hg(0)), inorganic (Hg(I) and Hg(II)), and organic mercury. These chemical forms impact its solubility and reactivity as well as its mobility, bioavailability, toxicity, bioaccumulation, and biomagnification [4]. Elemental mercury has a high vapor pressure (14 mg/m^3 at 20°C) and is soluble in water up to approximately 60 µg/L. Inorganic mercury occurs as Hg(I) and Hg(II) salts. Many Hg(II) salts are readily soluble in water and thus are highly mobile and toxic. A notable exception is HgS, which has a solubility of ~10 ng/L. Inorganic mercury has a high affinity for selenium, which can explain the protective role it plays in mercury toxicity. Inorganic mercury also has a high affinity for sulfur, including amino acids such as cysteine and methionine, which explains its high toxicity. Hg(I) is less stable than Hg(II) and is only sparingly soluble, resulting in lower toxicity. Organic mercury consists of a covalent bond between a divalent Hg atom and carbon. These compounds can react with biologically important ligands and can easily cross biological membranes.

Mercury can cycle between the atmosphere (air), hydrosphere (water), and lithosphere (land), as well as transfer through the food chain. The most common forms of Hg found in the environment are metallic Hg, mercuric sulfide, mercuric chloride, and methylmercury. The main dissolved Hg species in aquatic environments are Hg(0), Hg(II) complexes, and organic Hg forms, primarily as monomethylmercury cation and dimethylmercury [3]. For the purposes of this work, the focus will be on aqueous Hg chemistry, excluding methylmercury.

Formation of hydration spheres. When an Hg^{2+} ion is placed in water, the hydrogen bonding network of the water is altered as the water molecules rotate so that

their negative dipoles face the opposite charge of the Hg ion, thus breaking hydrogen bonds. This group of water molecules is called a hydration shell. The new orientation results in a net charge of the same sign as the ion on the outside of this hydration shell (Figure 2-1). This charge then tends to orient nearby water molecules, causing a second hydration shell and resulting in further disruption of the hydrogen bonding network.

In the first hydration sphere, the attraction of the water's negative dipole to the metal cation causes a distortion in the water's O-H electron cloud, weakening the bond and allowing for easier dissociation of the water molecule. This phenomenon results in the metal ion acting as a polyprotic acid as the complexed water deprotonates [5].

Mercury complexation with H_2O. Without complexing ligands present, hydrolysis plays a large role in speciation. At a low pH (below pH 2), the hexaqua ion, $Hg(H_2O)_6^{2+}$, is octahedrally coordinated by water molecules with equal Hg – O bond lengths (Figure 2-2). As the pH increases, the octahedral coordination is distorted. This results in two axial oxygen atoms with a shortened Hg – O bond length and four equatorial oxygen atoms with lengthened Hg – O bond lengths [6]. Up to two protons can be released from the waters of hydration surrounding the Hg^{2+} ion (Equations 2-1 to 2-2 [7]) as Hg^{2+} hydrolyzes to $HgOH^+$ and $Hg(OH)_2$ (Figure 2-3). In the absence of complexing ligands, $Hg(OH)_2$ is the dominant inorganic species at pH 6 [8].

$$Hg^{2+} + H_2O \rightleftharpoons HgOH^+ + H^+ \qquad {}^*K_1 = 10^{-3.4} = \{H^+\}\{HgOH^+\}/\{Hg^{2+}\} \qquad (2\text{-}1)$$

$$HgOH^+ + H_2O \rightleftharpoons Hg(OH)_2 + H^+ \qquad {}^*K_2 = 10^{-2.7} = \{H^+\}\{Hg(OH)_2\}/\{HgOH^+\} \qquad (2\text{-}2)$$

$$Hg^{2+} + 2H_2O \rightleftharpoons Hg(OH)_2 + 2H^+ \qquad K_{overall} = 10^{-6.1} = \{H^+\}^2\{Hg(OH)_2\}/\{HgOH^+\} \quad (2\text{-}3)$$
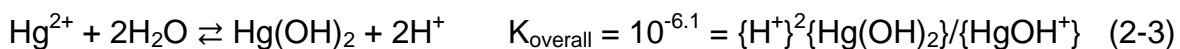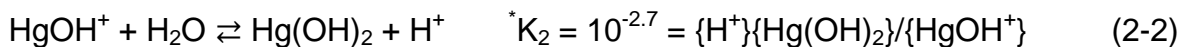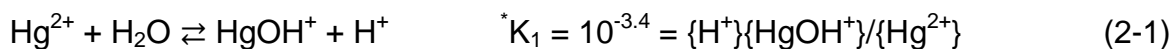
Mercury Complexation with Ligands. Association with various ligands is strongly dependent upon environmental conditions, including the type and concentration of Lewis bases present, the redox status (pE), Eh, pH, and pCl (Figure 2-4) [9,10]. The Hg ion can react with a ligand through inner or outer sphere complexation. Inner sphere complexation (e.g. ion exchange) involves the exchange of a hydration water for the ligand (Equations 2-4 and 2-5, where L = ligand) [10]. The loss of the water molecule from the hydration sphere is often the rate determining step. Outer sphere complexation (e.g. hydrogen bonding) is an electron transfer that involves separate chemical components that remain separate during the entire electron transfer event, as opposed to inner sphere electron transfer, in which the two chemical components are connected via a chemical bridge [10,11]. Ligands alter the adsorption of metal cations in the following ways: the formation of stable non-adsorbing complexes, the formation of ternary surface complexes, competitive adsorption of ligands onto the adsorbent surface, and reduction of the positive charge at the adsorbent surface through adsorption of the ligand [12].

$$Hg(H_2O)_6{}^{2+} + L^- \rightleftarrows Hg(H_2O)_6 \cdot L^+ \tag{2-4}$$

$$Hg(H_2O)_6 \cdot L^+ \rightleftarrows Hg(H_2O)_5 L^+ + H_2O \tag{2-5}$$

Mercury complexation with chloride. In aqueous solution, Hg can complex with chloride ligands to form very stable Hg-Cl complexes even at very low chloride concentrations (Figure 2-5). Up to four water molecules from the hydration sphere can be exchanged for chloride ions, depending upon the chloride concentration (Equations 2-6 to 2-10 [7]). The mass balance for a system containing Cl^- and OH^- as ligands is represented in Equation 2-11.

$$Hg^{2+} + Cl^- \rightleftharpoons HgCl^+ \qquad K_1 = \{HgCl^+\}/\{Hg^{2+}\}\{Cl^-\} \qquad (2\text{-}6)$$

$$HgCl^+ + Cl^- \rightleftharpoons HgCl_2 \qquad K_2 = \{HgCl_2\}/\{HgCl^+\}\{Cl^-\} \qquad (2\text{-}7)$$

$$HgCl_2 + Cl^- \rightleftharpoons HgCl_3^- \qquad K_3 = \{HgCl_3^-\}/\{HgCl_2\}\{Cl^-\} \qquad (2\text{-}8)$$

$$HgCl_3^- + Cl^- \rightleftharpoons HgCl_4^{2-} \qquad K_4 = \{HgCl_4^{2-}\}/\{HgCl_3^-\}\{Cl^-\} \qquad (2\text{-}9)$$

$$Hg^{2+} + 4Cl^- \rightleftharpoons HgCl_4^{2-} \qquad \beta_4 = \{HgCl_4^{2-}\}/\{Hg^{2+}\}\{Cl^-\}^4 \qquad (2\text{-}10)$$
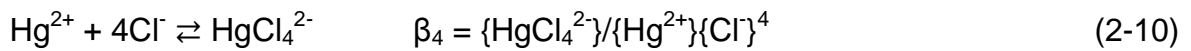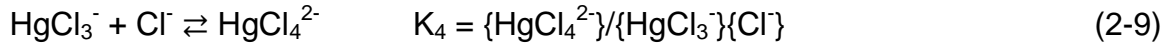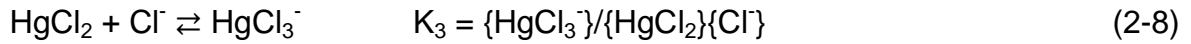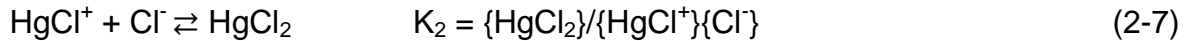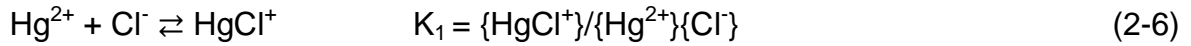
$$TOT\text{Hg} = \{Hg^{2+}\} + \Sigma_{i=1}^{2}\{Hg(OH)_i\} + \Sigma_{i=1}^{4}\{HgCl_i\}$$

$$= \{Hg^{2+}\}(1 + \Sigma_{i=1}^{2}\beta_{OH,i}\{OH^-\}^i + \Sigma_{i=1}^{4}\beta_{Cl,i}\{Cl^-\}^i \qquad (2\text{-}11)$$

A overall stability constant (β) is an equilibrium constant that describes a ligand displacement equilibrium reaction. The constant is derived by fitting experimental data into a chemical model of the equilibrium system so values are found to vary with the source of the data (Table 2-1). As seen in equation 2-12, the differences in stability constant values can impact the predicted speciation. A large stability constant denotes a strong tendency to form a complex. Thus, based on the log K values given by Benjamin, the Hg-Cl species are more likely to form than the Hg-OH species [7].

Hahne and Kroontje [13] performed a thorough examination of the effect of chloride concentrations on Hg speciation. Using the stability constants provided by Benjamin [7], using concentrations rather than activities, and verified by Visual MINTEQ, the following conclusions have been drawn. At pH 2, chloride levels of just 3.5 µg/L (pCl 7) result in the shift of Hg speciation from 50% Hg^{2+} and 50% $HgOH^+$ to include approximately 25% of the total Hg as Hg-Cl complexes $HgCl^+$ and $HgCl_2$ (Figure 2-6). When chloride concentrations reach 500 mg/L (pCl 1.85), Hg is present entirely as Hg-Cl complexes, with 85% as $HgCl_2$. Increasing the chloride concentration to levels

commonly found in chlor-alkali wastewater (25,000 mg/L) further alters the speciation to primarily $HgCl_4^{2-}$ [13].

The major difference between Hg speciation at pH 2 and pH 4 is present at 3.5 µg/L Cl^-. At pH 2, Hg exists as 25% Hg-Cl complexes, while at pH 4 all Hg is hydrolyzed as mono- and dihydroxy species and no chloro-complexes are present. At the other chloride concentrations investigated, the speciation did not differ much between the two pH values [13]. At pH 6, 100% of the Hg at pCl 12 and 7 exists as fully hydrolyzed $Hg(OH)_2$. The speciation of Hg at higher chloride concentrations remains similar to the distribution at the more acidic pH values of 2 and 4 [13]. Increasing to an alkaline pH value of 8, the fully hydrolyzed Hg species is dominant, constituting 100% of the total Hg for pCl 12 and pCl 7. At pCl 1.85, $Hg(OH)_2$ accounts for 70% of the Hg. At this point, $HgCl_2$ accounts for 28% of total Hg, as opposed to the 85-89% at pH 2, 4, and 6 [13].

Mercury complexation with sulfur. Mercury is sulfophilic, with a strong affinity for ligands containing sulfur [10]. Mercuric sulfide, HgS, is one of the least soluble salts known and readily precipitates from aqueous solution. In the presence of chloride ions and oxidizing conditions, Hg-Cl complexes will predominate, while reducing conditions allow for Hg-S complexes to predominate. More soluble than mercuric sulfide, HgS_2^{2-} forms at high pH and $Hg(SH)_2$ forms at low pH.

Mercuric complexation with nitrate. $Hg(NO_3)_2$ completely ionizes in solution to form Hg^{2+} and 2 NO_3^-.In this system, no complexation occurs beyond Hg hydrolysis. This reaction is relevant due to the laboratory use of $Hg(NO_3)_2$ standards.

Mobility and solubility of Hg complexes

Speciation can determine the solubility and mobility of Hg in the environment, with the degree of mobilization depending upon the degree of complexation. Hg-Cl

complexation increases solubility while Hg-S complexation decreases solubility, with K_{s0} values of 2.59 x 10^{-15} and 2 x 10^{-53} respectively. Without chloride ions present, the mobility of Hg is restricted both due to the solubility of Hg(OH)$_2$ and the potential for adsorption of Hg^{2+} and HgOH$^+$. Hg(OH)$_2$ is soluble up to 107 mg/L (5.37 x 10^{-4} M), at which point precipitation will take place. But with just 0.35 µg/L chloride at pH 6, most of the Hg will be present as Hg-Cl complexes, which are highly soluble [8]. Previous researchers have determined that the introduction of chloride ions to solution can release Hg from sediments into solution [14]. As stated earlier regarding the stability constants, the source of the equilibrium values can impact the predicted total soluble Hg concentration present at a given pH in a system in equilibrium with Hg(OH)$_{2(s)}$, OH$^-$, and Cl$^-$ (Equation 2-12).

$$TOT\text{Hg}_{\text{diss}} = \;^{*}\text{K}_{\text{sp}}/\{\text{OH}^-\}^2(1 + \Sigma_{i=1}^{2}\beta_{\text{OH},i}\{\text{OH}^1\}^i + \Sigma_{i=1}^{4}\beta_{\text{Cl},i}\{\text{Cl}^-\}^i \qquad (2\text{-}12)$$

Health Impacts

Human health impacts

Toxicokinetics and toxicodynamics. The chemical speciation of Hg influences its toxicokinetics (absorption, distribution, metabolism, and excretion) [15]. Elemental Hg exposure occurs primarily through inhalation, as it is rapidly absorbed through the lungs with approximately 80% of inhaled vapors absorbed by lung tissues [15]. Once absorbed, elemental Hg can penetrate both the placental and the blood-brain barrier to act as a neurotoxicant [4]. Elemental Hg is eliminated through urine, feces, exhalation, sweat, and saliva, dependent upon the extent of oxidation. Symptoms of elemental Hg exposure include tremors, lethargy, insomnia, memory loss, cognitive impairment, and headaches as well as kidney, pulmonary, and thyroid effects [16].

Absorption Hg(I) and Hg(II) occurs primarily through the gastrointestinal tract; therefore, most exposure occurs through diet. Even soluble mercury salts are not well absorbed, with uptake ranging between 7-15% [3]. Because inorganic Hg is not lipid soluble, it has very limited ability to cross both the blood-brain and placental barriers. Symptoms of inorganic Hg exposure include gastrointestinal pain, vomiting, diarrhea, loosening of the teeth, and renal damage [16].

Methylmercury is rapidly absorbed through the gastrointestinal tract and easily penetrates both blood-brain and placental barriers in humans and animals [15]. Symptoms of methylmercury exposure include blurred vision or blindness, deafness, speech impairment, headaches, tremor, and loss of coordination or memory. The developing fetus is particularly sensitive to methylmercury exposure. Prenatal exposure can result in developmental neurological abnormalities such as delayed onset of walking or talking and cerebral palsy [4].

Epidemiological studies. Studies have not reliably addressed the effects of maternal exposure to elemental Hg on the developing fetus [15]. No studies on developmental toxicity associated with inorganic Hg exposure are available.

The first epidemiologic report of methylmercury poisoning is centered on the chronic methylmercury exposure that occurred in Minamata, Japan between 1953 and 1960. The Chisso Corporation factory released wastewater with high levels of Hg into the harbor, resulting in bioaccumulation of methylmercury in fish and shellfish ranging from 10 to 35 mg/L. Subsequent consumption of these fish resulted in neurological symptoms in adults, and both neurological and developmental symptoms in prenatally exposed children [17]. In one study of 628 human cases, 78 deaths occurred [15].

The effects of acute high level methylmercury poisoning were demonstrated in Iraq in 1971 when methylmercury fungicide-treated seed designated for planting was instead ground into flour and baked into bread for human consumption. Prenatally exposed children exhibited symptoms including blindness, deafness, and paralysis [18].

Environmental health impacts

Methylmercury can be formed in aquatic ecosystems through microbial metabolism and chemical processes. Sulfate-reducing bacteria take up Hg in its inorganic form and convert it to methylmercury. Methylmercury moves through the food chain when these bacteria are consumed or release the methylmercury into the aquatic ecosystem. Top predators in the aquatic food chain, such as large fish, otter, mink, and raptors have the highest tissue levels of Hg [19]. The process of Hg bioaccumulation is complex and involves biogeochemical cycling and ecological interactions [4].

Natural unpolluted surface waters are reported to have total Hg levels ranging between 0.1 and 5 ng/L. Assuming 1 ng/L total Hg and recognizing that methylmercury accounts for 1 to 10% of total Hg, the methylmercury concentration will range from 10 to 100 pg/L, which could easily exceed the Wildlife Criteria [4].

Mercury Emissions

Mercury release can occur from natural sources such as volcanic activity and weathering of rocks and, to a greater degree, from anthropogenic activity, both current and historic (Table 2-2). The average abundance of Hg in the Earth's crust is 50mg/kg [3]. Coal-fired power production is the single largest global source of atmospheric Hg emissions, due to both an increasing global demand for power production and decreasing intentional use of Hg in industrialized countries.

The chemical form of released Hg depends upon its source, the environment, and other minor factors. As an element, Hg is persistent and cannot be broken down to less toxic substances. It is important to recognize that local releases of Hg have a global effect. Mercury can transport long distances through ocean and air currents. Elemental Hg has an atmospheric residence time of several months to one year. Some models suggest that up to 50% of Hg deposited in North America is from external sources [4].

Major pathways of anthropogenic Hg sources to water include direct discharge, indirect discharge, atmospheric deposition, and surface run-off and leachate from contaminated soil and landfills. The majority of Hg in surface waters is due to air deposition related to anthropogenic activities, both domestic and international [20]. Major point sources of Hg release to water in western countries include chlor-alkali facilities, pharmaceutical industries, metal processing plants, offshore oil activities, and coal-fired power plants.

Chlor-alkali industry

The chlor-alkali industry manufactures chlorine, hydrogen, and sodium hydroxide (caustic soda). The manufacturing process involves electrolysis of a salt solution to convert chloride ions to elemental chlorine. Three basic process variations for electrolytic production of chlorine are diaphragm cell, Hg cell, and membrane cell, with each using a different method to keep the chlorine product separate from the hydrogen and caustic soda. In the Hg cell process, Hg is used as the cathode where elemental sodium will accumulate, while the chlorine will migrate to the anode. The chlorine is treated for sale and the sodium forms an amalgam with Hg. This amalgam is then used to produce hydrogen gas and caustic soda [21]. Approximately 1 kg of Hg per 1000 kg chlorine produced is lost from the process, including atmospheric losses and effluent

waste stream [22]. Although reliance on Hg cells at chlor-alkali facilities is diminishing, 5

Hg cell facilities are still in operation in the United States and contribute approximately

7.1 tons per year anthropogenic Hg release [19].

The reported constituent concentration ranges for chlor-alkali wastewater are

listed in Table 2-3. There is potential for a portion of the total Hg in chlor-alkali

wastewater to be in the elemental state. Due to the influence of pH on Hg speciation, it

is important to note that the pH of chlor-alkali wastewater tends to be either acidic (~pH

2) or basic (~pH 12) [23,24].

In 2003, the EPA lowered the Hg national emission standard for hazardous air

pollutants (NESHAP) by 3,068 kg per year, applicable to Hg cell chlor-alkali plants, Hg

ore processing facilities, and sludge incineration and drying plants. Specifically, the final

rule limited Hg emissions from Hg cell chlor-alkali plants to 2.3 kg Hg/day [25]. In March

2011, the EPA proposed further reduction of Hg NESHAP by either eliminating the use

of Hg fuel cell technology or improving work practices to reduce fugitive Hg emissions

from the cell room to near-zero levels.

Flue gas desulphurization

Hg occurs naturally in coal in varying concentrations. COALQUAL, a database that

contains analyses of over 7,000 coal samples, identifies the mean Hg concentration in

coal as 0.17 µg/g [26]. When the coal is burned, Hg is released as an air pollutant,

contributing 13-26% of the total airborne emissions of Hg in the United States [26]. This

necessitates the use of pollution control devices, such as activated carbon injection that

directly targets Hg, or flue gas desulphurization (FGD) scrubbers that target sulfur

dioxide but also co-capture oxidized Hg.

FGD wastewater typically contains 10-800 µg/L Hg, primarily in the oxidized state [19, 27, 95]]. The wastewater also tends to contain high levels of dissolved solids, suspended solids, and organic compounds (Table 2-4). The pH of FGD wastewater typically falls within the range of 4.5 to 9.

The EPA is currently working to revise the effluent limitations guidelines and standards for the steam electric power generating point source category. This category includes FGD wastewater effluent. These new guidelines will likely address discharge limits for a variety of metals, including Hg [28].

Mercury emission regulations

Mercury discharge is regulated under the Clean Water Act (CWA) and the Resource Conservation and Recovery Act (RCRA). Mercury is listed as a toxic pollutant under section 307(a) of the Clean Water Act. For the protection of aquatic life, the Clean Water Act established mercury water quality standards (WQS) of 1.4 µg/L for an acute dose and 0.77 µg/L for chronic exposure. Over 8,000 bodies of water in the United States exceed WQS for Hg [20]. Some regions of the U.S. has established more strict Hg regulations. The maximum ambient water concentration is an average 1.3 ng/L, according to the Great Lakes Initiative Wildlife Criteria

RCRA requires that the EPA manage hazardous waste with a cradle to grave responsibility. Because of its toxicity, Hg is considered a hazardous waste. The EPA has established standards for the generation, transportation, storage, treatment, disposal, and recycling of hazardous waste, including mercury-containing waste. Land disposal restrictions exist that may require waste to be treated prior to landfilling.

Aqueous mercury removal technologies

Sulfide precipitation. Sulfide precipitation, capable of achieving a minimum effluent of 10-100 µg/L Hg, is a common remediation method for Hg-laden wastewater from both chlor-alkali industry and coal-fired power plants utilizing FGD wet scrubbers [29]. As presented in Eq. 2-13, organic and inorganic sulfides react to form insoluble Hg-sulfide (K_{sp} at 25°C is 2×10^{-53}) but these compounds can be difficult to remove from the wastewater, necessitating additional treatments such as pH adjustment, coagulation, flocculation, gravity settling, or filtration [29]. Outside of the ideal near-neutral pH range, soluble Hg-S species form. HgS_2^{2-} forms at high pH while $Hg(SH)_2$ which forms at low pH [29,30].

$$Hg^0 + Hg_2^{2+} + Hg^{2+} + S^{2-} \leftrightarrow 2Hg^0 + 2HgS_{(s)} \tag{2-13}$$

Disadvantages of sulfide precipitation include the potential for Hg to resolubilize in certain landfill conditions, difficulty monitoring real-time sulfide levels, the presence of toxic residual sulfide in the effluent, and the difficulty of treating and disposing of Hg and sulfide-laden sludges [29]. The reducing conditions of sulfide precipitation are ineffective for insolubilizing elemental Hg [31].The sludge produced often requires a treatment such as mineral encapsulation to ensure it is inert. The costs of treating chlor-alkali wastewater using sulfide precipitation were reported as $1.50/1000 gal, adjusted for inflation [32]. This cost is higher if additional treatments are applied.

Coagulation/co-precipitation. As an alternative or used in conjunction with sulfide precipitation, coagulation/co-precipitation using aluminum sulfate (alum) or iron salts can be used to treat aqueous Hg in wastewater. This treatment is capable of achieving effluent Hg concentrations of 5 to 10 µg/L using alum and 0.5 – 12.8 µg/L

using iron salts [29]. Coagulation is most efficient when used in conjunction with pH adjustment and filtration.

Adsorption Processes. Adsorbents have the potential to achieve high Hg removal efficiencies. Activated carbon, the predominantly applied adsorbent, is known to adsorb Hg(II) from aqueous solutions and can reach effluent levels of 0.5 to 20 µg/L [22,29,33-37]. However, removal levels depend highly upon the initial concentrations, the pH, and the concentration of other pollutants competing for adsorption sites [29]. Due to isothermal behavior of the adsorbent, incremental adsorbent dosage results in increased treatment efficiency but, unless recovery of the adsorbent is feasible, this increases the wastewater treatment residuals that require ultimate disposal. Granular activated carbon (GAC) is often applied as a fixed-bed unit with columns in parallel or series. Powdered activated carbon (PAC) is often applied as a slurry and requires subsequent solids separation. Modification of activated carbon, such as impregnation with carbon disulfide, bromine, or ozone, have been shown to enhance Hg removal [29,38,39]. In anticipation of new and more stringent water quality based standards, adsorption can be used as a polishing technique to reach lower Hg concentrations in industrial wastewater effluent [40].

Activated Carbon

Synthesis of Activated Carbon

Activated carbon is made in two steps by first heating a carbonaceous precursor in an inert atmosphere to eliminate light and heavy carbon-based oils and non-carbon elements as volatile gases and then activating thermally (physically) or chemically. After activation, the surface of the carbon is heterogeneous with a typical elemental composition of 88% C, 0.5% H, 0.5% N, 1% S, 6-7% O, and ash constituents [41]. The

amount of oxygen can range from 1-20% depending on raw material, activation, and additional treatments. The heteroatoms typically occur at edges and corners of the graphene sheet and behave similarly to the functional groups commonly found in aromatic compounds [35,42]. The properties of activated carbon, such as surface area and pore size, are affected by the nature of the activation method as well as the source material [35].

Thermal activation

Porosity. Thermal activation is performed using CO_2 or $H_2O_{(g)}$ at temperatures over 400°C to remove carbon atoms, thus creating meso- and macroporosity according to the stoichiometry shown in Equations 2-14 and 2-15 [35]. Porosity development occurs by the opening of previously inaccessible pores, the creation of new pores by selective gasification of certain structural components, and the widening of existing pores. At temperatures over 400°F, the carbon atom attached to a surface oxygen complex is a common site for gasification.

$$\underline{C} + CO_{2(g)} \rightarrow 2CO_{(g)} \tag{2-14}$$

$$\underline{C} + H_2O_{(g)} \rightarrow CO_{(g)} + H_{2(g)} \tag{2-15}$$
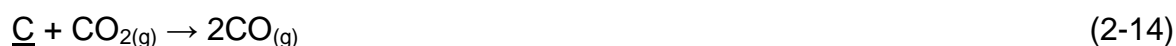
Surface oxygen functionality. At temperatures below 400°C, the reactions of CO_2, steam, and O_2 with carbon can result in chemisorbed oxygen (Equations 2-16 and 2-17). Surface oxygen complex formation is selective based on carbon surface heterogeneity and results in C(O) group with wide ranges of functionality with variable stability. These groups can influence the wettability, polarity, acidity, adsorption behavior, and catalytic and chemical reactivity of the carbon.

$$\underline{C} + O_2 \xrightarrow{<400°C} C(O) \tag{2-16}$$

$$\underline{C} + H_2O(g) \xrightarrow{<400°C} C(O) \tag{2-17}$$
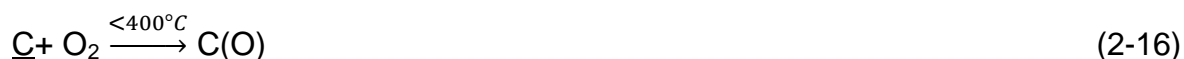
Possible basic C(O) groups formed are pyrone, first proposed by Boehm and Voll

in 1970, and chromene, first proposed by Garten and Weiss in 1957 [42]. Although the

main source of carbon basicity is a result of these basic groups, π-basicity can weakly

contribute to the basic nature of a carbon [42].

Possible acidic groups are carboxyl, quinone, hydroxyl, carbonyl, carboxylic

anhydride, and lactone [35]. Acidic surface groups cause the carbon surface to be

hydrophilic and polar. [22] Usually, both acidic and basic groups are present on the

carbon surface. Consequently, activated carbon is amphoteric.

Chemical activation

As thermal activation primarily creates meso- and macro-pores, controlled wet

chemical activation can be used to create microporosity. Chemical activation is

commonly performed by carbonizing the precursor at 450 to 600°C in the presence of

$ZnCl_2$, KOH, or H_3PO_4 [35].

Activated Carbon Modification

Modification of existing activated carbon surface chemistry features can be

performed chemically (acidic treatment or impregnation) or physically (heat treatment).

Acidic treatment enhances C(O) [43]. Physical modification enhances surface area,

pore volume, and C(O). Activated carbon surface chemistry can be manipulated using

these techniques to produce adsorbents that are tailored for a particular function.

Enhanced surface oxygen functionality

C(O) groups can be formed through acid treatment with the amount of oxygen

gained dependent upon the method and the precursor used [44-49]. Wet chemical

31

oxidation uses oxidizing aqueous solutions such as ozone [50], nitric acid [43,45,48,51], and hydrogen peroxide [45,51]. Nitric acid is the most widely used method of increasing the total acidity in a wet chemical oxidation [48,50]. Wet oxidations are generally thought to minimally alter other surface chemistry characteristics such as pore size distribution [43,45,47,49,52,52] but several researchers have found that concentrated nitric acid oxidation reduced the BET surface area and total pore volume while the pore width increased due to pore collapse [53-57]. Salame noted a loss in mesopore volume specifically associated with oxidation using concentration nitric acid and ammonium persulfate [58]. Oxidation with hydrogen peroxide increases the volume of pores having a diameter of ~6A [45,47,59].

Iron impregnation

Researchers have previously experimented with magnetic adsorbents. Oliveira et al. [60] created an activated carbon/iron oxide magnetic composite via fast hydrolysis at pH 10 of a 2:1 Fe(III) : Fe(II) and 1:1, 2:1, and 3:1 C:Fe. Magnetization, X-ray diffraction, and Mossbauer data suggest that the main magnetic phase present in the composite is maghemite. Temperature programmed reduction (TPR) data suggests that the iron oxides present can be reduced to magnetite, enhancing the magnetization. The experiment also determined that the surface area loss was proportional to the iron loading. The composites did not significantly lose magnetic strength in the pH range of 5-11. Oliveira et al. [61] also synthesized a magnetic zeolite for Cr^{3+}, Cu^{2+}, and Zn^{2+} removal from water. Gorria et al. [62] synthesized a magnetic adsorbent by depositing nickel nanoparticles on activated carbon.

Magnetism. Iron (Fe) is a malleable transition metal with an atomic number of 26, atomic mass of 55.85, and an electron configuration of $[Ar]4s^2 3d^6$. Iron exists in two

main oxidation states, Fe(II) (Fe^{2+}, ferrous Fe) and Fe(III) (Fe^{3+}, ferric Fe). Ferrous iron spontaneously oxidizes to ferric iron, reducing solubility. The 3d electrons determine magnetic properties. Each d orbital occupies a different orientation in space: d_{xy} d_{yz} d_{xz} d_{z2} d_{x2-y2}. Coordination to oxygen or hydroxyl causes unequal energy distribution in the d-orbitals [63].

Magnetic properties arise because of interactions between the spin moments of the electrons and the orbital moment. Ferromagnetic materials possess parallel electron spins, resulting in an overall net magnetic moment with large permeability (ratio of magnetic flux density to external field strength) and large positive susceptibility (strong attraction) to an external magnetic field. Ferromagnetic materials are spontaneously magnetic and retain their magnetic properties after the external field has been removed [63]. Antiferromagnetic materials possess electron spins of equal magnetic moment with antiparallel alignment, resulting in zero overall magnetic moment, positive permeability, and a small positive susceptibility.

Magnetite. Magnetite (Iron (II,III) Oxide) is a naturally occurring ferrimagnetic iron oxide with inverse spinel structure and a face-centered cubic unit cell based on 32 O^{2-} ions. The tetrahedral sublattice (A) contains one Fe^{3+} atom surrounded by four oxygen atoms while the octahedral sublattice (B) contains one iron atom, either Fe^{3+} or Fe^{2+}, surrounded by six oxygen atoms, thus forming the two interpenetrating magnetic sublattices. The saturation magnetism of magnetite ranges from 92 to 100 Am^2/kg. Magnetite contains eight formula units, $Y[XY]O_4$ ($X=Fe^{2+}$, $Y = Fe^{3+}$), per unit cell. The unit cell edge length is 0.839 nm and surface area ranges between 4 and 100 m^2/g. Magnetite is frequently non-stoichiometric and iron can be partly of fully replaced by

other metal ions depending upon steric hinderance (based on atomic radii and valence). Substitution changes the unit cell edge length and therefore can be identified via XRD analysis [63]. Cation substitution of mercury for iron in the iron oxide structure can be ruled out based on Goldschmidt's rules of isomorphous substitution; The ionic radius of mercury is too large to substitute for either ferrous or ferric ions [64].

Maghemite. Maghemite, a structural polymorph of magnetite, is a naturally occurring ferrimagnetic iron oxide with spinel ferrite structure. Maghemite has a cubic unit cell based on 32 O^{2-} ions and a unit cell length of 0.834 nm. Each unit cell contains 32 O^{2-} ions, 21 ⅓ Fe^{3+} ions, and 2 ⅓ vacancies. Maghemite can be considered an Fe^{2+} deficient magnetite. The iron cations are randomly distributed over 8 tetrahedral (A) and 16 octahedral (B) sublattices with randomly distributed vacancies limited to the octahedral sites. Due to the structure of maghemite, the saturation magnetism can vary from 60 to 80 Am^2/kg. Maghemite has a surface area ranging from 8 to130 m^2/g [63].

Adsorption

Adsorption theory

The current understanding identifies adsorption as a surface phenomenon that results from unsaturated and unbalanced molecular forces on a solid surface that are satisfied by attracting adsorbate molecules, atoms, or ions, resulting in a higher concentration of these particles on the solid surface relative to the bulk solution. Activated carbon adsorption can by physical or chemical.

Physisorption occurs through van der Waals attraction (dispersion forces). Asymmetry of the electron distribution in the adsorbate particle causes a transient dipole moment that, when it is approaching the solid adsorbent surface, can induce an appropriately oriented dipole moment in a surface molecule, producing instantaneous

attraction. These forces are greater in the micropores where the adsorbate molecules can be closer to each other than in the bulk aqueous phase [35]. Physisorption is a reversible exothermic process that is not site-specific and can result in multimolecular thickness of the adsorbed phase.

Chemisorption forces arise from redistribution of electrons between the adsorbent and adsorbate, resulting in a site-specific irreversible chemical bond [65]. Chemisorption results in unimolecular thickness of the adsorbed phase. Due to the nature of chemisorption, it is much stronger than physisorption.

Three successive steps are commonly proposed to describe adsorption dynamics on porous adsorbents. First, the solute is transported from bulk solution through a liquid film to the carbon's external surface (external diffusion). Next, most of the solute that was transported from the bulk solution diffuses into the pores while a small quantity remains on the external surface (internal diffusion). This is the rate limiting step. Finally, the solute is adsorbed on the interior surface of the pores and capillary spaces of the adsorbent, reaching equilibrium. These steps are influenced by the affinity of the solute for the surface, the solvent for the surface, and the solute for the solvent [66].

Adsorption is an equilibrium process. Initially, adsorption proceeds at a rapid rate due to the availability of surface sites for adsorption but, as adsorption sites fill, the rate of adsorption slows while the rate of desorption increases until reaching equilibrium where the rate of adsorption equals the rate of desorption. At a constant temperature, adsorption equilibrium can be represented as an adsorption isotherm. Two common isotherm equations applied to liquid phase adsorption, Freundlich and Langmuir, apply to both chemisorption and physisorption.

Isotherm theory

Adsorption isotherms utilize controlled physisorption and desorption onto a

sorbent. An adsorption isotherm is the graphical representation of the relationship

between the bulk adsorbate and the amount adsorbed at a given temperature [67]. The

International Union of Pure and Applied Chemistry (IUPAC) classifies adsorption

isotherms into six categories as follows (Figure 2-7) [35,68]:

1. Type I isotherms, also referred to as Langmuir isotherms, are concave with respect to P/P_0. This isotherm reaches a maximum value of adsorption. The steepness of the slope of the isotherm from P/P_0 values of zero to 0.05 indicates the narrowness of the micropores. It is generally accepted that Type I isotherms represent microporous solids with a small external surface area such as activated carbon and zeolites.

2. Type II isotherms describe adsorption in the presence of both micropores and open surface. This isotherm contains an inflection point where the curve changes from concave to convex, representing where monolayer coverage ends and multilayer adsorption begins. These isotherms represent solids that are either non-porous or macroporous.

3. Type III isotherms are convex and are typical of adsorption at sites with low adsorption potential, such as organic polymeric systems.

4. Type IV isotherms are similar to Type II isotherms but includes mesoporosity. Activated carbons will not typically present a plateau in the high relative pressure region.

5. Type V isotherms are characteristic of a low energy, homogeneous, mesoporous solid.

6. Type VI isotherms characterize extremely homogeneous surfaces such as pyrolytic graphite. Measurement is performed using argon or methane rather than nitrogen.

Desorption can be slower than adsorption due to a higher activation energy, forming a

hysteresis in which the adsorption and desorption curves of the isotherms do not follow

the same path (Figure 2-8). Line PQ describes adsorption in microporosity and open

surface; smaller pore size results in a steeper PQ line. Line QR indicates reversible

adsorption in the smallest mesopores. Line RS indicates capillary condensation. Upon lowering the pressure, desorption follows the line SUR.

IUPAC has established four categories of hysteresis loops (Figure 2-9). When a hysteresis loop occurs within the multilayer range of a gas adsorption isotherm (relative pressure of >0.2), it is usually associated with capillary condensation in mesopores, shown as H1 and H4. The H2 and H3 hysteresis loops are intermediate between these two extremes. The dashed lines represent low pressure hysteresis due to microporosity. Hysteresis shape is often identified with specific pore structures. Type H1 loops are often associated with porous materials consisting of approximately uniform spheres in a regular array and thus a narrow pore size distribution. Type H2 loops do not have a well defined pore size distribution or shape. This hysteresis at one point was attributed to ink bottle pores but this view is now recognized as over-simplified. Type H3 loops is associated with slit-shaped pores due to plate-like particles. Type H4 is also associated with slit-shaped pores but the Type I isotherm character indicates microporosity [68].

Langmuir Isotherm equation. The Langmuir equation was the first adsorption isotherm equation developed (Equation 2-18). This equation relates the amount adsorbed to the equilibrium concentration of the adsorbate in the bulk solution where Y/M is the concentration of adsorbate adsorbed (mg/L) divided by the carbon concentration (mg/L); C is the equilibrium concentration (mg/L), and *a* and *b* are constants, determined graphically. The assumptions in this equation are 1) adsorbate is attached to the surface at definite localized sites, 2) each site accepts one adsorbate particle 3) the energy state of the adsorbate is equal at all sites (energetically

37

homogenous surface with negligible lateral interactions). This equation is idealized and thus its significance in interpreting adsorption data can be limited.

$$\frac{Y}{M} = \frac{abC}{(1+aC)} \qquad (2\text{-}18)$$

Freundlich Isotherm equation. The Freundlich equation relates the solute concentration on the adsorbent surface to the concentration of the solute in the bulk solution where Y/M is the concentration of adsorbate adsorbed (mg/L) divided by the carbon concentration (mg/L), C is the equilibrium concentration of the adsorbate in the bulk solution (mg/L), and both k and 1/n are constants. (Equation 2-19). A plot of log Y/M versus log C yields a straight line with a slope of 1/n and a y-intercept of k, which holds true over a wide range of concentration values including dilute solutions [69]. The Freundlich equation is often applied to physisorption and adsorption of solids of limited solubility.

$$Y/M = kC^{1/n} \qquad (2\text{-}19)$$

Aqueous phase metal adsorption

Aqueous phase adsorption involves interactions between the solute and surface, the solvent and surface, and the solute and the solvent. Issues that must be considered are competitive adsorption, chemical changes of the solute, and concentration changes of the solute. The solution pH can play a large role in adsorption as the concentration of acidic molecules is function of pH and both the dissociated and the non-dissociated forms may adsorb. In general, low solubility favors aqueous adsorption. [42]

There are several theories regarding adsorption of metal ions. The first theory is electrostatic adsorbate-adsorbent interaction (ion exchange). This process is entirely dependent upon the functionality of the carbon, particularly the C(O) complexes. The

second theory is that enhanced adsorption potentials (dispersion forces in the narrowest micropores) are strong enough to retain metal ions. The third theory is that of hard and soft acids and bases (HSAB) in response to the amphoteric nature of the carbon surface [35].

Metal adsorption can be influenced by various characteristics of the adsorbent, matrix, and adsorbate. Adsorbent surface chemistry characteristics that influence adsorption include surface area, pore size distribution, as well as C(O) and other heteroatom functionality. The role C(O) complexes is determined by a correlation between the amount of ion adsorbed and the amount of participating oxygen functionality. Matrix characteristics that can influence metal ion adsorption include the pH, temperature, and presence of competitively binding ions. Chemical and physical properties of the metal ion adsorbate influence on adsorption; adsorption is affected by ionic radius (access to porosity), solubility (hydrophobic interactions), and pKa (controls dissociation) [35].

Mercury adsorption from aqueous solution

Hg(0) adsorption by activated carbon. While the low solubility of $Hg(OH)_2$ allowed for removal of Hg via preferential precipitation, Hg(0) does not precipitate and its low solubility and high volatility result in more difficult aqueous removal than oxidized species [22,56,70,71]. Vapor phase Hg(0) adsorption by activated carbon is known to be affected by various matrix and sorbent characteristics, including surface oxygen functionality [22,27,56,70,71].

Gas phase research implicates C(O) complexes, reporting that two carbons with similar sulfur, chlorine, bromine, and iodine distribution displayed very different sorption capacities for Hg(0), most likely due to differences in surface oxygen functionality [72].

Li et al. [56] proposed that C(O) complexes, particularly the reducible lactone and carbonyl groups, are possible active sites for gas phase Hg(0) adsorption, potentially involving electron transfer from the Hg(0) to the lactone or carbonyl, followed by subsequent adsorption of Hg(II) through well studied mechanisms. Adsorbed Hg(0) was desorbed as Hg(II), lending support to the oxidation hypothesis. In a theoretical study, Liu et al. [73] concluded that lactone and carbonyl favor gas phase Hg(0) adsorption while phenol and carboxyl reduced Hg(0) capture [73]. The role of C(O) complexes in aqueous Hg(0) adsorption is not defined in literature.

Hg(II) adsorption by activated carbon. Activated carbon is known to have a high affinity for Hg (II). Multiple factors can influence Hg(II) adsorption, including temperature, surface area and pore volume, and particle size [22,72,74-76].

Aqueous Hg(II) can be removed from solution by physisorption, ion exchange, hydrogen bonding, surface precipitation, or reduction/volatilization. C(O) functionality can contribute to Hg removal from solution [75,77]. When the pH < pzc, cationic Hg must overcome electrostatic repulsion to exchange with the H^+ of a surface oxygen group (Equation 2-20) while anionic Hg is electrostatically attracted to the positive carbon surface [22,35,75]. When the pH > pzc, cationic Hg is electrostatically attracted to the deprotonated C(O) group (Equation 2-21) while mercury anions are electrostatically repelled by the negative sorbent surface [78].

$$2 \underline{C}\text{-COOH} + Hg^{2+} \rightarrow (\underline{C}\text{-COO})_2 \bullet Hg + 2H^+ \tag{2-20}$$

$$2 \underline{C}\text{-COO-} + Hg^{2+} \rightarrow (\underline{C}\text{-COO})_2 \bullet Hg \tag{2-21}$$
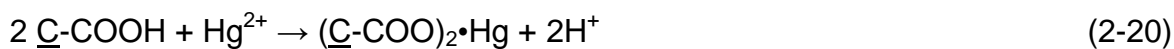
Hydrogen bonding can take place between an H atom on hydrolyzed Hg and an electronegative surface oxygen. When $Hg(OH)_2$ has reached its intrinsic solubility, it will preferentially precipitate on the carbon surface rather than in solution [79].

Activated carbon has been shown at high pH values to remove mercury via reduction and volatilization as Hg(0) [33,80]. Phenolic and hydroquinonic surface oxygen groups have been proposed as reduction sites (Equation 2-22) [36]. Confirmed by scanning electron microscopy, $HgCl_2$ reduction to the sparingly Hg_2Cl_2 will cause preferential precipitation onto the carbon surface while a complete reduction to Hg(0) result in Hg volatilization from solution [81]. Many researchers do not attempt to distinguish the mercury removed via adsorption from the mercury removed via reduction and volatilization. The amount of Hg adsorbed can be determined by the mass balance equation (Equation 2-23).

$$2(\text{-OH}) + 2HgCl_2 \rightarrow 2(\text{=O}) + Hg_2\,Cl_2 + 2HCl \tag{2-22}$$

$$[TOTHg] = [Hg(II)_{aq}] + [Hg(0)_g] + [Hg(II)_{ads}] + [Hg(0)_{ads}] \tag{2-23}$$

Hg adsorption by iron oxides. Iron oxides including magnetite, goethite, and ferrihydrite have been shown to adsorb aqueous Hg(II) [82-84]. The ion loading, as with activated carbon, is a function of matrix pH (Equation 2-24 and 2-25) [63,83]. Ternary surface complexes can also form between the surface, Hg^{2+}, and OH^- or Cl^- (Equations 2-26 and 2-27) [85]. Hg is likely to chemisorb onto Fe-oxides than to physisorb [63].

$$\underline{Fe}OH + Hg^{2+} \rightarrow \underline{Fe}\text{-O-Hg}^+ + H^+ \tag{2-24}$$

$$(\underline{Fe}OH)_2 + Hg^{2+} \rightarrow (\underline{Fe}\text{-O})_2 \bullet Hg + 2H^+ \tag{2-25}$$

$$\underline{Fe}OH + Hg^{2+} + H_2O \rightarrow \underline{Fe}\text{-O-Hg-OH} + 2H^+ \tag{2-26}$$

$$\underline{Fe}OH + Hg^{2+} + Cl^- \rightarrow \underline{Fe}\text{-OH-Hg-Cl} + H^+ \tag{2-27}$$
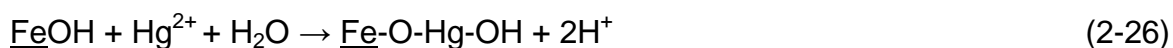
The presence of specific ligands can influence the adsorption of mercury onto iron oxides [86]. Sulfate has been shown to increase Hg(II) sorption onto iron oxides by reducing the positive surface charge and thereby reducing the electrostatic repulsion that can inhibit adsorption of Hg cations onto the oxide surface [12].

Hg reduction by iron oxides. Oxidation of iron oxides can occur with the reduction of an aqueous transition metal [64,87-90]. In anoxic conditions, Hg(II) is lost as Hg(0) in the presence of magnetite, shown in Equation 2-28, in which n is the charge transfer number and z is the valence state of the transition metal [82,90]. Reduction rates decrease with pH.

$$3[Fe^{2+} \ Fe_2^{3+}]O_4 + \frac{2}{n}m^z \rightarrow 4[Fe_2^{3+}]O_3 + Fe^{2+} + \frac{2}{n}m^{z-1} \qquad (2\text{-}28)$$
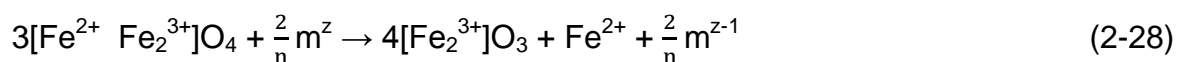
Hg oxidation by iron oxides. In the air phase, magnetite and maghemite have been shown to oxidize Hg(0) to Hg(II) [91]. The water content and surface area have been shown to impact the Hg(0) oxidation [92,93]. Indirect evidence for Hg(0) oxidation is seen in reduced adsorption in the presence of chloride ions; Elemental mercury must ionize in order to complex with chloride ions [83,84].

Table 2-1. Stability constant values for Hg-OH and Hg-Cl compounds

Benjamin				Snoeyink				Hahne & Kroontje			
Ligand	Complex	log K_1	log β	Ligand	Complex	log K_1	log β	Ligand	Complex	log K_1	log β
OH-	$HgOH^+$	10.6	10.6	OH-	$HgOH^+$			OH-	$HgOH^+$	11.86	11.86
	$Hg(OH)_2$	11.3	21.9		$Hg(OH)_2$				$Hg(OH)_2$	10.27	22.13
Cl-	$HgCl^+$	6.75	6.75	Cl-	$HgCl^+$	7.15	7.15	Cl-	$HgCl^+$	6.74	6.74
	$HgCl_2$	6.37	13.12		$HgCl_2^o$	6.9	14.05		$HgCl_2^o$	6.48	13.22
	$HgCl_3^{-1}$	0.90	14.02		$HgCl_3^{-1}$	2.0	15.15		$HgCl_3^{-1}$	0.9	14.07
	$HgCl_4^{-2}$	0.41	14.43		$HgCl_4^{-2}$	0.7	15.75		$HgCl_4^{-2}$	1.0	15.07

Table 2-2. Select anthropogenic releases of Hg [4]

Mobilization of Hg impurities	Coal-fired power and heat production
	Cement production (Hg in lime)
	Mining and other metallurgic activities
Intentional extraction and use	Hg mining
	Chlor-alkali production
	Use of fluorescent lamps
Waste treatment	Waste incineration
	Landfills

Table 2-3. Reported ranges of chlor-alkali wastewater constituents [23,24]

Constituent	Concentration range (mg/L)
Total Hg	1.6 - 7.6
Hg(0)	0.004 - 0.036
Chloride	460 - 25,000
Ammonium	0 - 0.8
Nitrite	0 - 1.7
Nitrate	<5 - 150
Sulfate	12 - 650
Ca	27.7
Cd	0.6
Mg	33.3
Na	311.2
Pb	2.9
Dissolved oxygen	6.8 - 9.1

Table 2-4. Reported ranges of FGD wastewater constituents [19,95]

Constituent	Concentration range (mg/L)
Hg	0.01 – 0.8
Suspended solids	250 - 20,000
Chloride	1,000 - 40,000
Ammonium	< 10 - 100
Nitrite	< 2
Nitrate	10 - 20,000
Sulfate	1,500 - 8,000
Sulfite	< 20
Sulfide	< 20
Ca	750 - 4,000
Cd	< 1
Cr	< 5
Cu	< 5
Mg	1,100 - 4,800
Na	670 - 4,800
Ni	< 5
Zn	< 10
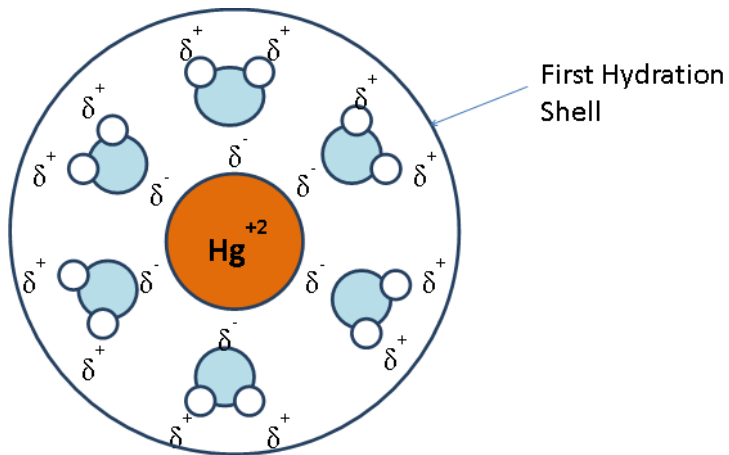
Figure 2-1. Hydration of Hg^{2+} ion in water
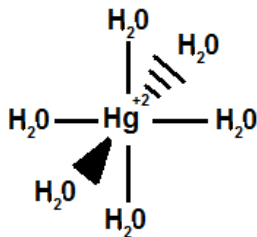
Figure 2-2. 3-dimensional geometry of Hg^{2+} hydration
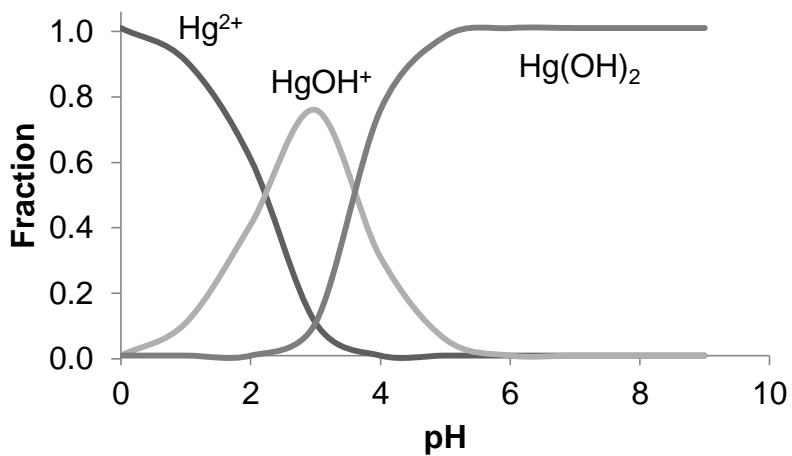
Figure 2-3. Distribution of Hg(II) at different pH values
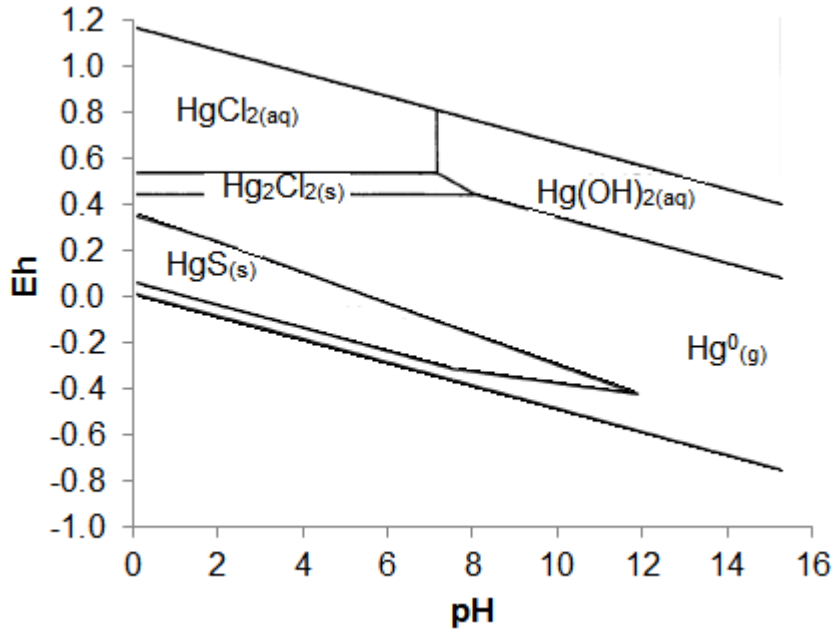
Figure 2-4. Mercury Eh-pH diagram for Hg-O-H-S-Cl system
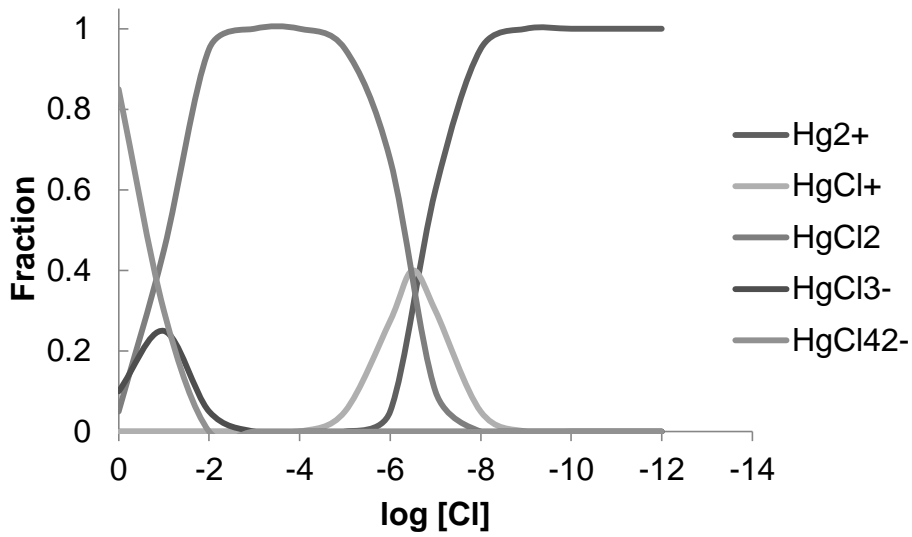
Figure 2-5. Distribution of Hg(II) at various chloride concentrations
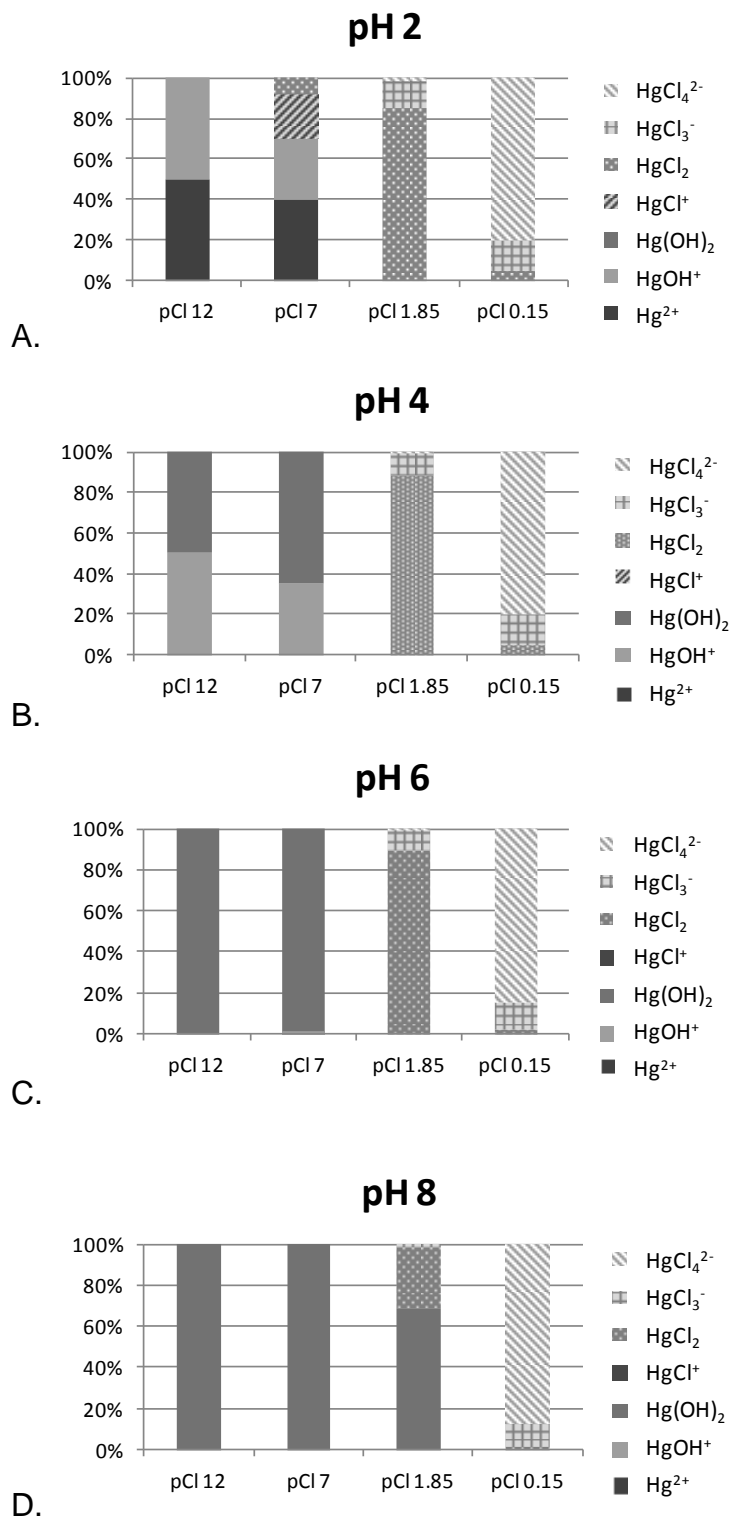
Figure 2-6. Hg(II) Speciation at varying pH and chloride concentrations. (pCl 7 is 3.5 µg/L, pCl 1.85 is 500 mg/L, and pCl 0.15 is 25,000 mg/L)
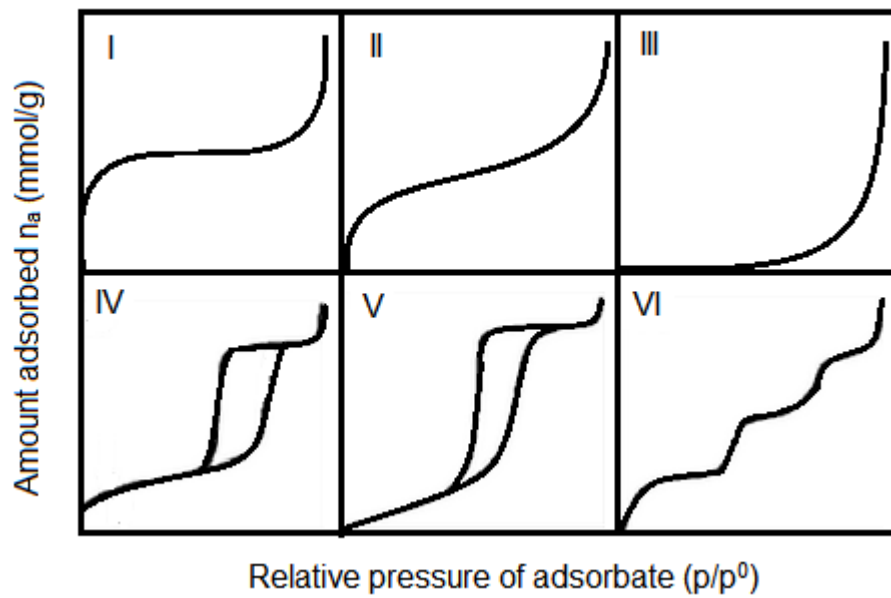
Figure 2-7. IUPAC gas adsorption isotherm classifications
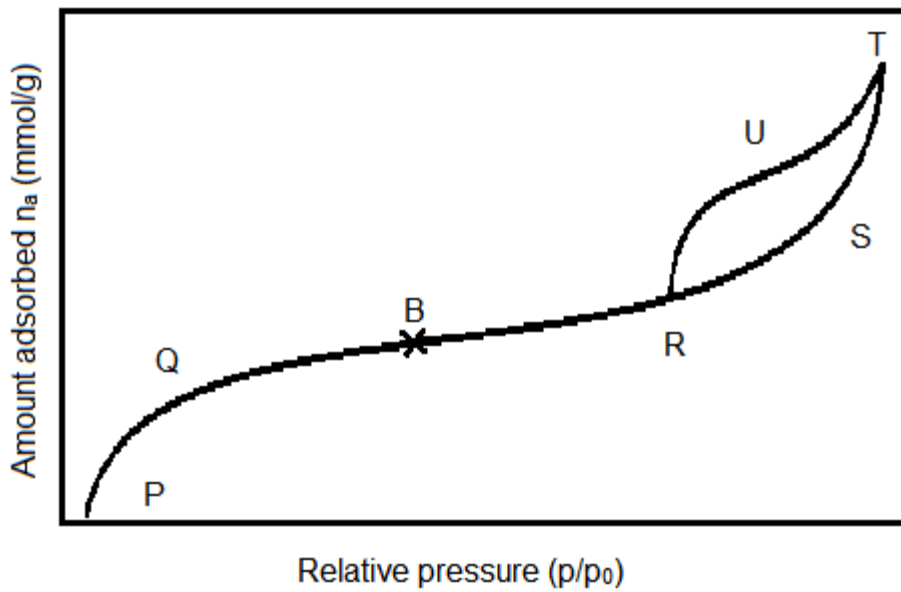
Figure 2-8. Nitrogen adsorption isotherm on micro- and mesoporous carbon exhibiting a closed hysteresis loop
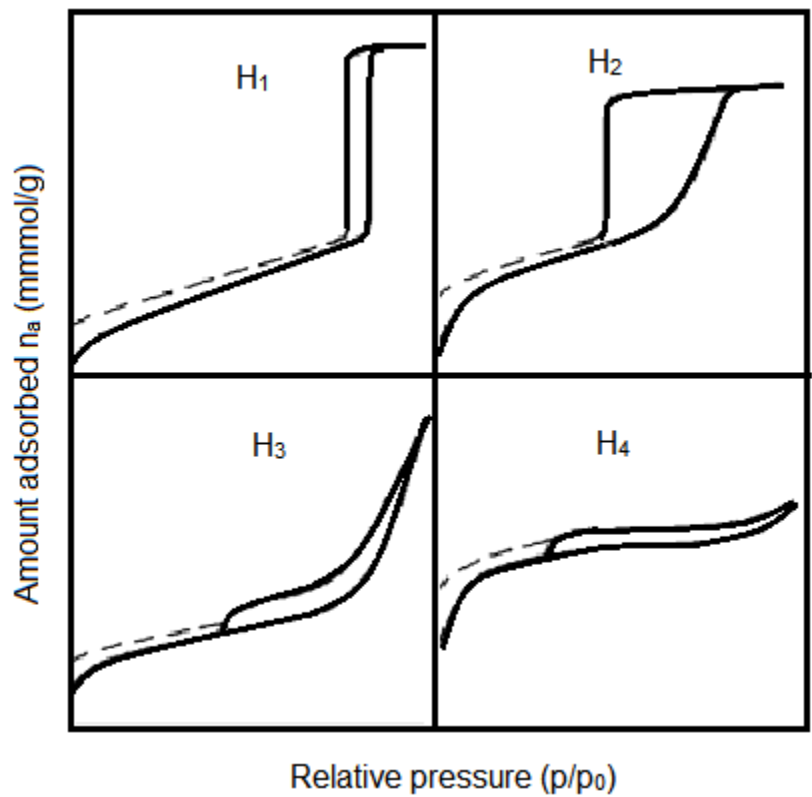
Figure 2-9. Types of hysteresis loops observed during adsorption

CHAPTER 3
MATERIALS AND METHODS

Chemicals and Materials

All chemicals used in this work were analytical grade and were applied without further purification. Solutions were prepared using ultrapure Type I water with a resistivity of 18.2 MΩ and a conductivity of 0.055 µS.

Hg(II) solutions were prepared by diluting 1000 mg/L stock $Hg(NO_3)_2$ standard solution (Fisher Scientific) in ultrapure water. Prior to preparing Hg(0) solutions, metallic Hg was washed with 0.1M HNO_3 and rinsed five times with ultrapure water to remove oxidized Hg compounds from the surface [98].Hg(0) solutions were prepared by mild heating of elemental Hg under $N_2(g)$ flow and bubbling the Hg-laden $N_2(g)$ through $N_2(g)$ purged ultrapure water for 2 hours to reach an aqueous concentration of 10 µg/L to 54 µg/L [99].

Commercially available carbons were oven-dried at 100°C for a minimum of 24 h prior to use. Calgon WPH® is a steam-activated powdered carbon made from bituminous coal with an approximate surface area of 1020 m^2/g. Norit CASPF® is a wood-based chemically activated powdered activated carbon with a surface area of about1200 m^2/g.

Materials Synthesis

Iron Impregnation

Magnetic powdered activated carbon (MPAC) composites were synthesized at room temperature by heterogeneous nucleation [11]. Fe(II) and Fe(III) salts (ferric chloride ($FeCl_3$) and ferrous-ferric oxide (FeO, Fe_2O_3)) were dissolved in ultrapure water with mechanical stirring. After carbon addition, rapid alkaline hydrolysis was induced by

adding 5 M NaOH dropwise to the solution to reach pH 10. The hydrolysis products,

$Fe(OH)^+$ and $Fe(OH)_2^+$, reacted to form ferrihydrite which preferentially precipitated onto

the WPH® carbon surface but, due to thermodynamic instability, transformed into

magnetite (Fe_3O_4) (Equations 3-1 and 3-2) [100]. In the presence of atmospheric

oxygen, the magnetite is susceptible to oxidation to maghemite [63].

$$2Fe(OH)_2^+ + Fe(OH)^+ + 3OH^- \rightarrow (Fe^{3+})_2(Fe^{2+})(OH^-)_8 \tag{3-1}$$

$$(Fe^{3+})_2(Fe^{2+})(OH^-)_8 \rightarrow Fe_3O_4 + 4H_2O \tag{3-2}$$
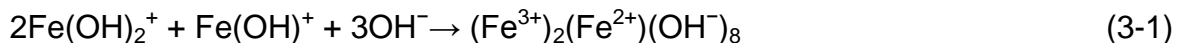
The amount of activated carbon was adjusted to obtain 1:1, 2:1, and 3:1 C:Fe

mass ratios. Samples were rinsed with ultrapure water to remove residual NaOH until a

constant water contact pH was achieved and subsequently oven-dried at 100°C

overnight.

Although maghemite is likely the predominant iron species present on the MPAC

surface due to the synthesis technique used, small amounts of non-magnetic iron

oxides (e.g. hematite or amorphous iron oxides) may occur. Thermal oxidation may

convert some of these amorphous iron oxides to magnetic iron oxides such as

magnetite or maghemite [63]. To compare the initial synthesis product to one having

undergone thermal oxidation, representative portions of the original MPAC were

subjected to oxidation in a programmable muffle furnace (Barnstead Thermolyne

47925-80) under atmospheric air flow. The program increased the temperature by 5°C

until the desired temperature was reached (250°C, 350°C, and 450°C), held for the

desired duration (3 or 6 h), and then gradually cooled.

Nomenclature for the materials is based on carbon to iron ratio, the oxidation temperature and time. For example,1:1-450-6h represents a WPH$^®$ carbon sample impregnated with a 1:1 mass ratio of Fe prior to a 6h thermal oxidation at 450°C.

Surface Oxygen Modification

Commercially available carbons were modified by wet chemical oxidation at room temperature by exposure to 1M, 5M, and 10M solutions of HNO_3, H_2SO_4, and NaOH for 6h. Samples were then rinsed with ultrapure water until reaching a constant water contact pH and subsequently oven-dried at 100°C overnight.

As a control, a sample of the virgin WPH$^®$ carbon was stripped of its surface oxygen groups at 950°C under 150 mL/min H_2(g) flow for 180 min [56,101-103]. While temperatures under 400°C result in the formation of C(O), temperatures over 400°C decompose acidic C(O) groups to CO_2 while basic groups decompose to CO (Equations 2-17 to 2-20) [22] [101]. Anhydrides are removed at 550°C, phenols at 630°C, lactones at 670°C, and 810°C for carbonyls and quinones [52]. The resulting carbon is basic due to Lewis base sites, primarily delocalized π electrons on the basal planes but also localized electron pairs at the edges of the graphene layers [101,101,104]. Using H_2 rather than N_2, He, or another inert gas flow minimizes O_2 chemisorption after stripping by producing relatively stable edge carbons without unpaired electrons, thus maintaining a hydrophobic carbon surface [50,101,105]. This treatment minimally influences porosity [49,52,56,106].

The modification process has the potential to form humic substances which may block adsorbent porosity, reducing Hg adsorption. A humic substance removal wash of 0.1 M NaOH followed by a 0.1 M HCl rinse was investigated [107].

Nomenclature for the materials is based on the activated carbon used and both the concentration and the identity of the modifying reagent. Nitric acid, sulfuric acid, and sodium hydroxide modified carbons are identified as NAC, SAC, and SHAC, respectively. For example, CASPF® carbon that was modified with 5M HNO_3 is represented as CASPF® NAC-5M. The H_2(g) stripped carbon is identified as ACH. The feasibility of modifying biochar rather than commercially activated carbon was also investigated (Appendix A).

Activated Carbon Characterization Methods

Porosity

Instrumentation

Nitrogen adsorption-desorption analyses were performed using a Quantachrome NOVA 2200e. The operating theory, based on ideal conditions, states that the moles of nitrogen transferred from the manifold of a given volume (V_m) at temperature T_a into an empty sample cell partly immersed in liquid nitrogen is equal to the moles of nitrogen transferred to the cell cold zone plus the moles transferred to the warm cell zone [108].

Each sample was outgassed at 110°C under vacuum for 24 h to removed physisorbed substances. Then, nitrogen was added and removed in finite volumes at specific pressures with temperature held constant at approximately 77K using a liquid nitrogen bath. The quantity of adsorbed gas plotted against the relative equilibrium pressure results in a hysteresis loop.

Surface area

The surface area of each sample was calculated by the Brunauer–Emmett–Teller (BET) equation (Equation 3-3 [109]) for P/P_0 = 0.1 to 0.3, in which W is the weight of the adsorbed gas at P/P_0, W_m is the weight of the adsorbed gas at monolayer coverage,

and C is the BET constant. The BET method is the most widely used procedure for surface area analysis of solids.

$$\frac{1}{W[(^{P_0}/_p)-1]} = \frac{1}{W_m C} + \frac{C-1}{W_m C} \left(\frac{P}{P_0}\right) \qquad (3\text{-}3)$$

The C constant, related to the enthalpy of adsorption of the monolayer, indicates the degree of attraction between the adsorbed gas and the solid is sufficient to achieve monolayer coverage. A C constant value over 200 indicates micropore filling. The BET method assumes adsorption sites are uniform and randomly occupied, monolayer molecules serve as sites for subsequent layer adsorption, and subsequent layers have liquid-like properties.

When analyzing data using the BET equation, it is important to use the following parameters to reduce the potential for error. The correlation coefficient (R^2) should be no less than 0.9975 and the C constant, calculated from the slope and y-intercept, must never be negative. Additionally, the P/P_0 value with the maximum single point BET value should be used as the upper limit for the multipoint BET range. A minimum of three, preferably five, relatively equally spaced data points should be used in the multipoint BET calculation. Finally, data points that curve upward from the straight line at low relative pressure and data points that curve downward from the straight line at high relative pressure should not be used in the multipoint BET calculation [108].

Pore volume

Total pore volume is calculated from the amount of vapor adsorbed at the limiting pressure, $P/P_0 = 0.99$. This assumes that all pore space is filled with adsorbate. If no macropores are present, the isotherm will remain nearly horizontal over the range of P/P_0 approaching unity. If macropores are present, the isotherm will rise rapidly as the

P/P_0 nears unity. If mesopores are present, the slope should plateau near the limiting pressure, indicating the all pore space is filled. The average pore size is estimated from the pore volume.

Pore size

Pore volume is distributed over various pore sizes, represented by a pore size distribution. IUPAC classifies pores according to width [68]. Macropores have a pore diameter over 500 Å (50nm) while micropores fall under 20 Å (2nm); Mesopores fall in between the two. Various relative pressures correspond to the sequence of gas adsorption (Table 3-1).

Pore size calculations were based upon the Kelvin equation, which relates the vapor pressure above a liquid to the pore diameter (Equation 3-4) [35] where γ is the surface tension, υ is the molar volume of the liquid, R is the molar gas constant (8.314×10^7 J/mol·K), and r_k is the effective radius of curvature. The equation is based on the principle that equilibrium vapor pressure over a concave meniscus of a liquid adsorbent is less than the saturation vapor pressure at the same temperature. Therefore, a gas can condense as a liquid inside the porosity of a solid with sufficiently small pore radii filling with liquid at lower equilibrium vapor pressure values, describing capillary condensation. The pore size distributions over the mesopore region were calculated using the Barrett–Joyner–Halenda (BJH) equation [110].

$$\ln\left(\frac{P}{P_0}\right) = -\frac{2\gamma\upsilon}{r_k RT} \tag{3-4}$$

Point of Zero Charge

The surface chemistry of activated carbon is dominated by its amphoteric nature which is dependent upon heteroatom content, mainly oxygen. When immersed in water,

carbon develops a surface charge from the dissociation of surface groups or the adsorption of ions from solution. A negative charge can result from dissociation of acidic C(O) while a positive charge may be due to basic C(O). When the pH is lower than the pzc value, water donates more H^+ than OH^- groups so the adsorbent surface is positively charged and attracts anions. When the pH is above the pzc value, surface groups will dissociate, leaving the sorbent surface negatively charged, attracting cations (Figure 3-1). Ion loading as a function of pH has also been demonstrated for the adsorption of many heavy metals ions by activated carbon [49,111,112].

The point of zero charge (pH_{pzc}) was determined using the abbreviated version (10% by weight). Ultrapure water was purged with $N_2(g)$ for 20 min before carbon addition for a 24 h contact time, after which the solution pH was obtained in duplicate under $N_2(g)$ headspace flow using an Accumet AB 15 pH meter. The manufacturer satted instrument sensitivity is between -1.99 and 19.99 with an accuracy of 0.01 pH units.

Total Acidity Titration

The Boehm titration technique is a classical equilibrium acid-base titration that provides information regarding acid/base features of the carbon surface [41,113]. Carbon samples were prepared for total acidity titration using the Boehm titration method by adding 0.5 g carbon and 0.1 g KCl to 25 mL of 0.05 N NaOH and 0.05 N HCl, respectively, and rotating end-over-end for 48 h [22,46,47]. The KCl was added to increase the ionic strength of the solution. The titration is performed against a blank with any base consumed due to neutralization of surface functional groups. Blank solutions were prepared using 25 mL 0.05 N NaOH and 0.05 N HCl, each with 0.1g KCl. After the elapsed contact time, carbon solutions were filtered using 0.45 μm mixed cellulose

filters (Fisher Scientific). Filtrate was purged with $N_2(g)$ for 10 min prior to titration. 0.05N NaOH samples were titrated with 0.1N H_2SO_4 to pH 4.5 while 0.05 N HCl solutions were titrated with 0.05 N NaOH to pH 11. Total acidity was calculated as the difference between the volume of titrant consumed in the sample titrations and the volume of titrant consumed in the appropriate blank titrations with the difference being due to neutralization of surface functional groups.

Elemental Analysis

Moisture content of the carbons was determined by the mass difference before and after heating at 90°C for 16 h. Ash content was determined by the mass difference after heating to 650°C for 16h. Elemental composition (C,H,N) was determined by a Carlo Erba EA 1108 elemental analyzer. Assuming negligible presence of other elements, oxygen content was determined by mass difference.

X-Ray Diffraction

X-ray diffraction (XRD) can be used to determine purity, crystal size, disorder, and degree of isomorphous substitution. XRD observes the interaction of electromagnetic waves with atoms of a crystal. Common radiation sources are CoKα (0.178890nm) or FeKα (0.193604nm). When the x-rays pass through a crystal, each atom in the structure scatters the waves uniformly in space but in certain directions all the waves combine for enhanced intensity. The direction of this occurrence is related to the distance between atomic planes and the angle that the x-rays enter and leave the crystal (Bragg angle). The XRD diagram is a plot of the observed diffracted intensity vs. Bragg angle [63].

X-ray diffraction (XRD) patterns of the MPAC were recorded using a Philips APD 3720 X-ray unit with Cu Kα radiation. XRD patterns were analyzed to identify the iron speciation on the MPAC surface. Components were identified using the powder

diffraction identification number according to the International Center for Diffraction Data. Peaks greater than 3σ of the baseline noise were used.

Vibrating Sample Magnetometry

Vibrating Sample Magnetometry (VSM) is used to measure magnetic properties as a function of the external magnetic field strength, temperature, and time. The theory of operation is based upon Faraday's law of induction where if a sample is placed in a uniform magnetic field (H), a magnetic moment (m) will be induced in the sample, producing a voltage in stationary sensing coils proportional to the magnetic moment induced (Figure 3-2). The data is presented as a hysteresis loop that shows the relationship between the induced magnetic flux density (B) and the magnetizing force (H) (Figure 3-3). Magnetic characteristics of the MPAC composites were measured using Princeton Measurements Co. MicroMag VSM 3900.

Saturation (value of B at points a and d), occurs when almost all magnetic domains are aligned. Therefore, increasing the magnetizing force will not significantly increase the magnetic flux. Retentivity (value of B at point b) indicates the remanence (level of residual magnetism) of the material when the magnetizing force is reduced to zero. This occurs as some magnetic domains remain aligned but others have lost their alignment. Coercivity, H_c, (value of H at point c) is the amount of reverse magnetic field required to return magnetic flux to zero. Permeability (μ), the ratio of flux density to magnetizing force, describes the ease with which a magnetic flux is established in the material [114].

Magnetic Adsorbent Recovery

MPAC, easily dispersed in aqueous solution, can be retrieved using a strong magnet such as neodymium, a rare-earth magnet. The recovery (%) of MPAC from

aqueous solution and adsorbent mass balance was determined using the dry mass captured by the magnet, the dry mass retained by a 0.45 μm nitrocellulose filter after vacuum filtration, and the dry mass of the initial MPAC dose. The contact time (5 min) and carbon dose (1 g/L) were held constant while the MPAC species varied based on synthesis variables. Preliminary experimentation indicated the use of a 5 min contact time because the results did not significantly vary above this contact time while a 1 min contact time produced considerably lower magnetic sorbent recovery from aqueous solution.

Adsorbent Stability

Iron. As Fe is redox sensitive with ferrous iron being highly soluble, Fe effluent levels were quantified using a spectrophotometer (Hach DR/4000 Spectrophotometer) and Hach's TPTZ powder pillow method 2190. This method requires 10 mL aqueous sample to which the TPTZ Iron Reagent Powder Pillow is added, shaken for 30 s, and allowed to react for 3 min prior to measurement. Each run was performed with standards including a blank. The manufacturer stated estimated detection limit is 0.022 mg/L total Fe.

Mercury. As the modified carbons have adsorbed toxic Hg, their disposal is potentially regulated under the Resource Conservation and Recovery Act. The Code of Federal Regulations (40 CFR §261.24) identifies Hg as a contaminant that must be tested for using the toxicity characteristic leaching procedure (TCLP; EPA method 1311). Resulting leaching must have an Hg level under 0.2mg/L in order to be considered non-hazardous. Higher leachate levels necessitate the treatment of the spent adsorbent as a hazardous waste, greatly increasing disposal costs as it cannot be disposed of in a sanitary landfill.

The appropriate extraction fluid is determined by the water contact pH. Because the water contact pH of the Hg-loaded sorbent was under pH 5, the following extraction fluid was prepared: 5.7 mL glacial acetic acid, 64.3 mL 1N NaOH, to 930 mL of ultrapure water. Ten ml of this extraction fluid was applied to 0.5 g Hg-loaded carbon and rotated at 30 rpm for 18 h. After the elapsed contact time, the carbon was separated from aqueous solution by vacuum filtration and the pH of the extract was obtained before processing for Hg quantification.

Aqueous Mercury Removal

Labware Preparation

All labware used in adsorption experiments was prepared by soaking for a minimum of 2 h in 20% HNO_3 and subsequently rinsing with ultrapure water a minimum of three times before air drying. Vessel blanks were performed on each batch of cleaned glassware to ensure labware was free from residual mercury contamination by exposing randomly selected labware items to a 20% HNO_3 solution for 5 min and processing as sample for analysis.

Mercury Quantification Methods

Cold vapor atomic absorption (CVAA) spectrometry is often used to quantify aqueous Hg concentrations due to its ease of use, rapidity, selectivity, and accuracy compared to other technologies [3]. CVAA has a detection limit of 0.1 µg/L. Atomic fluorescence spectrometry is used to reach ng/L detection limits. The EPA has developed several standardized methods associated with this technology.

The total mercury is determined for each aqueous sample by reducing all Hg species present to Hg(0) with $SnCl_2$ before transporting the vapor into the path of radiation from a cathode ray tube (Figure 3-4). The ground state of elemental mercury

atoms absorb radiation from the lamp in proportion to the concentration. The reduced signal reaching the detector is recorded. This process is based on the Beer-Lambert Law.

In this study, total aqueous Hg concentrations were measured on a Teledyne Hydra Atomic Absorption Mercury Analyzer using EPA method 245.1, which uses a thermal digestion and $SnCl_2$ reduction technique. The EPA method has a detection range between 0.2 µg/L and 100 µg/L, which may be extended based upon sample size, matrix characteristics, operating conditions, and instrumentation configuration. The manufacturer-stated instrumentation detection limit is 0.2 µg/L but the operating method detection limit (MDL) was determined to be 0.4 µg/L.

Within 24 h of collection, each sample was acidified to under pH 2 using 0.5 mL HNO_3 and 1mL H_2SO_4. Standards were prepared with each run. According to EPA method 245.1, each sample was thermally digested prior to analysis using 3mL of 0.32 M $KMnO_4$ (Fisher Scientific), 1.6 mL of 0.18 M $K_2S_2O_8$ (Fisher Scientific), and 1.2 mL of NaCl–hydroxylamine sulfate solution (2.1M NaCl, 0.73M hydroxylamine sulfate) (Fisher Scientific).

Test Stand

The batch reactor contained a sealed Teflon mercury-carbon contact chamber with 0.8 L/min headspace $N_2(g)$ flow through an inlet/outlet port to an oxidizing purge trap (Figure 3-5). The oxidizing purge trap to capture volatilized Hg was prepared using 0.25 M $KMnO_4$ (Fisher Scientific) in 10% H_2SO_4 (Fisher Scientific) solution. All Hg(0) experiments were performed in a glove bag under $N_2(g)$ flow. The carbons were applied as a slurry at a 1g/L dose to Hg-spiked ultrapure water for a specified contact time, after

which the adsorbent was separated from solution via vacuum filtration using 0.45μm mixed cellulose filter (Fisher Scientific).

Hg Mass Balance

An integral Hg mass balance verifies the Hg-removal performance of an adsorbent. Based on published aqueous Hg(II) mass balances, acceptable mass balance closure was determined to be within approximately ±15% [115,116]. This was achieved by quantifying the residual aqueous Hg, adsorbed Hg extracted from MPAC by HF digestion (or sequential chemical extraction where specified), and volatilized Hg captured in the $KMnO_4$ trap.

A total digestion was applied to quantify total adsorbed Hg. This digestion was also applied to virgin carbons to determine trace levels of Hg contamination in the activated carbon from the raw source material. These trace levels of contamination were accounted for in the mass balance calculations. The HF digestion was performed using 400 μL aqua regia (3:1, v/v concentrated HCl (J.T. Baker) to concentrated HNO_3 (Fisher Scientific)), 2 mL of concentrated HF (Acros Organics), and 20 mL of saturated H_3BO_3 (Acros Organics).

Batch Studies

Identifying a contact time is essential in order to reach adsorption equilibrium during the isotherm assay. Based on the protocol described by Calgon, a 1 g/L dose of carbon was applied to 100 μg/L Hg solution for 0–180 min [69].

Isotherm analysis is useful in evaluating the capacity of the carbon for adsorption of specific contaminants. Isotherm analysis was performed by applying varying weights of dried powdered activated carbon to constant volumes of Hg solution for the equilibrium contact time previously identified, after which samples were vacuum filtered

using 0.45μm mixed cellulose filter (Fisher Scientific). Results were analyzed using both the Freundlich and Langmuir isotherms.

MPAC adsorption experiments were performed at the pseudo-equilibrium contact time of 180 min with a carbon dose of 1g/L and a mercury concentration of 100 μg/L. Surface modified carbon adsorption experiments were performed with a contact time of 30 s due to the volatile nature of Hg(0). The carbon dose applied was lowered to 150mg/L as higher doses resulted in nearly 100% removal for most carbons. Controlled by the solubility of Hg(0), Hg(0) doses ranged between 40 and 60 μg/L; Hg(II) solution concentration was 50 μg/L.

Investigation of Adsorption Mechanisms

Influence of pH and pCl

Mercury speciation in the presence of a known chloride concentration at given pH values is well understood. By manipulating these variables, Hg speciation can be controlled and binding mechanisms can be predicted. This concept can be used to investigate the efficiency of the SCE for predicting binding mechanisms based on extraction fraction. Hg speciation at the identified pH and pCl values was predicted using Visual MINTEQ. The pCl was adjusted using NaCl while pH was adjusted using 0.25M H_2SO_4 or 0.25 NaOH. Ionic strength, calculated using the Debye-Huckel equation, was held constant using Na_2SO_4. The optimal pH and pCl for Hg(II) adsorption by MPAC was found using a fractional factorial approach by manipulating the pH (2, 6, and 10) and pCl (12, 6, and 0).

Sequential chemical extraction

Sequential chemical extractions (SCEs), first becoming popular in the 1980s, are used to provide information regarding the speciation, bioavailability, and mobility of

metals by applying selective extractants with increasing strength to the same sample aliquot [117,118]. The goal is to convert the bound metal into a soluble form using specific extractants as to elucidate the binding mechanism and speciation. Once extracted, the metals are analyzed by the appropriate analytical technique. If the chemistry of the adsorbate is understood, extractants can be meticulously applied to elucidating the operating binding mechanisms.

When designing an SCE, major factors to consider include the chemical nature of the extractant, efficiency and selectivity of extractants, matrix effects such as re-adsorption, order of extractants, and the nature of the targeted metal [118,119]. Problems with sequential extractions include selectivity less than 100%, control of reaction conditions, and inconsistencies between extraction protocols [118,120]. It is also possible that in removing a fraction of the metal ion, the ion may then redistribute itself among the remaining phases (phase transformation) [121].

Several factors have been experimentally determined to have significant affects on the results. Shaking speed should be maintained at 30 rpm [99]. The temperature during extractions should remain at 20°C ± 2°C [99,120]. Extraction times should reach 18 ± 4 hours [99,120]. Samples should be dried until constant weight and the sample slurries should be formulated with a 1:100 solid to extractant ratio [99,117,120,122]. When properly designed, an SCE can reach detection levels as low as 0.5 µg/L [120].

In this study, sequential chemical extraction was performed by applying the following extractants with increasing strength to the same sample aliquot: water soluble, ion exchangeable, surface precipitated, surface bound, poorly reducible (iron-associated), and residual. The water soluble fraction used ultrapure water to target the

labile non-adsorbed Hg within the pores. The ion exchangeable fraction used 1M

ammonium nitrate to target weakly electrostatically adsorbed Hg. Ammonium nitrate

was selected because nitrate will not complex with mercury; therefore, any mercury

mobilized will be due to cation exchange with ammonium on the carbon surface. The

surface precipitated fraction was targeted using 0.11M acetic acid. At higher pH values,

acetic acid has been shown to have little to no effect on organic carbon or free iron

concentrations [122]. The surface bound mercury was targeted using 0,1M 2,3-meso-

dimercaptosuccinic acid (DMSA), a chelating agent that sequesters Hg. The poorly

reducible fraction used 0.128M diothinite, 0.3M citrate, and 1M bicarbonate (DCB) to

target the metals associated with the iron oxides by reducing Fe^{3+} to the more soluble

Fe^{2+} form, thus releasing chemisorbed Hg [118]. Due to potential metal impurities in this

reagent, a reagent blank was performed to prevent Hg contamination [122]. Residual

Hg was quantified in the final fraction using aqua regia, HF, and H_3BO_3 as described

above for total digestion.

Data Analysis

All experiments were performed in triplicate and average values reported. All

replicate data falls within the 95% confidence interval. Error bars represent the standard

error of the mean. The Box Behnken experimental design for response surface

methodology was used to identify the optimal MPAC for Hg removal according to the

three variables specified. The design required 17 total runs with 12 experiments and 5

replicates of the center point. The experimental design was analyzed using Design-

Expert software (version 6.0.5). Visual MINTEQ 2.61, a chemical equilibrium model,

was used to calculate metal speciation, complexation reactions, and solubility equilibria.

Linear regression and ANOVA analyses were performed using the statistical software

R, version 2.14.1.

Table 3-1. Surface Area Calculation Methods by P/P_0 range utilized [108]

P/P_0 range	Mechanism	Calculation method
<0.1	Micropore filling	DFT, HK, SF, DA, DR
0.01 – 0.1	Sub-monolayer formation	DR, MP
0.05 – 0.3	Monolayer formation	BET, Langmuir, DR, MP
>0.2	Multilayer formation	t-plot, alpha-s, FHH, MP
>0.35	Capillary condensation	BJH, DH, Fractal-FHH, NK
0.1-0.5	Capillary condensation in M_{41}S-type materials	DFT, BJH, DH
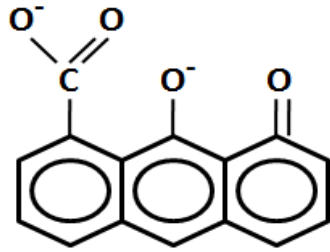
Figure 3-1. Common acidic surface oxygen groups on activated carbon with pH above the pHpzc (left to right: carboxyl, phenol, carbonyl)
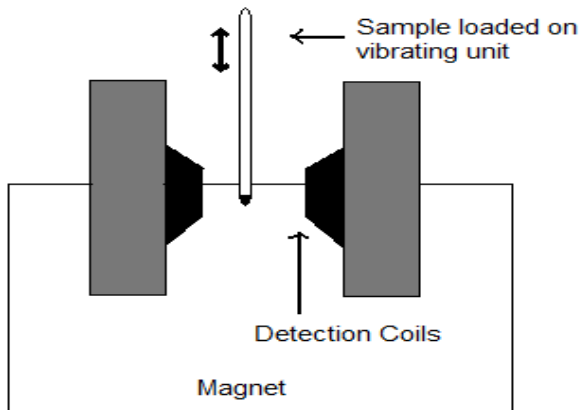
Figure 3-2. Vibrating Sample Magnetometer Schematic
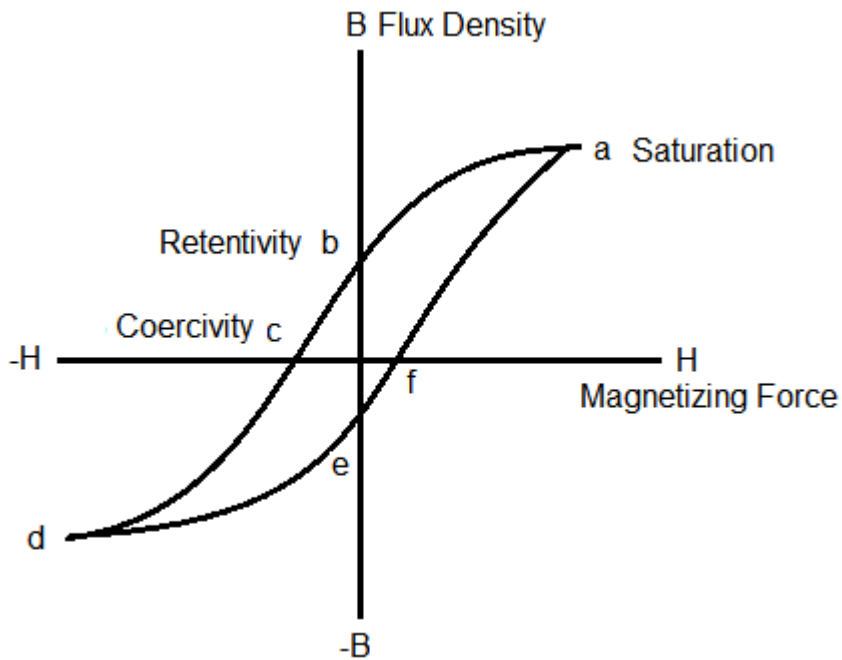
Figure 3-3. Hysteresis loop resulting from VSM analysis
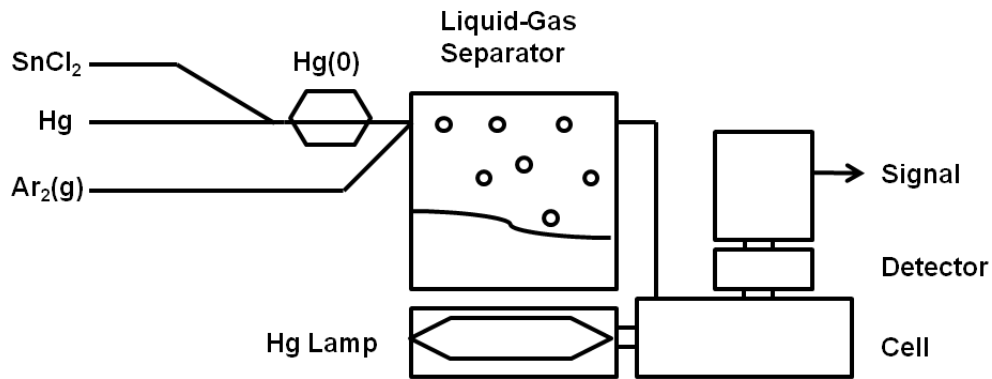
Figure 3-4. Cold Vapor Atomic Absorption Spectroscopy Schematic
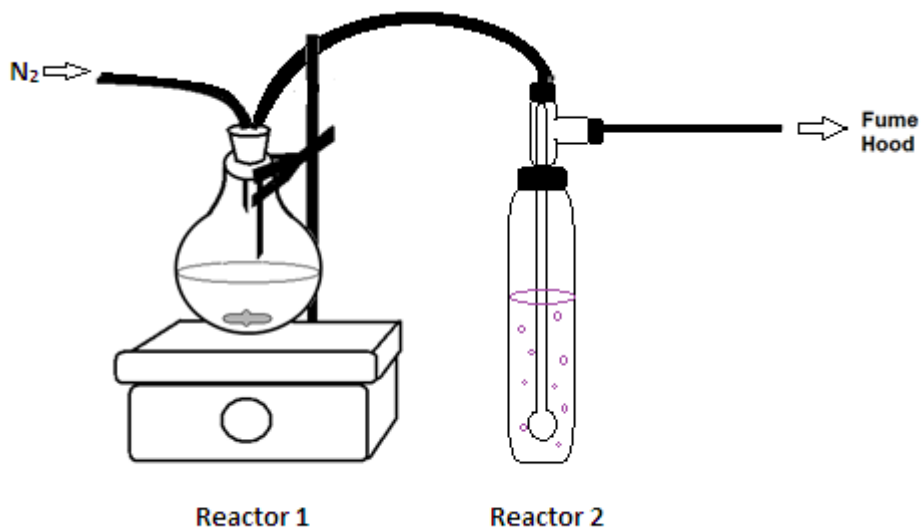
Figure 3-5. Schematic of batch adsorption test stand

CHARACTERIZATION OF MODIFIED ACTIVATED CARBON

Many carbon modifications are discussed in the literature. The applications of the materials prepared in this work are unique, as iron impregnation for Hg adsorption has not been investigated, nor has the influence of surface oxygen functionality on aqueous elemental Hg adsorption been studied. In order to best understand the application of these materials to Hg-laden wastewaters, knowledge of the material characteristics is necessary.

The following discussion addresses the characterization of the carbon adsorbents in terms of porosity, surface charge, crystalline nature, elemental composition, magnetic characteristics, and sorbent stability. The objectives were to 1) synthesize magnetic carbons that are at least 95% recoverable through magnetic separation, 2) increase acidic C(O) on activated carbon surfaces with minimal pore degradation, and 3) characterize carbons with techniques including nitrogen adsorption-desorption, X-ray diffraction, point of zero charge, and total acidity.

MPAC Characterization

Porosity

Nitrogen adsorption-desorption isotherms for virgin WPH® and CASPF® carbons are shown in Figure 4-1. The isotherms are Type I, common for microporous substances such as activated carbon. Both carbons display H4 hysteresis loops, indicative of a microporous characteristic with slit-shaped pores.

Isotherms were analyzed to produce BET surface area, average pore diameter, and total pore volume data. The process of iron impregnation was expected to reduce the available surface area relative to the virgin activated carbon due to the minimal

surface area of the iron oxides (1.9 m^2/g). As expected, the 1:1 C:Fe resulted in a ~50% reduction of surface area relative to the raw WPH$^{®}$ carbon while the 2:1 and 3:1 C:Fe showed surface areas reduced by the expected ~33% and ~25%, respectively (Table 4-1). The replicates of each average porosity characteristic reported below have a coefficient of variation (CV) of approximately 7%.

With the purpose of converting amorphous iron oxides to ferromagnetic magnetite or maghemite, portions of the synthesized MPAC were subjected to thermal oxidation for varying temperatures and durations (250°C, 350°C, and 450°C for 3 h and 6 h). Figure 4-2 demonstrates that thermal oxidation of a 1:1 C:Fe MPAC at 250°C had little effect on porosity (surface area, pore volume, and pore size) regardless of duration while temperatures of 350°C and 450°C increasingly reduced the surface area and pore volume while increasing the average pore size. This adverse degradation of porosity is likely due to decomposition of surface oxygen groups and, to a greater extent, gasification of carbon at temperatures over approximately 400°C [22].

The 1:1, 2:1, and 3:1 C:Fe MPACs exhibited similar BJH pore size distributions (PSD) to the virgin carbon as calculated from nitrogen adsorption isotherms (Figure 4-3). Thermal oxidation of the samples caused pore degradation/collapse, demonstrated by the reduction in cumulative pore volume and slight skewing of the pore volume to higher pore diameters, seen in the highly oxidized sample (3:1-450-3h). PSD replicates indicated no greater than a 5.5% CV.

Magnetic Characteristics

X-ray diffraction

Maghemite is the most likely iron oxide produced in the synthesis of MPAC but other iron oxides have the potential to precipitate onto the carbon surface. An XRD

analysis was performed to identify the iron oxide species present on the carbon surface. The raw 3:1 C:Fe as well as the oxidized 3:1 C:Fe samples were analyzed (Figure 4-4).

All samples investigated displayed peaks with positions and relative intensities that match well with those for maghemite-c (39-1346) and maghemite-q (25-1402). The samples exposed to 350°C and 450°C exhibited additional peaks identified as hematite (33-0664), a non-magnetic iron oxide. All major diffraction peaks were associated with the iron oxides identified.

Several specific features of interest are present in these XRD patterns. The raw 3:1 carbon exhibits an amorphous characteristic from roughly 2θ 15° to 34° and from 2θ 40° to 50°. As the oxidation temperature increased, this amorphous characteristic was reduced and the crystalline structure enhanced, seen in the progressively flattened baseline and the increased sharpness of nearby peaks. It was hypothesized that the thermal oxidation would force amorphous iron oxides to magnetite or maghemite. Although there is no overwhelming evidence of this effect seen in the XRD patterns, two unique aspects in the patterns suggest this change may occur. Maghemite-c is known to exhibit small diffraction peaks at 2θ 32.152° and 44.743° which are present only in the 450°C carbon. It could be argued that the emergence of minor peaks at 2θ 23.791° and 26.125° in the samples that underwent higher thermal oxidation temperatures is evidence of this change but these peaks could have been present in the original 3:1 sample and only became clear due to the progressively increased crystallinity and thus flattened baseline.

In several locations, there was clear evidence of the formation of hematite through the thermal oxidation process. Hematite formation was expected due to the conversion

of maghemite to hematite in the range from 350°C to 750°C, depending upon the grain size, degree of oxidation, and defects in the crystal lattice [123]. Notice the development of a hematite peak as thermal oxidation temperature increased at 2θ 24.158°, 33.181°, 40.890°, 49.523°, and 64.049°. Transformation to hematite may be indicated at approximately 2θ 35.5 but interpretation is unclear due to overlapping peaks of hematite at 2θ 35.642°, maghemite-c at 2θ 35.661°, maghemite-q at 2θ 35.715°, and magnetite at 2θ 35.453°. Also of note is the formation of a hematite shoulder peak (2θ 62.507°) in the maghemite-c (2θ 62.983°) and maghemite q (2θ 63.069°) peak for carbons exposed to 450°C for 6 h.

Due to the synthesis technique, magnetite (19-0629) may be present on the carbon surface. Distinguishing magnetite from maghemite XRD patterns can be challenging, as most of magnetite's strong peaks are very close to the location of maghemite-c, maghemite-q, and hematite peaks. Magnetite's strongest peak, unfortunately, is muddled with the other peaks at approximately 2θ 35.5°. The only strong magnetite peak that would stand apart from the other iron oxides known to be present is at 2θ 56.994°; this peak is absent in all XRD patterns presented. As magnetite slowly oxidizes over time under atmospheric oxygen exposure, it is possible that a freshly synthesized sample may display a magnetite peak at this location.

Vibrating sample magnetometry

The magnetic properties of MPAC were tested by vibrating sample magnetometry as shown in Table 4-2. To enable manipulation using conventional magnets, the sorbent must exhibit sufficient saturation magnetization (Ms) of at least 4.5 Am^2/kg and a remanence (residual magnetization, Mr) high enough to allow for recapture but not so high as to cause clumping [62]. All MPACs tested showed sufficiently strong saturation

74

magnetism to allow for recapture. Thermal oxidation at 250°C and 350°C slightly increased Ms for the 6h duration. The 450°C oxidation dramatically increased Ms for the 3h duration but declined for the 6h duration, likely due to the conversion of maghemite and magnetite to non-magnetic hematite. Remanence values tended to increase at all thermal oxidation temperatures with 450°C resulting in the highest Mr values of the samples tested. No samples exhibited excessive clumping upon water contact.

Magnetic adsorbent recovery

MPAC was retrieved from the aqueous solution via magnetic solid-phase extraction. With a coefficient of variation of only 4.0%, the C:Fe did not significantly influence the recoverability of the adsorbent (Table 4-3). Sorbent recovery slightly decreased as the thermal oxidation temperature increased. The relative percent difference between the raw MPAC and the sample exposed to 450°C for 6 h was 15.9% and 27.3% for the 1:1 and 3:1 C:Fe, respectively. Although VSM and XRD data indicated improved magnetic qualities with thermal oxidation, this improvement did not translate to improved sorbent recovery. The 3:1 MPAC meets the objective of being 95% recoverable. The average adsorbent mass balance closure was 92.3% and ranged from 88.1% to 96.5% with a CV of 9.5%.

Adsorbent Stability: Iron

Typically, iron is not a concern from a regulatory standpoint and is commonly a constituent of industrial wastewaters. At unadjusted pH, the MPAC adsorbent is quite stable and Fe effluent concentrations fell below the detection limit (0.022 mg/L total Fe) for all contact times investigated, between 0.5–180 min.

Because Fe leaching is sensitive to matrix pH, the stability of the 3:1 MPAC adsorbent at extreme pH values was determined. At pH 2, 1.2 mg Fe leached per gram

75

MPAC. The leaching did not cause discoloration of the water. At pH 10, the Fe effluent concentrations fell below the detection limit. The leaching of Fe at lower pH values did not impact recoverability, with 98% of the MPAC being recovered.

C(O) Modified Carbon Characterization

Porosity

Nitrogen adsorption-desorption isotherms were analyzed to produce BET surface area, average pore diameter, and total pore volume data (Table 4-4). Consistent with literature, the $H_2(g)$ stripping process did not negatively influence porosity [49,52,56,106]. Literature indicated the potential for damage to porosity through the wet chemical oxidation process due to either pore damage or the formation of pore-blocking humic substances [107]. Nitric acid modified samples exhibited progressive porosity damage with increasing concentration. Conversely, sulfuric acid and sodium hydroxide modifications did not result in damage to porosity. The humics removal wash did not significantly influence the adsorbent porosity (CV of only 0.4%) and thus was not applied to carbon samples. The modified carbons and $H_2(g)$ stripped carbons exhibited similar BJH pore size distributions to the virgin WPH® carbon (Figure 4-5). PSD replicates indicated no greater than a 3.2% CV. The treatment of CASPF® carbon impacted porosity similarly to the WPH® modification.

Surface Oxygen Functionality

With a basic pH_{pzc} and a relatively low oxygen content, the total acidity of WPH® carbon was expectedly low, at only 85 meq/g [0.05] NaOH (Table 4-4). On the contrary, CASPF® carbon displayed an acidic pH_{pzc} and higher oxygen content, resulting in greater total acidity relative to WPH®. The control carbon, stripped of nearly all C(O), demonstrated a very basic pH_{pzc} and a total acidity near zero.

In the modification of WPH$^®$ with nitric acid, as the acid concentration increased, the oxygen content and total acidity increased while the pH$_{pzc}$ fell. Relative to 10M HNO$_3$ treatment, the 10M H$_2$SO$_4$ treatment was less effective at adding surface oxygen groups, seen in the reduced oxygen content and the lower total acidity. Interestingly, the pH$_{pzc}$ of SAC-10M was slightly lower than NAC-10M for both WPH$^®$ and CASPF$^®$ carbons. Also note the lack of response in SAC and SHAC carbons to acid concentration; total acidity, pH$_{pzc}$, and oxygen content remained relatively stable.

The CASPF$^®$ modified carbons interestingly showed an increase in pH$_{pzc}$ upon modification though the values remained very acidic. Modification with 10 M HNO$_3$ resulted in an oxygen content of 21.2% and a high total acidity of 425 meq/g, a 37% increase from raw CASPF$^®$ carbon. Modification with 10 M H$_2$SO$_4$ actually reduced the oxygen content and total acidity relative to the raw CASPF$^®$.

Table 4-1. Porosity of various MPACs

Sample	Surface area (m^2/g)	Mean pore size (Å)	Pore volume (cm^3/g)
1:1	579	24.2	0.333
2:1	709	24.3	0.430
3:1	790	23.2	0.457
3:1-450-3h	46	82.4	0.124

Table 4-2. Magnetic characteristics of various MPACs

Sample	Hc (mT)	Mr (Am^2/kg)	Ms (Am^2/kg)
3:1	2.75	1.3	10.92
3:1-250-3h	3.17	1.2	10.90
3:1-250-6h	7.10	2.0	11.23
3:1-350-3h	3.65	1.6	10.89
3:1-350-6h	11.96	2.7	11.98
3:1-450-3h	9.28	3.9	19.43
3:1-450-6h	7.29	3.2	14.99

Table 4-3. Magnetic solid phase extraction results for various MPACs

Sample	Sorbent recovery (%)
1:1	92.6
2:1	88.1
3:1	95.0
1:1-250-6h	85.4
1:1-350-6h	76.5
1:1-450-6h	75.6
3:1-250-6h	87.8
3:1-350-6h	81.5
3:1-450-6h	72.2

Table 4-4. Characterization of various C(O) modified carbons

Sample	Surface area (m^2/g)	Pore size (Å)	Pore volume (cm^3/g)	% N	% H	% O	% Ash	pH$_{pzc}$	Total acidity (meq/g [0.05] NaOH)	Total basicity (meq/g [0.05] HCl)
WPH	1020	11.2	0.55	0.0%	0.2%	6.9%	7.4%	8.36	85	136
ACH	1044	15.0	0.58	0.0%	0.3%	1.9%	8.1%	10.10	11	212
WPH NAC-1M	991	11.2	0.58	0.0%	0.2%	8.4%	6.3%	6.56	94	99
WPH NAC-5M	978	11.0	0.54	0.6%	0.6%	15.8%	6.4%	5.02	139	107
WPH NAC-10M	878	11.0	0.49	0.5%	1.1%	19.6%	6.6%	3.99	231	91
WPH SAC-1M	975	11.1	0.54	0.4%	0.3%	6.1%	6.3%	3.78	112	48
WPH SAC-5M	989	11.1	0.55	0.3%	0.3%	5.9%	6.4%	3.90	112	33
WPH SAC-10M	975	11.2	0.55	0.3%	0.4%	10.5%	5.7%	3.36	118	26
WPH SHAC-1M	994	11.1	0.54	0.4%	0.2%	3.8%	6.8%	7.37	60	105
WPH SHAC-5M	1000	11.1	0.55	0.4%	0.2%	5.1%	6.8%	7.25	64	147
WPH SHAC-10M	1001	11.1	0.54	0.4%	0.2%	6.3%	6.2%	7.13	70	156
CASPF	1201	11.0	0.91	0.0%	2.3%	19.8%	0.7%	1.93	293	0
CASPF NAC-10M	817	11.7	0.51	2.4%	1.9%	21.2%	0.9%	2.83	425	10
CASPF SAC-10M	1269	11.8	0.93	0.1%	2.3%	13.8%	0.4%	2.77	278	2
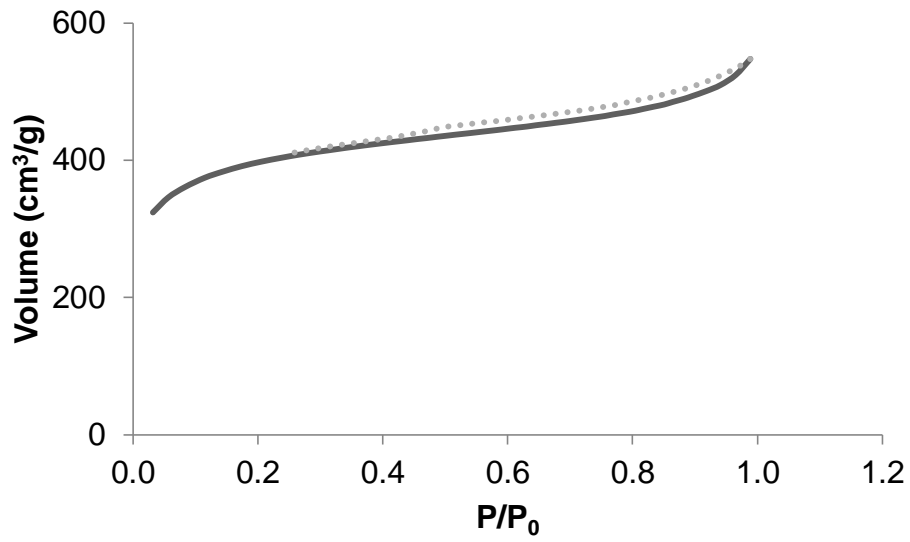
A.
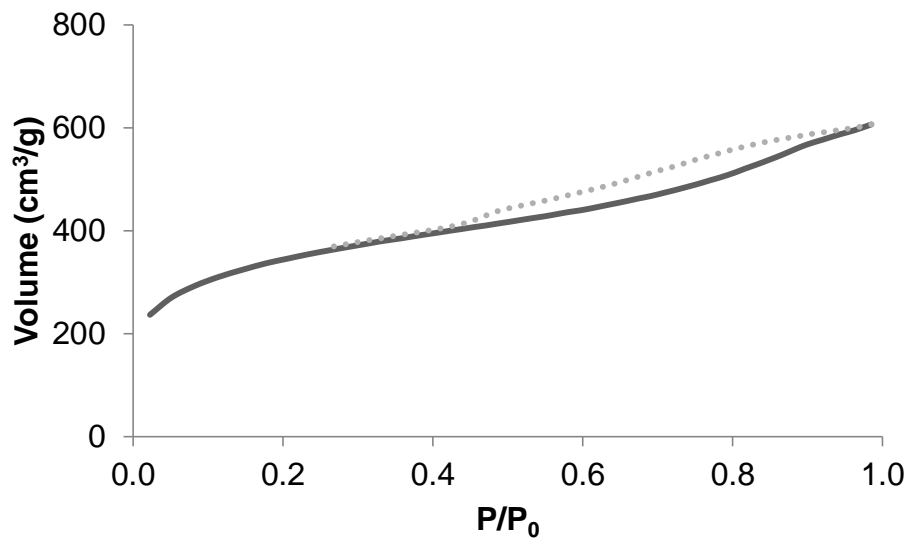
B.

Figure 4-1. MPAC nitrogen adsorption-desorption isotherms A) WPH B) CASPF
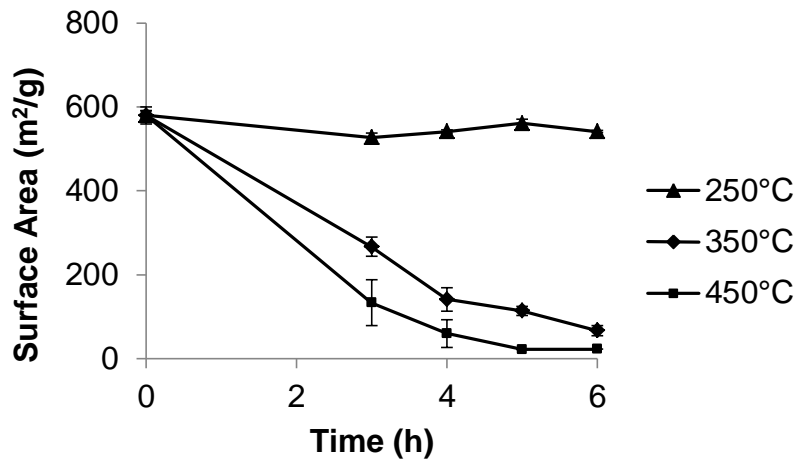
A.
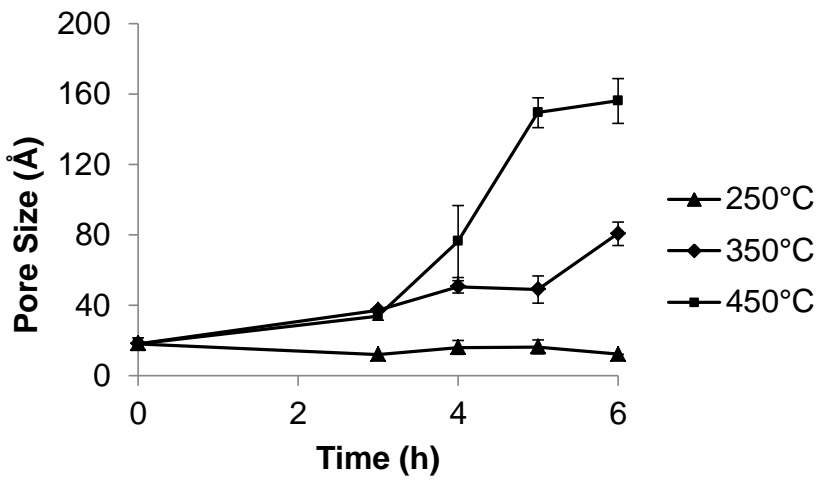
B.
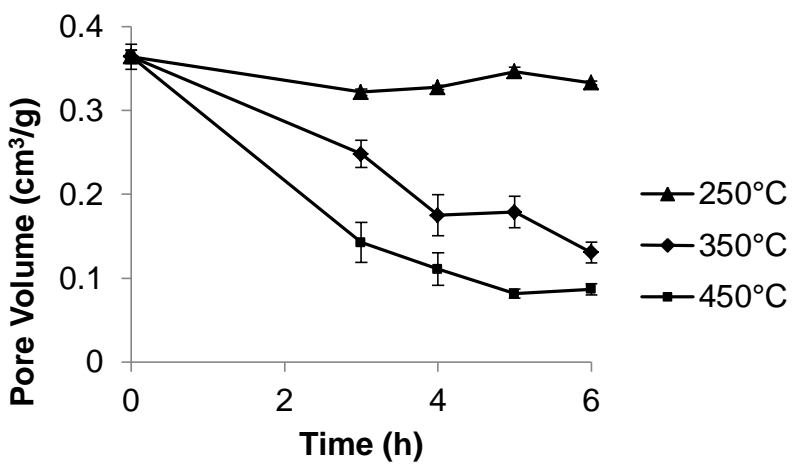
C.

Figure 4-2. Effect of thermal oxidation on porosity of 1:1 C:Fe. A) surface area, B) pore size, and C) pore volume
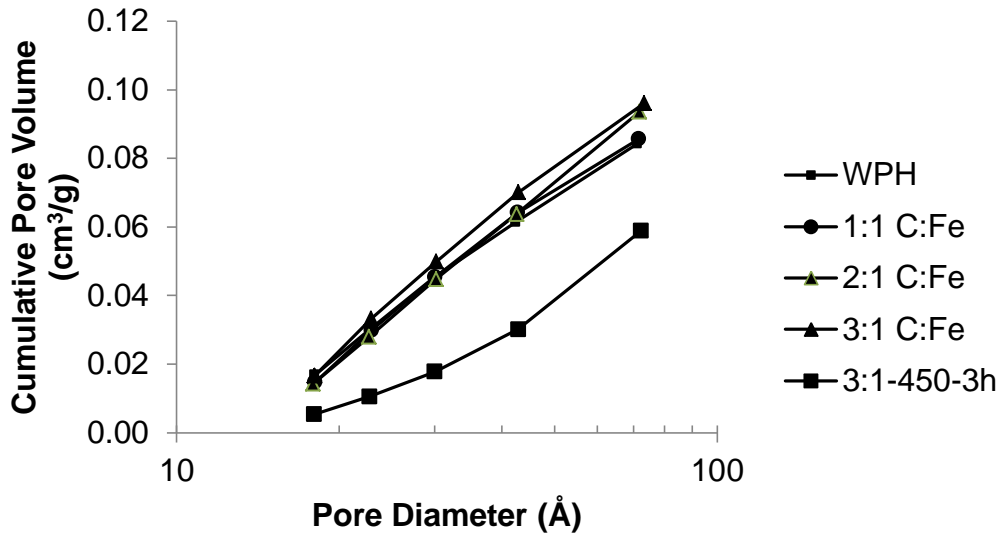
Figure 4-3. BJH pore size distribution of select MPACs
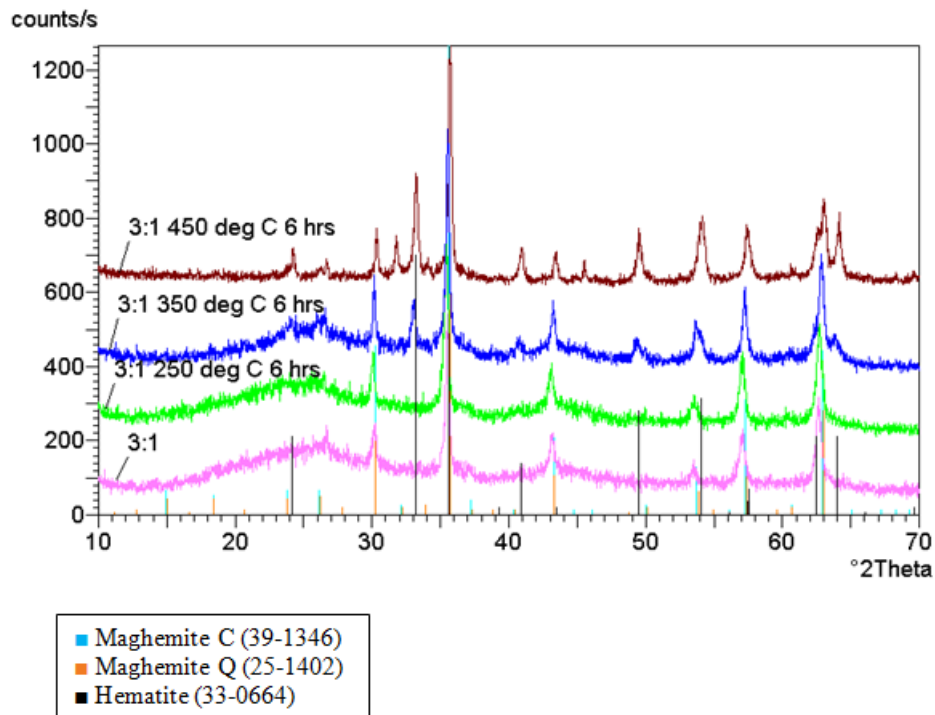
Figure 4-4. Powder XRD patterns of MPAC particles before and after thermal oxidation
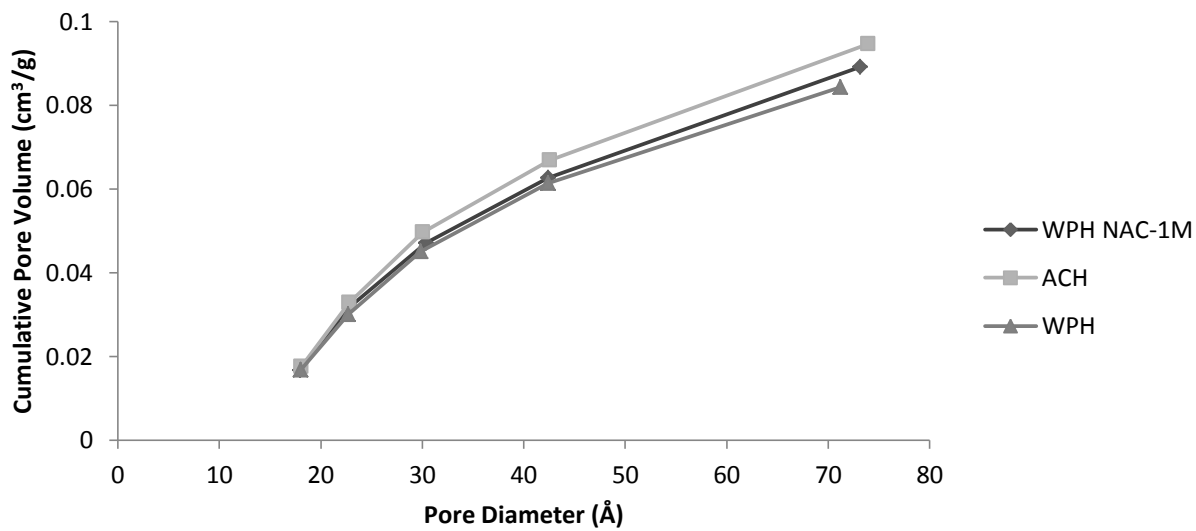
Figure 4-5. BJH pore size distribution of select C(O) modified carbons

CHAPTER 5
TRACE LEVEL AQUEOUS MERCURY REMOVAL USING MODIFIED ACTIVATED CARBON

The following discussion investigates the adsorption of Hg using commercially available activated carbon modified by several approaches. Previous literature has investigated the application of activated carbon to aqueous Hg adsorption [22,72,74,75]. However, the literature has not addressed aqueous Hg removal using a magnetic adsorbent. The literature is scarce regarding aqueous Hg adsorption using an activated carbon with enhanced surface oxygen functionality [36,75,77]. In fact, little is known regarding aqueous adsorption of Hg(0) or the role of surface oxygen groups in its adsorption. The objective of this study was to determine which experimental conditions yielded the highest removal of aqueous Hg.

MPAC Results

Controls

Prior to performing Hg adsorption experiments, it was imperative to perform control runs. To verify that the batch reactor was free from residual Hg contamination, an air blank was performed periodically. This was accomplished by running the test stand with only ultrapure water, in the absence of carbon and mercury. Hg levels were quantified in the mercury-carbon contact chamber and volatilization trap. A sorbent blank, determined via aqua regia and hydrofluoric acid digestion, identified trace levels of Hg in the adsorbent averaging 0.125 µg Hg/g virgin WPH[®]. Bituminous coal is the raw material used in the production of WPH[®] activated carbon; coal is known to contain trace levels of Hg. These values were considered in the mass balance calculations. A background analysis was performed by running Hg-spiked ultrapure water through the batch reactor in the absence of carbon. The analysis revealed the following: low levels

of Hg volatilization occurred in the absence of carbon, quantifiable Hg residues (9%

total Hg) formed in test stand labware necessitating an HNO_3 rinse to fully quantify the

residual Hg, and an average 6% Hg was fugitive (Figure 5-1). The fugitive Hg was likely

due to mass and volume measurement errors amplified by the small scale of the

experiment.

Pseudo Equilibrium Adsorption

The amount of adsorption was calculated based on the difference before and after

adsorption according to the following equation:

$$q_e = \frac{C_0 - C_e}{m} \times V$$ (5-1)

where q_e is the equilibrium adsorption capacity of Hg(II) (mg/g), C_0 is the initial

concentration of Hg(II) (mg/L), V is the volume of the Hg(II) solution (mL), and m is the

adsorbent dosage (mg).

Contact time

A 1 g/L dose of 3:1 MPAC was applied to 100 µg/L Hg solution to study the effect

of contact time on the adsorption of Hg(II) shown in Figure 5-2. The initial adsorption

rate was rapid with over 90% of the Hg(II) removed during the first minute of contact.

This was followed by a much slower adsorption rate, reaching pseudo-equilibrium at

120 min. Before carbon addition, the aqueous solution pH averaged 4.7 with a

percentage change in the pH of 6.5% in the first 30 seconds of contact. Beyond the first

30 s, the pH stabilized to an average of 6.2.

Batch testing of synthetic waters

Effect of iron loading. Because of its influence on the adsorbent surface

characteristics, it was possible for iron loading to impact the removal of Hg from 100

μg/L aqueous solution (Figure 5-3). 1:1 and 2:1 C:Fe performed similarly, with a CV of 2.78%. The 3:1 C:Fe exhibited the best Hg removal. As the iron loading influenced porosity (Table 4-1), the effect of surface area changes due to both Fe loading and thermal oxidation is discussed below.

Effect of thermal oxidation. Figure 5-4 demonstrates that the thermal oxidation temperatures investigated in this study minimally influenced the aqueous mercury removal capabilities of MPAC despite the pore damage incurred at oxidation temperatures over 250°C. For each C:Fe, the CV between the raw samples and oxidized samples only varied between 0% and 4.5%. At all oxidation temperatures, the 3:1 MPAC achieved the highest mercury removal. The 1:1 and 2:1 C:Fe performed similarly for Hg removal, with CV values under 2.8% at each temperature.

Effect of surface area. This work does not show a strong correlation between surface area alone and mercury removal. The experimental data best fit a three variable model with an adjusted R^2 of 0.464, identifying surface area, pore volume, and point of zero charge as the variables influencing Hg(II) adsorption in the system. An ANOVA test identified the sums of squares for the surface area, pore volume, and pH_{pzc} of 113.1, 2.1, and 341.1, respectively. The pH_{pzc} is the primary variable influencing results. As the R^2 is not close to 1, there are likely other variables influencing the efficiency of Hg(II) removal; Hg adsorption can be influenced by other sorbent characteristics such as surface oxygen functionality [35,76].

Mercury mass balance. The average Hg mass balance closure for experiments was 99.5% with a standard deviation of 8.8%. The mass balance closures ranged from 88.3% to 116.8% but many runs did not fall within the 95% confidence intervals; the

observed distribution fits a random distribution curve (Figure 5-5). The challenge in obtaining mass balance closure was likely due to HF extraction inefficiency in quantifying the adsorbed Hg, mechanical loss of C resulting in lower Hg masses extracted in the HF digestion, and volumetric measurement errors amplified due to the small scale of the experiment.

The mass balance for Hg adsorption onto 3:1 C:Fe MPAC is presented in Figure 5-6. At unadjusted pH, approximately 95% of the Hg was removed from aqueous solution with 2% volatilized and 87% adsorbed while 6% remained fugitive.

Optimization. Box Behnken fractional factorial design was used to identify the optimal MPAC for both Hg removal and MPAC recovery (equally weighted in the experimental design) according to the following variables: C:Fe and thermal oxidation temperature and time. The following criteria were used in the numerical optimization: C:Fe within range, minimized oxidation temperature and time, maximized magnetic recovery, and maximized Hg removal. Oxidation parameters were minimized to reduce the cost of MPAC synthesis. Based on these criteria, the optimal synthesis variables of 3:1 C:Fe with no thermal oxidation would achieve a predicted sorbent recovery of 92.5% (±8.3%) and Hg removal of 96.3% (±9%).

Adsorption Isotherms

The effect of the dose of MPAC on Hg(II) adsorption was investigated by varying the MPAC dose from 0.5 to 10 g/L (Figure 5-7). The Langmuir equation is derived from the assumption of monolayer adsorption on specific homogenous sites, while the Freundlich model represents physical adsorption on heterogeneous surfaces. The good fitting results of both models, seen in Figure 5-7A, implied that both chemisorption and physisorption mechanisms took place in the adsorption system. The term 1/n was

between 0 and 1, indicating heterogeneity of the MPAC and affinity of the adsorbate for the adsorbent, resulting in favorable adsorption of Hg(II) by the 3:1 C:Fe MPAC [124]. The dimensionless Langmuir constant separation factor, R_L, given as $R_L - 1/(1+BC_o)$ where C_o is the initial concentration and b is the Langmuir constant. The R_L indicates favorable adsorption between 0 and 1 while $R_L>1$ indicates unfavorable adsorption, $R_L =1$ is linear, and $R_L = 0$ indicates irreversible adsorption. The value of R_L was found to be 0.002, indicating favorable and nearly irreversible adsorption.

Kinetics Studies

Three kinetic models have been proposed for Hg(II) adsorption by MPAC: 1) intraparticle diffusion [125] 2) pseudo-first order kinetic model [126], and 3) pseudo-second order kinetic model [127]. The intraparticle diffusion model can be described according to the Weber and Morris equation as:

$$q_t = k_{id} t^{1/2} + C \tag{5-2}$$

where k_{id} is the intraparticle diffusion rate constant ($\mu g/g \cdot min^{1/2}$), C is the y-intercept ($\mu g/g$), and q_t is the adsorption capacity of Hg(II) ($\mu g/g$) at time t (min). The plot of q_t vs $t^{1/2}$ is not linear and does not pass through the origin, therefore intraparticle diffusion is not the sole rate-limiting step (Figure 5-8). Multiple rate-limiting steps might take place in this system.

The pseudo-first order rate law was integrated to a linear rate law (Equation 5-3) where k is the equilibrium rate constant (1/min). The pseudo-second order model (Equation 5-4) was expressed where k_2 is the pseudo-second order rate constant of adsorption (g/μg•min). The applicability of these models was assessed by comparing the R^2 values of the linear plot of log($q_e - q_t$) vs. t and (t/q_t) vs. t, respectively (Figure 5-

8). The data fit the pseudo-second order model with an R^2 of 0.9999, indicating that adsorption was due to chemisorption [128]. The p-value for the slope was 7.22 x 10^{-13}.

$$\log (q_e - q_t) = \log q_e - \frac{k_1}{2.303} t \tag{5-3}$$

$$\frac{t}{q_t} = \frac{1}{k_2 q_e^2} + \left(\frac{1}{q_e}\right) t \tag{5-4}$$

Adsorbent Stability: Hg

The mobility of Hg once adsorbed to the 3:1 C:Fe was investigated using the standardized TCLP test. The effluent Hg concentrations remained under the regulated limit of 200 µg/L until reaching an Hg loading ratio of 1000 µg Hg :1 g MPAC, where the effluent concentration was found to be double the allowable limit for sanitary landfill disposal (Figure 5-9).

<div align="center">

C(O) Results

</div>

Controls

As previously described, an air blank was performed to verify that the batch reactor was free from residual Hg contamination. Reagent blanks verified all solutions and ultrapure water were free from trace levels of mercury. A sorbent blank identified trace levels of Hg present in the virgin carbons with WPH® containing 0.125 µg Hg/g and CASPF® containing 0.071 µg Hg/g. Through a procedural blank, this residual Hg was not shown to influence aqueous or volatilized Hg levels.

Due to the volatile nature of Hg(0), it was important to understand the rate of volatilization in the absence of carbon. Figure 5-10 demonstrates that, in the absence of carbon, nearly 50% of the Hg volatilizes after 30 s, with only 1.2 % of the Hg(0) fugitive. Because of this high rate of volatilization, Hg(0) adsorption experiments were performed at a 30 s contact time rather than at pseudo-equilibrium.

The HF/H$_3$BO$_3$ total digestion employed when quantifying adsorbed Hg for the MPAC carbons did not produce replicable results with the C(O) modified carbons. For these experiments, mass balance was determined by assuming Hg that did not either volatilize or remain in aqueous solution was adsorbed.

Batch Testing of Synthetic Waters

Effect of C(O) on Hg adsorption

Due to the multitude of variables that can influence adsorption, the influence of one specific variable requires regression analysis. A t-test with a significance level of α = 0.05 revealed oxygen content as a good regression parameter for Hg(II) adsorption (p-value = 0.00328) but the same does not hold true for Hg(0) adsorption (p-value = 0.28850). This could be due, in part, to water cluster formation. Acidic C(O) groups tend to adsorb water by hydrogen bonding and dispersion forces, followed by clustering of additional water molecules at these adsorption sites [129]. These water clusters can block adsorbate access to the activated carbon porosity [130]. Studies have shown a drop in adsorption capacity of organic pollutants with an increase in the amount of C(O) groups, evidence of the water adsorption effect [131,132]. As Hg(0) is uncharged, it is possible that there are not sufficient attractive forces to overcome the pore blocking effect due to water cluster formation. Although the speciation in the Hg(II) system exists primarily as the uncharged Hg(OH)$_2$, the carbon particles serve as a nucleation point for the precipitation of solid Hg(OH)$_2$ which may be able to overcome the pore blocking of the water clusters.

As seen in Figure 5-11, the virgin WPH$^®$ carbon performed fairly well for Hg(II) removal, but when applied to Hg(0) adsorption resulted in relatively high levels of volatilization. SAC and SHAC carbons achieved high levels of Hg(0) adsorption with

minimal losses through volatilization. The annealed carbon, with the lowest oxygen content, displayed the lowest Hg (0) and Hg(II) removal.

Effect of porosity on Hg adsorption

Hg(II). A t-test revealed that surface area alone was poorly correlated to Hg(II) removal, with an R^2 value of 0.004. An ANOVA test on the influence of surface area, pore size, and pore volume on Hg(II) removal revealed that pore volume had significantly more influence than surface area and pore size, with a sums of squares value of 569.75 compared to 5.31 and 97.47, respectively.

The two-variable model that best fits the Hg(II) removal data indicates oxygen content and pH_{pzc} as important variables, resulting in an R^2 value of 0.499. An ANOVA test indicated oxygen content to be the primary variable influencing adsorption with sums of squares of 666.82 while the pHpzc sums of squares was only 62.06.

Hg(0). Surface area also poorly correlated to Hg(0) removal, with an R^2 value of 0.093. A t-test analysis of the influence of surface area, pore size, and pore volume on Hg(0) removal resulted in a negative adjusted R^2, making an ANOVA test impractical.

The best regression model to fit the Hg(0) data indicates that surface area, pore volume, surface oxygen functionality, and the point of zero charge as important variables, resulting in an R^2 value of 0.5886. The t-test identified the pHpzc as a good regression parameter (>95% confidence). An ANOVA test indicated the point of zero charge as the primary variable influencing adsorption with sums of squares of 1041.72. As no model using the measured variables achieved a strong R^2 value, it is possible that an unquantified variable was influencing the results of both Hg(II) and Hg(0) adsorption.

Adsorption Isotherms

The effect of the dose of C(O) modified carbons on Hg(II) adsorption was investigated by varying the carbon dose (Figure 5-12). The good fitting of the experimental data to both models, seen in Figure 5-12A, implied that both chemisorption and physisorption mechanisms were occurring in the adsorption system. The Freundlich term 1/n was 0.86, indicating heterogeneity of the carbon surface and affinity of the adsorbate for the adsorbent, resulting in favorable adsorption of Hg(II) by NAC-1M. The value of R_L was found to be ≈ 0, indicating irreversible adsorption.

Kinetic Studies

As with MPAC, three kinetic models were investigated for Hg(II) adsorption by NAC-1M (Figure 5-13). The plot of q_t vs $t^{1/2}$ is fairly linear for ACH, NAC-1M, SAC-1M, and SHAC-1M, with R^2 values of 0.7596, 0.7892, 0.8938, and 0.8322, respectively. The linearity of the experimental data for NAC-1M, SAC-1M, and SHAC-1M indicated that intraparticle diffusion may be a rate limiting step in these systems. The ACH carbon demonstrated immediate uptake of Hg(II) at a much higher capacity than the other carbons, likely due to the absence of surface oxygen groups and therefore an absence of water clusters on the adsorbent surface. Interestingly, the adsorption capacity decreased as time progressed. This may be due to competitive adsorption between Hg(II) and H_2O for the available adsorption sites on the carbon surface where equilibrium with water proceeds slower, thus the decrease in adsorption capacity as equilibrium is approached.

The applicability of the pseudo-first order and pseudo-second order models was assessed by comparing the R^2 values of the linear plots. Due to the negative slope of ACH, it could not be assessed for pseudo-first order kinetics. NAC-1M, SAC-1M, and

SHAC-1M all fit the pseudo-first order model with R^2 values of 0.9188, 0.9822, and 0.8975, respectively. Even so, the data showed a stronger fit with the pseudo-second order kinetic model, with R^2 values higher than 0.99, indicating that chemisorption played a large role in Hg(II) removal. The p-values for the slopes were very low, ranging from 1.2×10^{-5} to 6.7×10^{-7}.

Adsorbent Stability

The mobility of Hg(II) once adsorbed to the surface modified carbons was investigated using the standardized TCLP test (Table 5-1). After loading the carbons with 100 µg Hg/ g C, the effluent remained under the regulated limit of 200 µg/L for all carbons tested.

Table 5-1. Hg leaching from various carbons under landfill conditions

Sample	Effluent (µg Hg)	Hg leaching (µg Hg/ g C)
ACH	8.4	16.7
WPH	6.9	13.8
CASPF	31.2	62.2
NAC-10M	36.1	72.2
SAC-10M	54.1	107.8
SHAC-10M	11.4	22.7
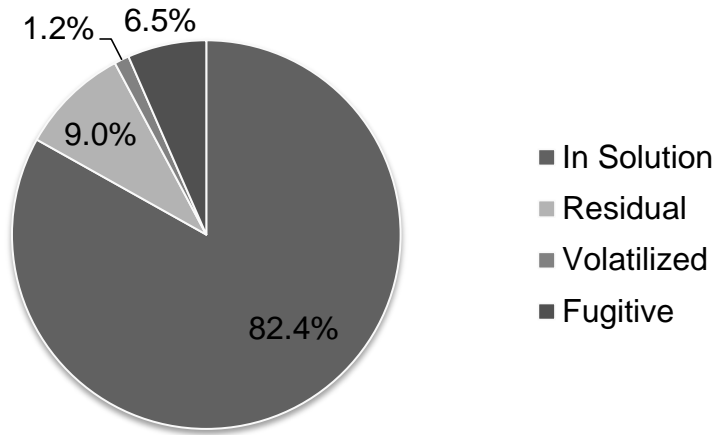
Figure 5-1. Background Hg(II) mass balance
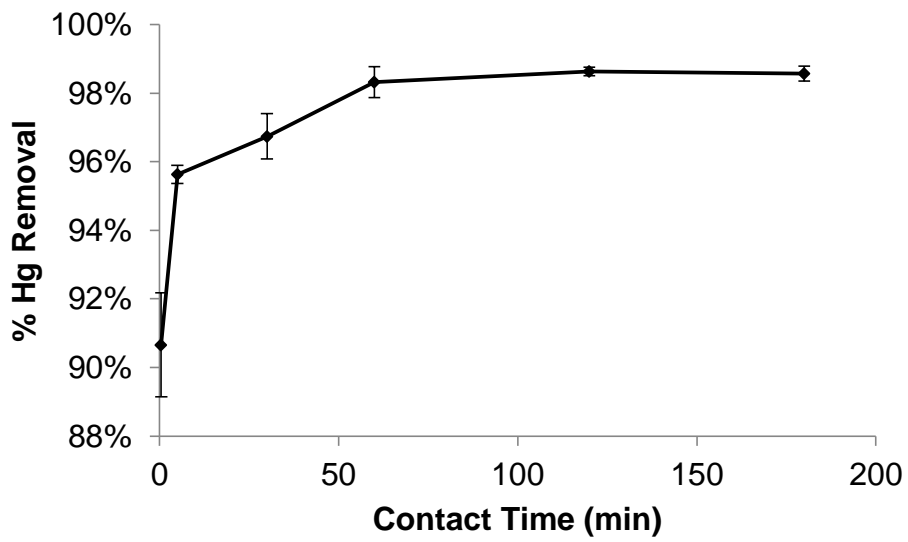
Figure 5-2. Effect of contact time on Hg(II) adsorption (3:1 C:Fe, 1g/L)
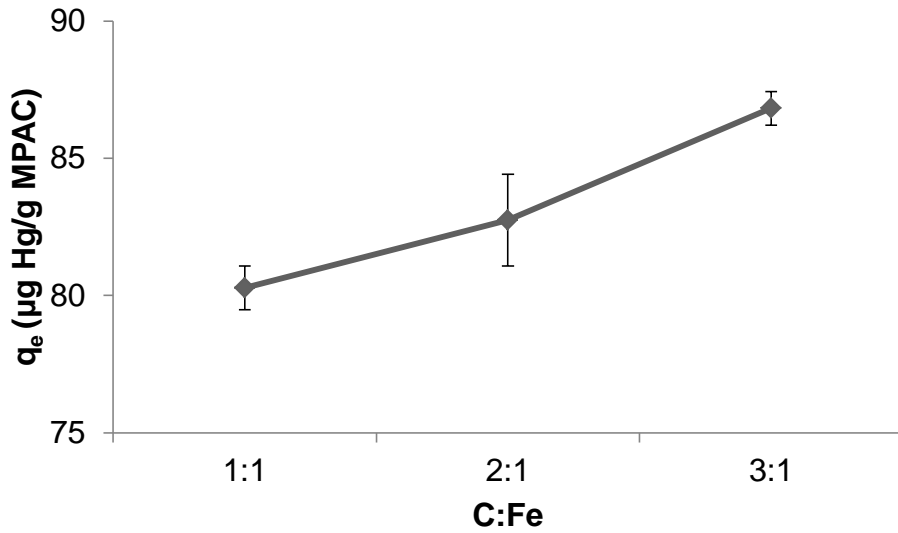
Figure 5-3. Effect of iron loading on pseudo-equilibrium adsorption of 100μg/L Hg(II)
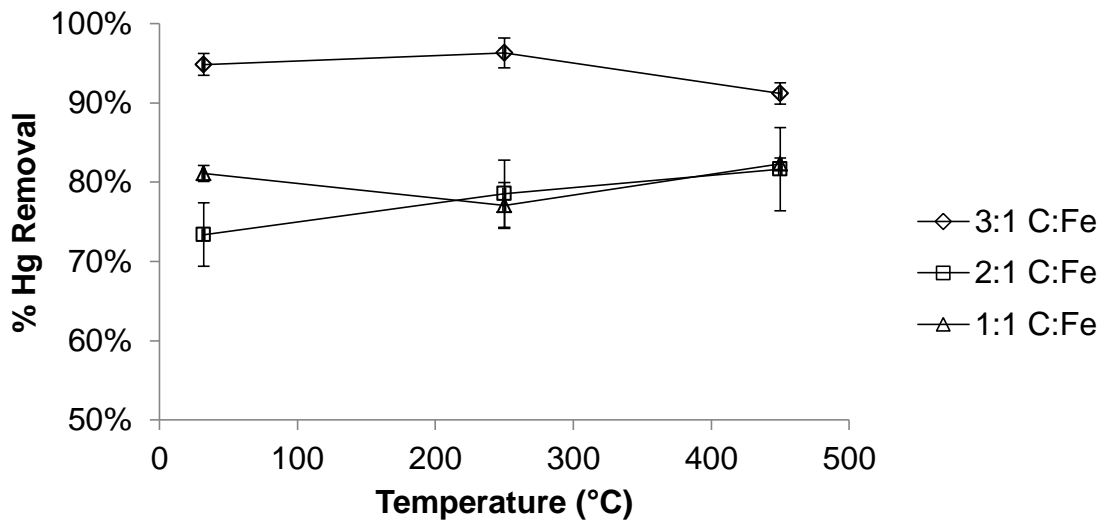
Figure 5-4. Influence of 3h oxidation at 250°C and 450°C on aqueous Hg(II) removal
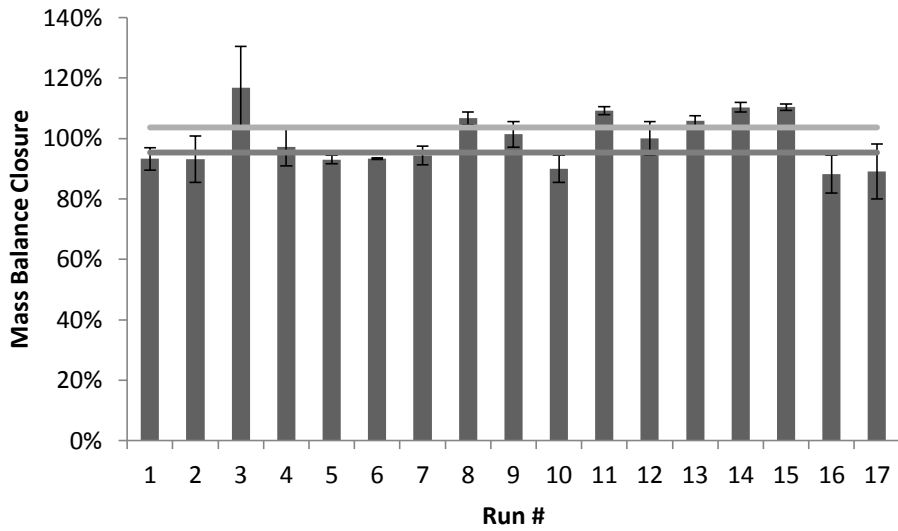
Figure 5-5. Mass balance distribution
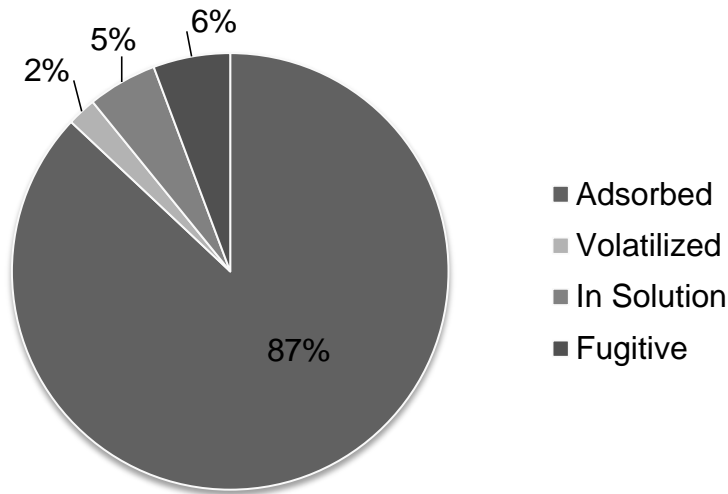
Figure 5-6. Hg mass balance for 3:1 C:Fe adsorbent
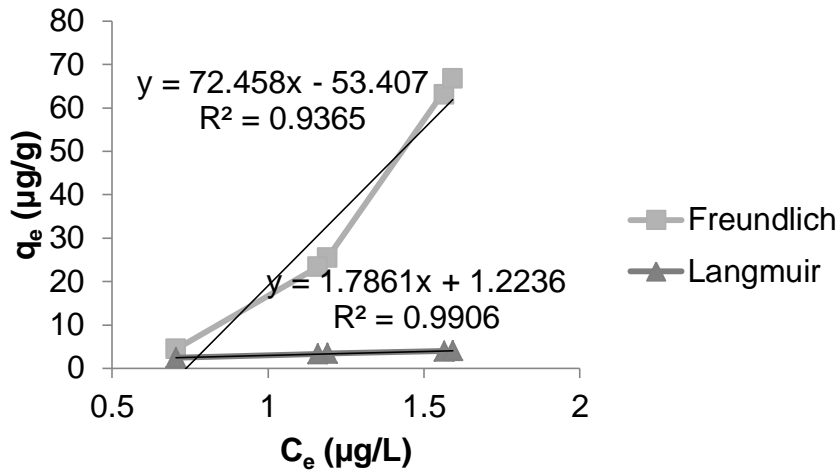
A.
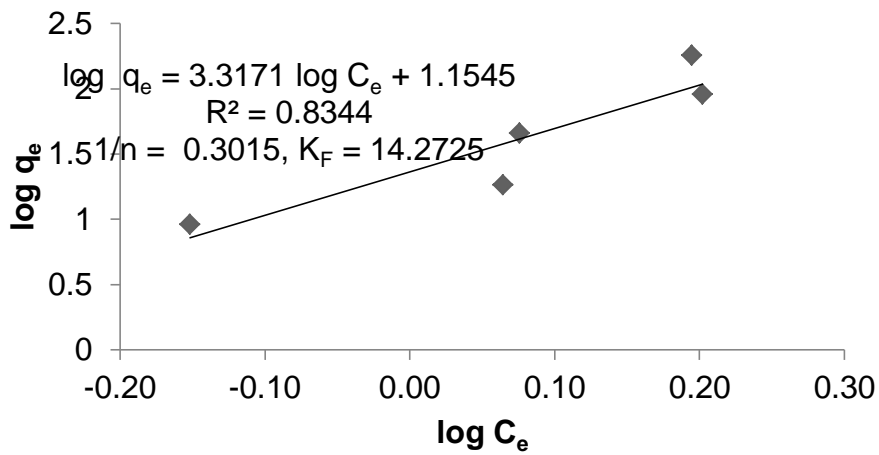
B.
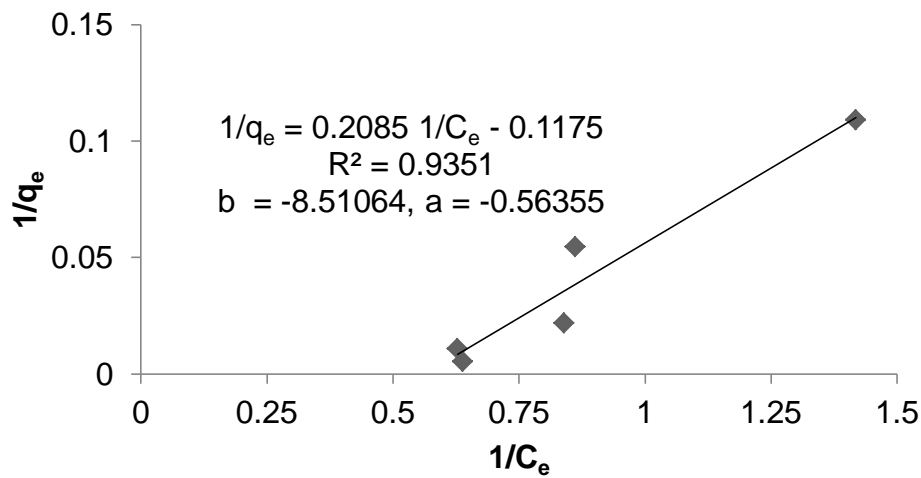
C.

Figure 5-7.   Hg(II) adsorption isotherm onto 3:1 MPAC. A) Nonlinearized adsorption
isotherm B) Freundlich model, and C) Langmuir model
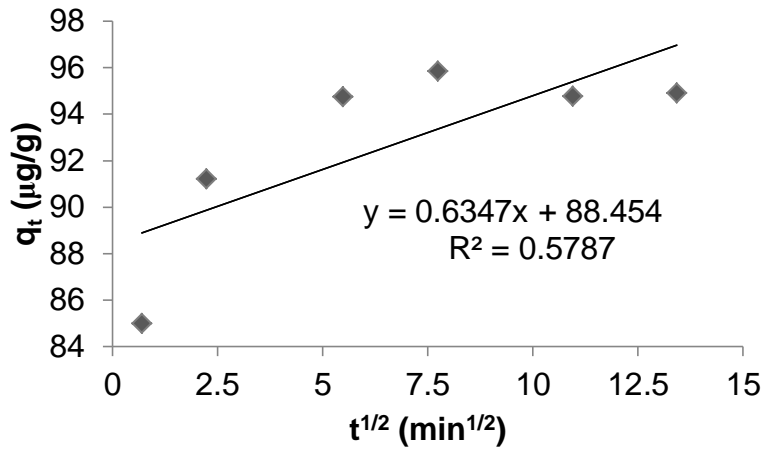
A.
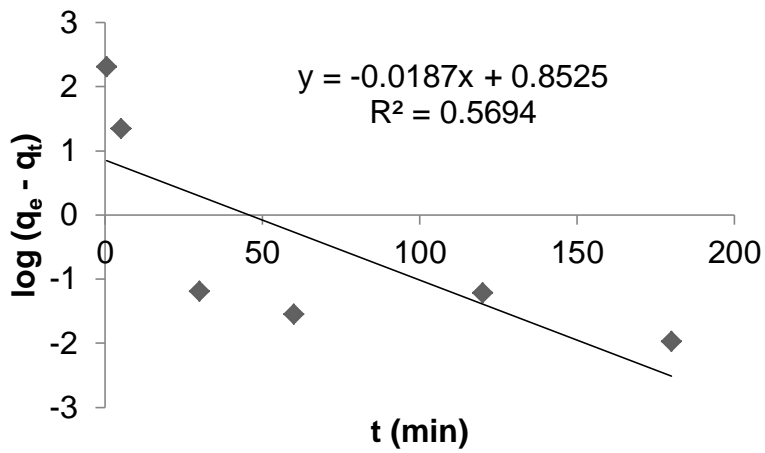
B.
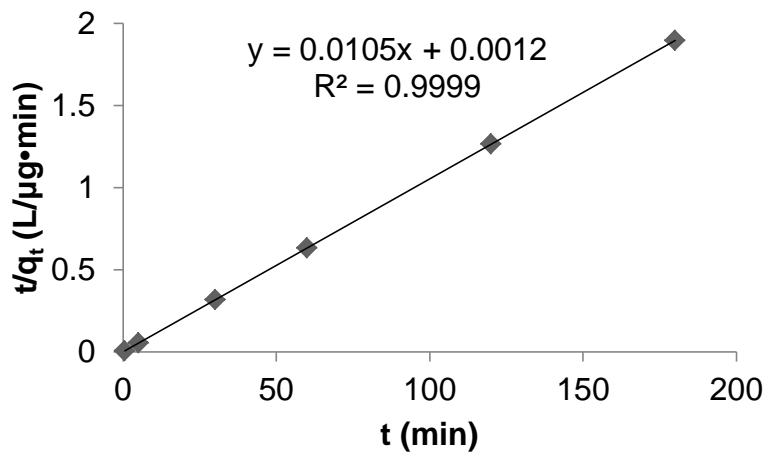
C.

Figure 5-8. Kinetic models for the adsorption of Hg(II) onto 3:1 MPAC. A) Intraparticle diffusion model, B) Pseudo-first order model, and C) Pseudo-second order model
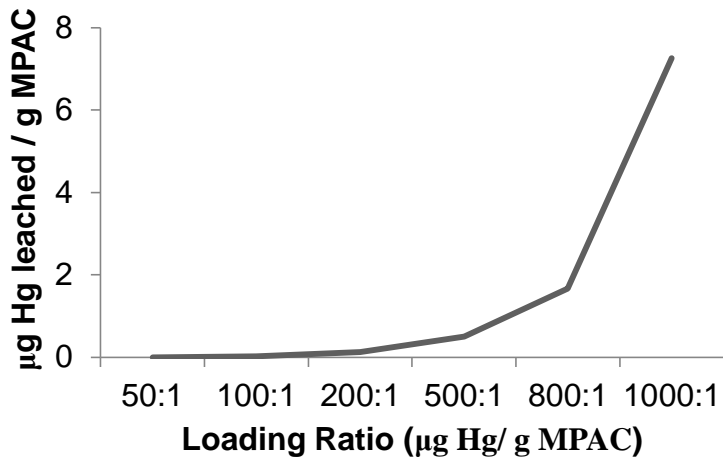
Figure 5-9. Hg leaching from 3:1 C:Fe at various loading rates under landfill conditions
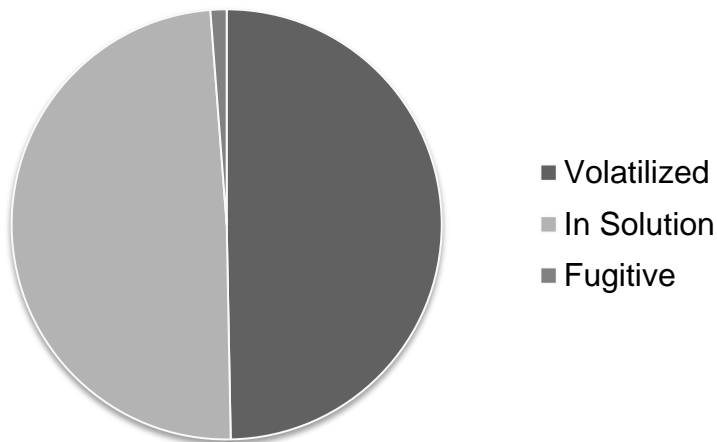
Figure 5-10. Background Hg(0) mass balance for a 30 s contact time
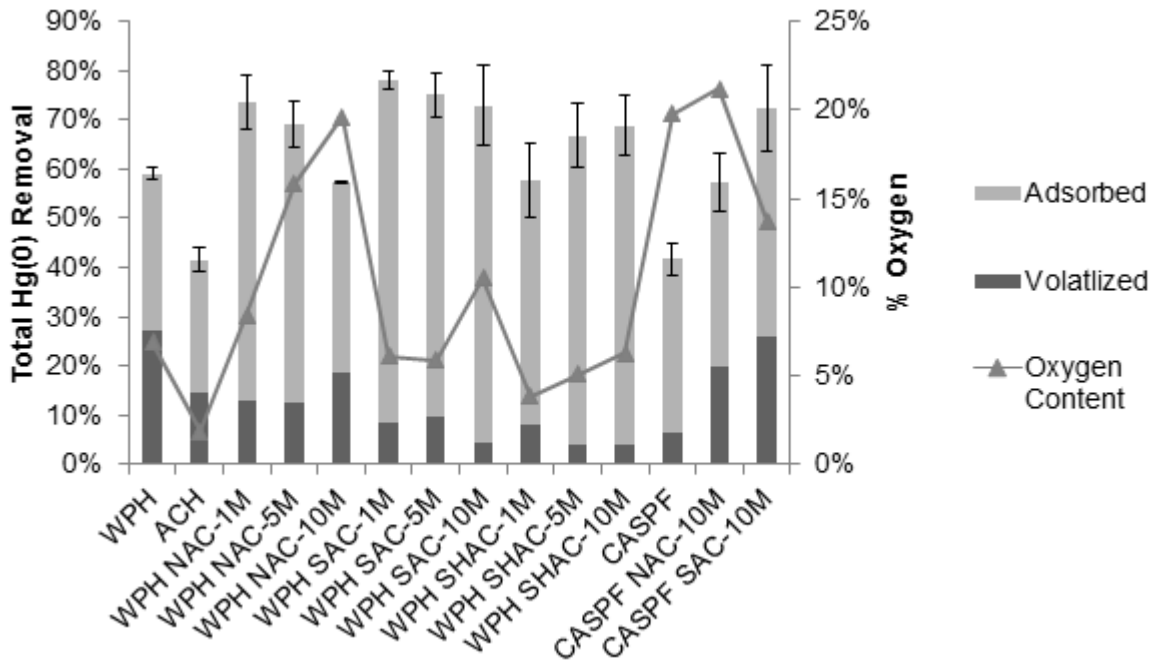
A.
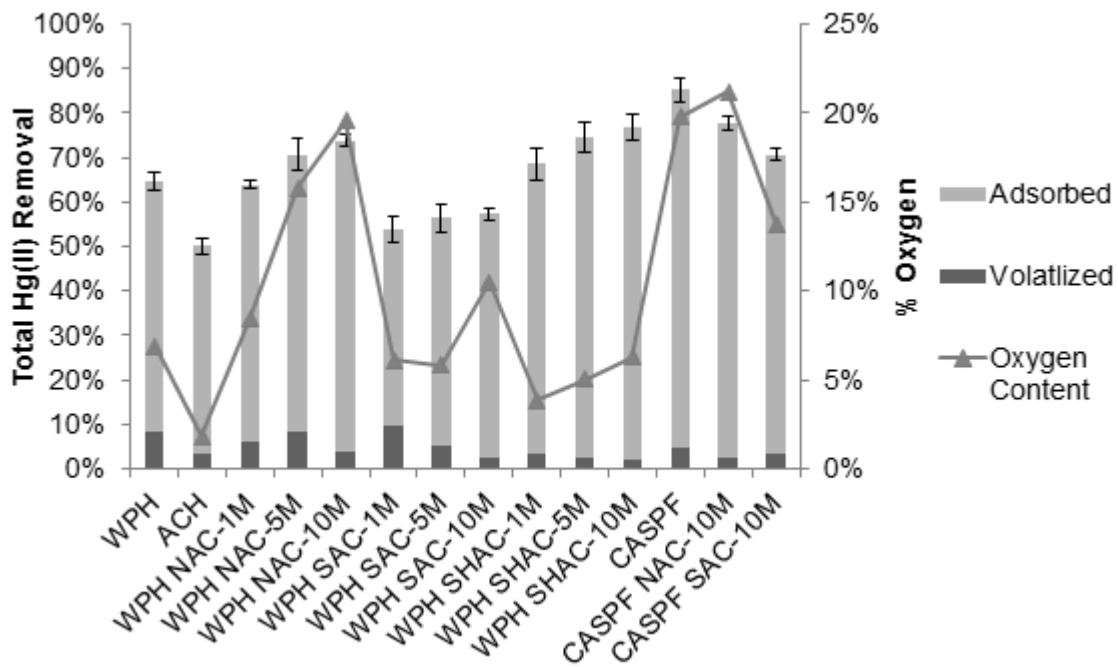
B.

Figure 5-11. Hg removal through adsorption and volatilization for various surface-modified carbons. A) Hg(II) B) Hg(0)
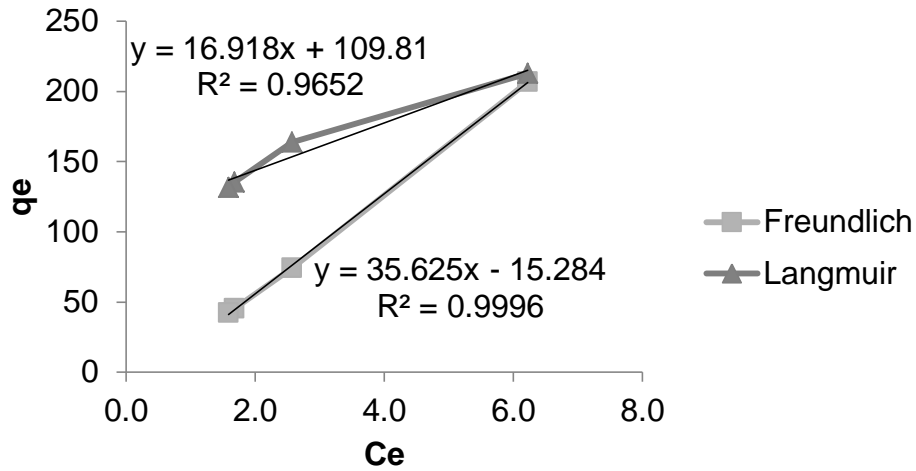
A.
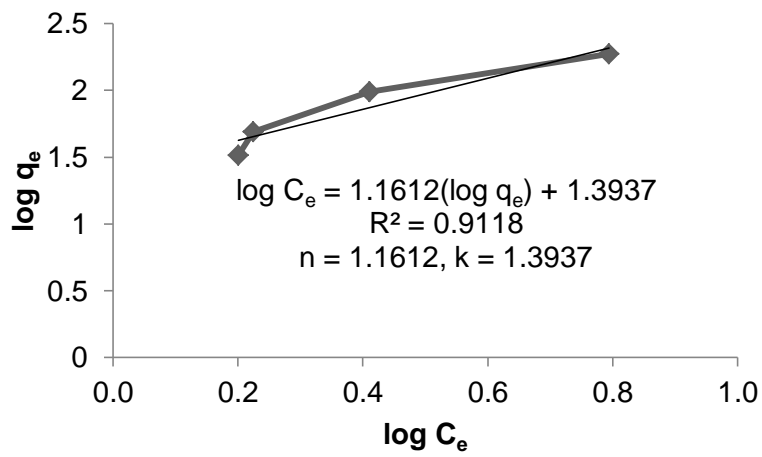
B.
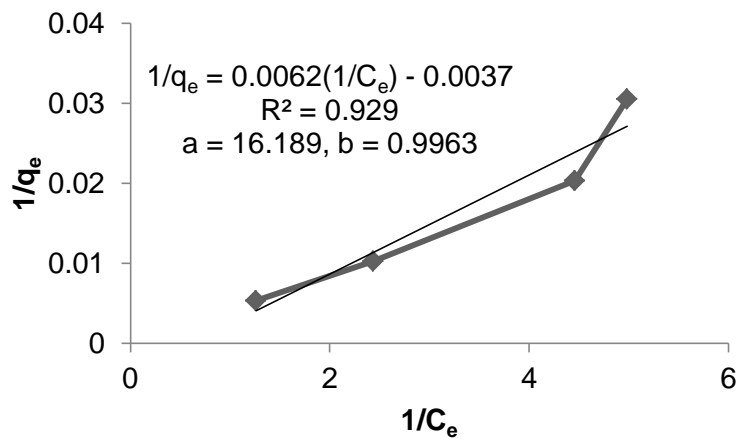
C.

Figure 5-12. Hg(II) adsorption isotherm onto NAC-1M. A) Nonlinearized adsorption isotherm B) Freundlich model, and C) Langmuir model
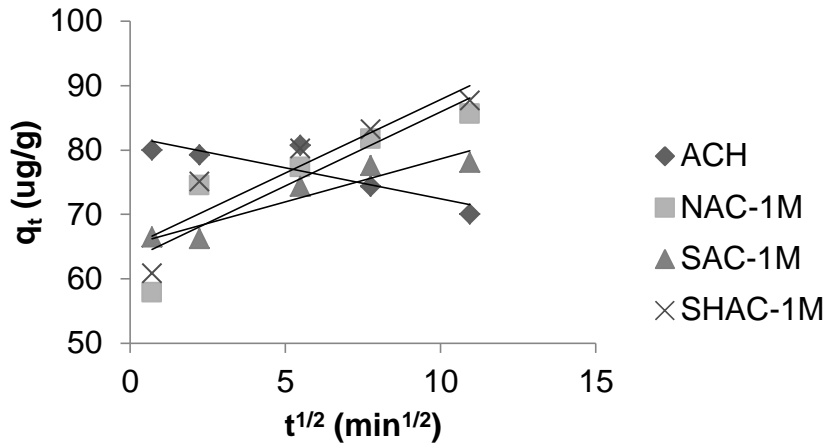
A.
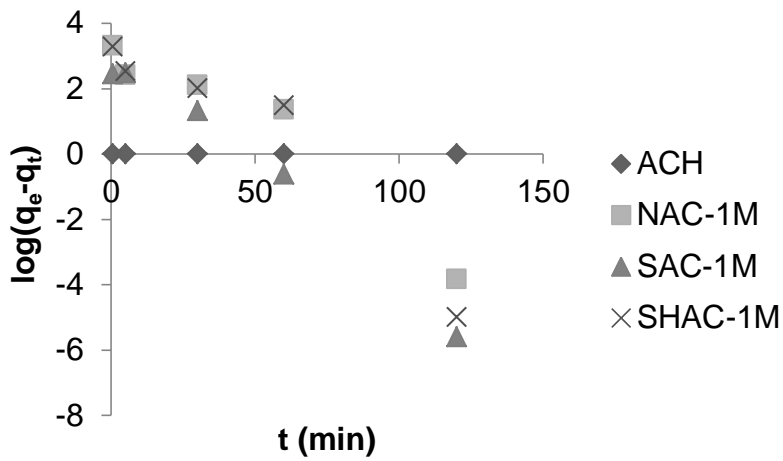
B.
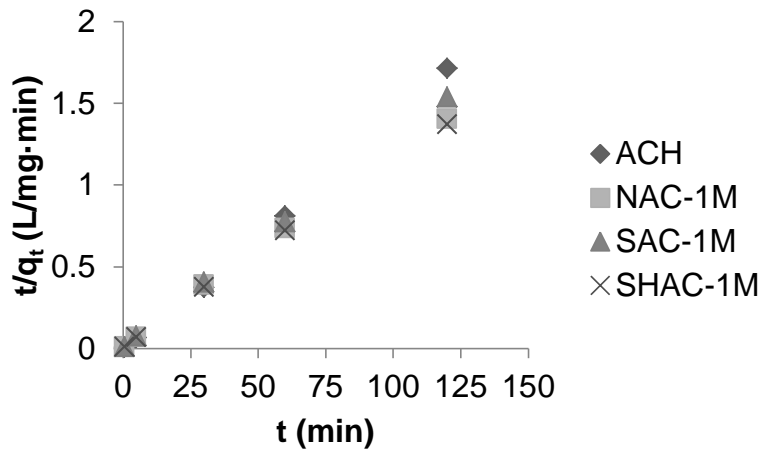
C.

Figure 5-13. Kinetic models for the adsorption of Hg(II) onto C(O)-modified carbons. A) Intraparticle diffusion model, B) pseudo-first order model, and C) pseudo-second order model

CHAPTER 6
ADSORPTION MECHANISMS

One objective of this study was to determine the influence of Hg speciation on adsorption mechanisms. The Hg speciation in each system was determined using Visual MINTEQ. The binding mechanisms were predicted based on this speciation. A sequential chemical extraction was designed with the goal of verifying these binding mechanisms. Prior to applying the SCE to the MPAC and C(O)-modified carbon systems, its performance was evaluated by forcing Hg to known speciation through manipulation of pH and pCl and quantifying Hg desorbed in each phase.

Proposed Adsorption Mechanisms

Mechanisms of Hg(II) Adsorption

The unadjusted matrix pH ranged between 4.4 and 4.7. Using the speciation program Visual MINTEQ 2.61, the mercury speciation in the given matrix conditions was predicted to be 96.5-99% $Hg(OH)_2$ and 1-3.5% $HgOH^+$.

MPAC. Upon addition of 3:1 C:Fe MPAC, the pH of the aqueous solution reached an equilibrium value of 6.2. Under these conditions, the Hg speciation was nearly 100% $Hg(OH)_2$ which was likely removed from aqueous solution by preferential precipitation onto the MPAC surface once maximum solubility was reached.

C(O)-modified carbons. The pH of the aqueous solution varied between 3.41 and 5.45, depending on the modification of the carbon (Table 6-1). The more basic systems contained Hg primarily as $Hg(OH)_2$ while the more acidic systems contained Hg in various states of hydrolysis, including Hg^{2+}, $HgOH^+$, and $Hg(OH)_2$. $Hg(OH)_2$ was likely removed due to preferential precipitation onto the carbon surface. For the systems with a contact pH below the pzc, the carbon surface was positively charged and

electrostatically repelled the Hg cations. The systems with a contact pH above the pzc, such as NAC 10M, SAC carbons, and CASPF® modified carbons, the carbon surface was negatively charged and thus Hg cations were electrostatically attracted to the surface.

Mechanisms of Hg(0) Adsorption

Aqueous Hg(0) can undergo physisorption. The matrix pH and pCl do not influence its adsorption. Gas phase research proposed Hg(0) oxidation by carbonyl-containing C(O) groups and subsequent adsorption via known Hg(II) adsorption mechanisms, while phenolic groups have been shown to decrease Hg(0) adsorption [72,73]. The lack of correlation of Hg adsorption with C(O) does not support this occurrence in the aqueous phase. Ideally, individual surface oxygen groups would be quantified in order to determine their specific relationship, if any, to adsorption. A chemical sequential extraction may provide more insight into the speciation of the elemental Hg, once adsorbed.

Influence of pH and pCl on Hg(II) adsorption

The adsorption of Hg by 3:1 MPAC was investigated at various pH and pCl values. Previously published literature reported a decrease in Hg adsorption onto activated carbon with an increase in chloride concentration [133]. This study supports those findings. As the pH increased from pH 2 to pH 10, Hg adsorption decreased for the three pCl values investigated (Figure 6-1). The system with the highest chloride concentration showed the most significant decrease in adsorption with increasing pH. The average mass balance closure of these runs was 95% $\pm$ 5%. With an adjusted R^2 of 0.557, a two variable model indicated both pH and pCl are good regression parameters with p-values of 0.0254 and 0.0096, respectively. An ANOVA test showed pH and pCl

have similar influence on the Hg(II) adsorption, with sum of squares of 34.2 and 50.8, respectively.

The influence of pH and pCl on Hg volatilization from the Hg(II) system is presented in Figure 6-2. At pH 2, little volatilization occurred at any chloride concentration. Regression analysis revealed that pH and pCl do not significantly influence Hg(0) volatilization, with an adjusted R^2 of -0.02.

Sequential Chemical Extraction

Protocol Verification

In order to ensure the extractant selections were sufficiently specific and efficient to predict speciation, the pH and pCl was adjusted to control speciation (Table 6-2). If properly designed, the distribution of Hg among the extraction fractions can be predicted.

Free Hg(II), although predicted to desorb in the ammonium nitrate fraction due to ion exchange, primarily desorbed in the acetic acid, DMSA, and HF residual fractions, indicating ion exchange was not the only primary binding mechanism (Table 6-3). Potential causes include: phase transformation that altered the adsorption mechanisms, the ammonium nitrate extractant was inefficient at targeting ion exchange, or if the Hg was not present as the predicted species. Surprisingly, a large amount of the Hg remained in solution, unadsorbed.

As predicted, the largest portion of uncharged $Hg(OH)_2$ desorbed in the acetic acid fraction, indicating surface precipitation. Although minimal, detectable levels were found in other extraction fractions, demonstrating phase transformation or non-ideal extractant performance due to a lack of specificity or poor extraction efficiency. Of note, a large

amount of Hg volatilized from this system, indicating an Hg(II) reduction mechanism that was not expected at the pH and pCl of the system.

HgCl$_2$ was expected to desorb in the surface bound fraction and to volatilize from solution as Hg(0). Although Hg desorbed in the expected fraction, a significant portion also desorbed in the acetic acid fraction. It is possible that HgCl$_2$ was reduced to Hg(0) and the highly insoluble Hg$_2$Cl$_2$, preferentially precipitating on the carbon surface [81].

Hg-Cl anions were expected to desorb primarily in the surface bound phase. With the adsorbent pH$_{pzc}$ of 9.3, the sorbent was positively charged, and should have resulted in an electrostatic attraction between the negatively charged Hg and the positively charged surface, enhancing adsorption. This was not realized as approximately 14% of the Hg remained in solution at equilibrium. While a large portion of the Hg desorbed in the DMSA extraction fraction, significant desorption also occurred in the acetic acid fraction. A very small percentage of the Hg was predicted to be present as HgCl$_2$ so reduction to Hg$_2$Cl$_2$ was not expected to largely influence the results. The low rate of volatilization, 1%, further indicates that this reduction does not account for the Hg association with the surface bound fraction.

Application

Although the results were interesting, it was clear that the SCE described could not accurately predict the speciation of Hg that was adsorbed from aqueous solution. It was beyond the scope of this study to pursue a stronger extraction scheme.

Table 6-1. Variation of 30 s Hg(II)-DI contact pH with pH_{pzc} of C(O) modified carbons

Sample	pH_{pzc}	Hg-DI contact pH
CASPF	1.93	3.41
WPH	8.36	5.16
ACH	10.10	5.45
NAC 1M	6.56	4.84
NAC 5M	5.02	4.82
NAC 10M	3.99	4.73
SAC 1M	3.78	4.91
SAC 5M	3.90	4.97
SAC-10M	3.36	4.90
SHAC 1M	7.37	5.23
SHAC 5M	7.25	5.35
CASPF SAC10M	2.83	4.51
CASPF NAC10M	2.77	4.25

Table 6-2. Predicted Hg speciation and SCE extraction fraction for given pH and pCl values

		Hg Speciation								
pH	pCl	Hg^{2+}	$HgOH^+$	$Hg(OH)_2$	$HgCl^+$	$HgCl_2$	$HgCl_3^-$	$HgCl_4^{2-}$	Description	Proposed extractants
1	12	100%							Free Hg	2, 5
6	12			100%					Precipitated	3
3	4				1%	99%			Uncharged Hg-Cl	4
8	0					6	27%	67%	Hg-Cl anions	?

Table 6-3. Hg distribution in SCE extraction fractions

Hg Speciation	Water	Ammonium nitrate	Acetic acid	DMSA	DCB	HF	Volatilized	In solution	Fugitive
Free Hg^{2+}	5.1%	3.1%	17.0%	27.4%	1.4%	15.2%	2.8%	17.7%	10.3%
$Hg(OH)_2$	2.5%	7.0%	25.9%	8.4%	0.4%	16.7%	20.8%	3.2%	15.1%
$HgCl_2$	2.1%	6.7%	23.9%	30.6%	0.9%	21.6%	7.5%	6.6%	0.1%
$HgCl_3^-$, $HgCl_4^{2-}$	1.1%	3.9%	21.0%	36.7%	2.5%	18.9%	1.0%	13.8%	1.1%
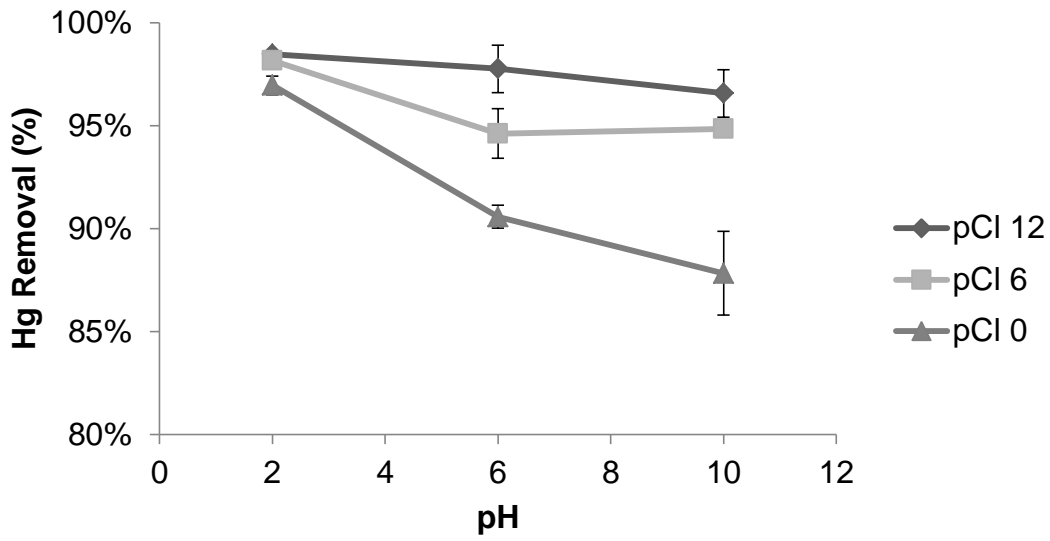
Figure 6-1. Influence of pH on aqueous Hg(II) adsorption
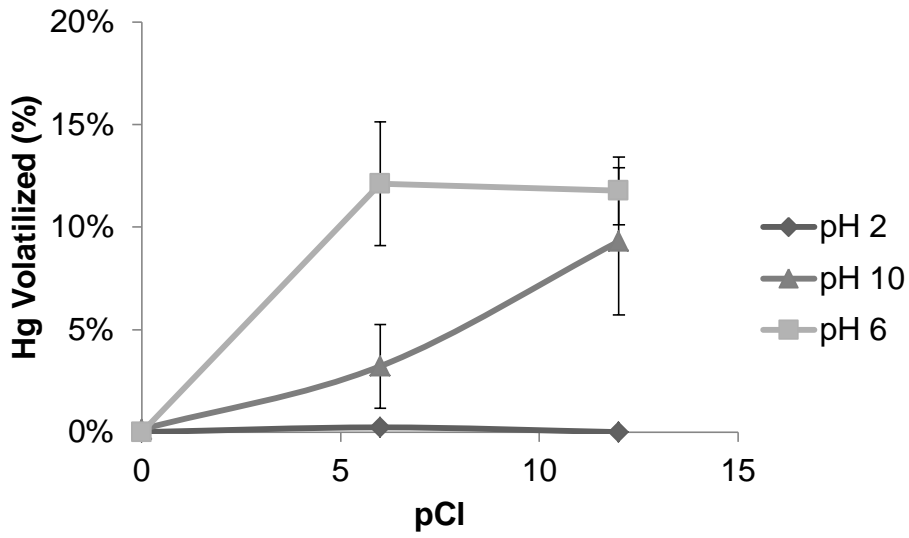
Figure 6-2. Influence of pCl on Hg(II) volatilization

CHAPTER 7
CONCLUSIONS AND RECOMMENDATIONS
Magnetic Powdered Activated Carbon

The magnetic powdered activated carbon, synthesized by iron impregnation and thermal oxidation, was optimized for mercury removal. The 3:1 C:Fe MPAC reached the goal of 95% sorbent recovery, with only a 25% decrease from the virgin carbon surface area. The presence of maghemite and amorphous iron oxides was confirmed on the 3:1 C:Fe MPAC. Thermal oxidation succeeded in decreasing the amorphous characteristic of the MPACs but did not provide a significant increase in magnetic recovery or Hg-removal performance. The potential benefits of thermal oxidation are not realized and are outweighed by the damaged porosity and increased cost in production. When exposed to an acidic matrix pH, the 3:1 MPAC leached low concentrations of Fe. Iron is not a concern from a regulatory standpoint and this leaching did not cause coloration of the water nor did it influence the sorbent recoverability.

In addition to ideal magnetic recovery, the 3:1 C:Fe MPAC outperformed other MPACs for Hg(II) removal. The 3:1 MPAC exhibited the highest adsorption capacity. At a pseudo-equilibrium contact time of 120 min with a 100 µg/L Hg solution at unadjusted pH, the 3:1 MPAC performed optimally, achieving 91% Hg removal with 2% volatilized, 84% adsorbed, while 4% remained fugitive. The average Hg mass balance closure for all 17 runs was 99.5% with a standard deviation of 8.8%, verifying the MPAC Hg removal performance. Surface area appears to influence adsorption in this system but, with a correlation of only 0.47, another factor is also influencing the system. The adsorption data fits both the Freundlich and Langmuir models, indicating that Hg adsorption proceeds both as chemisorption and physisorption. As the data strongly fits

the pseudo-second order model, chemisorption is clearly involved in this system. Once

adsorbed, the Hg is strongly bound to the MPAC surface. Hg leaching does not

necessitate special residuals handling until a loading of greater than 800 µg Hg/ g

MPAC.

Matrix pH and pCl are known to influence Hg speciation. Both pH and pCl were

shown to influence Hg adsorption onto 3:1 C:Fe MPAC. This influence was used

investigate the use of a sequential chemical extraction to predict Hg speciation and

binding mechanisms. The results clearly showed that the SCE described could not

accurately predict the speciation of Hg that was adsorbed from aqueous solution.

Surface Oxygen Modified Carbon

Commercially available activated carbons underwent wet chemical oxidation with

HNO_3, H_2SO_4, and NaOH, increasing surface oxygen functionality with the goal of

increased Hg(II) and Hg(0) adsorption. Nitric acid modification produced the most

surface oxygen groups but resulted in slight damage to porosity. Sulfuric acid and

sodium hydroxide modification did not damage porosity but were less effective than

nitric acid at increasing the surface oxygen functionality.

The model that best fit Hg(II) adsorption identified oxygen content and pH_{pzc} as

important variables, with oxygen content being the primary variable influencing the

results. Hg(0) adsorption data best fit a four variable model, indicating that surface area,

pore volume, surface oxygen functionality, and the pH_{pzc} as good regression

parameters, with the pH_{pzc} as the primary variable influencing the results. Neither model

achieved a strong R^2 value. It is possible that an unquantified variable influenced these

results. Due to the uncharged nature of Hg(0), it is possible that water cluster formation,

due to C(O) groups, limited adsorption. A minimum of surface oxygen groups are

required for the surface to be sufficiently hydrophilic, allowing the surface to be wetted by water and thus useful for water treatment applications. Therefore, a moderate amount of surface oxygen groups are optimal for Hg(0) adsorption from aqueous solution.

As no carbons violated TCLP effluent limits, it can be inferred that the Hg is strongly bound to the surface. Hg(II) adsorption onto the C(O) modified carbons fit both the Freundlich and Langmuir models, indicating that both physisorption and chemisorption occur. The data fit both pseudo-first order and pseudo-second order models very well, also supporting the occurrence of both physisorption and chemisorption.

In summary, it is possible to tailor activated carbon to allow for magnetic recapture. It also possible to enhance aqueous Hg(II) capture through surface oxygen modification, although Hg(0) adsorption is not influenced by these surface groups. Both carbons produced are stable and, under the experimental loading conditions applied, do not require special handling or disposal as a hazardous waste. The most effective aqueous Hg treatment method will depend on water chemistry, sorbent surface chemistry, and Hg speciation.

Contributions to Science

- Demonstrated that magnetic recovery is possible with low C:Fe without significant changes to surface area, pore size, and pore volume.

- Found that thermal oxidation, although achieving the goal of converting amorphous iron oxides to more crystalline form, did not result in improved sorbent recapture.

- Identified 3:1 C:Fe without thermal oxidation as the optimal synthesis parameters for trace level aqueous Hg removal.

- Increased understanding of Hg adsorption mechanisms by:

- Suggesting the influence of water cluster formation on aqueous Hg(0) adsorption.

- Demonstrated that surface oxygen functionality alone is not strongly correlated to aqueous Hg(0) adsorption.

- Identified porosity, adsorbent surface charge, and oxygen content as significant variables in aqueous Hg(0) adsorption.

- Demonstrated that, although porosity was not exerting a large influence on aqueous Hg(II) adsorption, pore volume influenced the results to a greater degree than surface area.

- Determined that pH and pCl do not significantly influence Hg volatilization from solution.

- Demonstrated that activated carbon can be used to adsorb aqueous Hg(0); improved aqueous capture is beneficial by reducing Hg losses to the atmosphere due to volatility.

Future Recommendations

- Combine the magnetic and surface oxygen group modification techniques.

- Apply the modified carbons to real wastewaters.

- Confirm oxidation of Hg(0) using SEM and XRD.

- Determine the identity and concentration of surface oxygen functional groups developed with the wet chemical oxidation methods; determine any correlation between these groups and Hg(II) and removal.

APPENDIX A
MODIFICATION OF SURFACE OXYGEN FUNCTIONALITY OF BIOCHAR FOR HG
ADSORPTION

In addition to wood and coal-based carbons, recent literature investigates the use of more sustainable biomass carbon sources [75,134,135]. Biochar, a sustainable and affordable pyrolyzed carbon commonly applied to soils to increase fertility and water retention, can exhibit high surface area and may act as a surface sorbent similar to activated carbon. Adsorption of Cu, Ni, Cd, and Pb onto biochar has been correlated with the amount of C(O) groups present, determined by O/C ratio, pHpzc, total acidity, and ^{1}H NMR analysis [136].

This study utilized the same surface oxygen modification applied to activated carbon. Table A-1 shows the biochar characterization results. No biochars investigated demonstrated high surface area. Modification did not significantly alter porosity or surface charge.

Table A-2 shows the Hg removal performance. Batch adsorption studies were performed at room temperature with a 150mg/L dose of biochar to 50 μg/L Hg-DI for a 30 s contact time. No biochars performed as well as the activated carbons previously discussed. The modification did not influence the Hg(II) adsorption efficiency. It is of interest that Hg does have an affinity for biochar, even if this affinity is lower than activated carbon and is not influenced by C(O) groups.

Table A-1. Biochar characterization data

Sample	Raw					10M H_2SO_4 Modification			
	pH_{pzc}	Surface Area (m^2/g)	Pore Size (Å)	Pore Volume (cm^3/g)	O/C	pH_{pzc}	Surface Area (m^2/g)	Pore Size (Å)	Pore Volume (cm^3/g)
Fresh Oak-250	3.9	1	99.7	0.00	0.8	3.7	0	117.2	0.00
Fresh Oak-650	9.7	46	17.8	0.04	0.2	9.4	85	15.1	0.06
Fresh Grass-250	4.4	2	6.7	0.01	0.8	4.5	6	45.3	0.01
Fresh Grass-650	9.7	12	45.1	0.03	0.5	9.6	2	54.0	0.01

Table A-2. Adsorption of aqueous Hg(II) by raw and modified biochar

Sample	Raw Hg Removal (%)	Modified Hg Removal (%)
Fresh Oak-250	39.3	35.9
Fresh Oak-650	34.4	40.0
Fresh Grass-250	41.4	38.7
Fresh Grass-650	19.1	22.5

LIST OF REFERENCES

[1] U.S. Environmental Protection Agency. Toxics release inventory: Reporting year 2007 public data release summary of key findings. 260-R-09-001, 2009.

[2] U.S. Code of Federal Regulations. Water quality criteria for the protection of wildlife. 40CFR132 Table 4, 2010.

[3] Drasch, Horvat M, Stoeppler M. Mercury. In: Merian E, Anke M, Ihnat M, Stoeppler M, editors. Elements and their compounds in the environment, . 2nd ed., Weinheim; Wiley-VCH; 2004 p. 931-1006.

[4] U.N.E.P Chemicals. Global mercury assessment. Geneva, Switzerland, 54790-01, 2002.

[5] Burgess J. Ions in solution: Basic principles of chemical interactions. 2nd ed. Coll House, England: Horwood Publishing; 1999.

[6] Kim CS, Rytuba JJ, Brown GE. EXAFS study of mercury(II) sorption to Fe- and Al-(hydr)oxides I. effects of pH. J Colloid Interface Sci 2004; 271(1): 1-15.

[7] Benjamin M. Water chemistry. Boston MA: McGraw-Hill; 2002.

[8] Hahne HC, Kroontje W. Significance of pH and chloride concentration on behavior of heavy metal pollutants: Mercury(II), cadmium(II), zinc(II), and lead(II). J Environ Qual. 1973; 2(4): 444-450.

[9] Davis A, Bloom NS, Hee SS. The environmental geochemistry and bioaccessibility of mercury in soils and sediments: A review. Risk Analysis 1997; 17(5): 557-569.

[10] Merian E editor. Metals and their compounds in the environment. Weinheim NY: VCH; 1999.

[11] Schwertmann U, Cornell RM. Iron oxides in the laboratory: Preparation and characterization. 2nd ed. Weinheim NY: Wiley-VCH; 2000.

[12] Kim CS, Rytuba JJ, Brown GE. EXAFS study of mercury(II) sorption to Fe- and Al-(hydr)oxides: II. effects of chloride and sulfate. J Colloid Interface Sci 2004; 270(1): 9-20.

[13] Hahne HCH, Kroontje W. The simultaneous effect of pH and chloride concentrations upon mercury(II) as a pollutant. Soil Sci Soc Am J 1973; 37(6): 838-843.

[14] Feick G, Yeaple D, Horne RA. Release of mercury from contaminated freshwater sediments by runoff of road deicing salt. Science 1972; 175(4026): 1142-1143.

[15] U.S. Environmental Protection Agency. Mercury study report to congress, volulme V: Health effects of mercury and mercury compounds. EPA-452/R-97-007, 1997.

[16] Langford N, Ferner R. Toxicity of mercury. J Hum Hypertens 1999; 13(10): 651-656.

[17] Harada H. Congenital Minimata disease: Intraeuterine methyl mercury poisoning. Teratology 1978(18): 285-288.

[18] Bakir F, Damluji S, Amin-Zski L. Methyl mercury poisoning in Iraq. Science 1973(181): 230-241.

[19] U.S. Environmental Protection Agency. Mercury study report to congress, volume II: An inventory of anthropogenic mercury emissions in the United States. Washington DC, EPA-452/R-97-004, 1997.

[20] U.S. Environmental Protection Agency. Roadmap for mercury. Washington DC, EPA-HW-QPPT-2005-0013, 2006.

[21] U.S. Environmental Protection Agency. Compilation of air pollutant emission factors, chapter 8: inorganic chemical industry. Research Triangle park NC, AP-42, 1995.

[22] Bansal R, Goyal M. Activated carbon adsorption. Boca Raton: CRC Press; 2005.

[23] Anirudhan TS, Divya L, Ramachandran M. Mercury(II) removal from aqueous solutions and wastewaters using a novel cation exchanger derived from coconut coir pith and its recovery. J Hazard Mater 2008; 157(2-3): 620-627.

[24] von Canstein H, Li Y, Timmis KN, Deckwer WD, Wagner-Dobler I. Removal of mercury from chloralkali electrolysis wastewater by a mercury-resistant *pseudomonas putida* strain. Appl Environ Microbiol 1999; 65(12): 5279-5284.

[25] U.S. Environmental Protection Agency. National emission standards for hazardous air pollutants: mercury emissions from mercury cell chlor-alkali plants; final rule. 40CFR63, 2003.

[26] Tewalt SJ, Bragg LJ, Finkelman, RB. Mercury in U.S. coal - abundance, distribution, and modes of occurrence. Washington DC, FS-095-01, 2001.

[27] Chang J, Ghorishi S. Simulation and evaluation of elemental mercury concentration increase in flue gas across a wet scrubber. Environ Sci Technol 2003; 37(24): 5763-5766.

[28] U.S. Environmental Protection Agency. Steam electric power generating effluent guidelines rulemaking, supplemental information package #2 for federalism and unfunded mandates reform act consultations, Washington DC, EPA 821-R-09-008, 2011.

[29] U.S. Environmental Protection Agency. Capsule report: Aqueous mercury treatment. Washington DC, EPA/625/R-97/004, 1997.

[30] Patterson, Luo B, Petropoulou C, Gasca E. Toxicity reduction methodologies. In: Ford D, editor. Toxicity reduction, evaluation, and control, . 2nd ed., Lancaster, PA; Technomic Publishing Co.; 1998 p. 109.

[31] Findlay DM, McLean RAN. Removal of elemental mercury from wastewaters using polysulfides. Environ Sci Technol 1981; 15(11): 1388-1390.

[32] Moorhouse J. Modern chlor-alkali technology, vol. 8. Oxford: Blackwell Science Ltd.; 2001.

[33] Huang CP, Blankenship DW. The removal of mercury(II) from dilute aqueous-solution by activated carbon. Water Res 1984; 18(1): 37-46.

[34] Humenick MJ, Schnoor JL. Improving mercury (II) removal by activated carbon. J Environ Eng-ASCE 1974; 100(NEE6): 1249-1262.

[35] Marsh H, Rodriguez-Reinoso F. Activated carbon. Amsterdam: Elsevier; 2006.

[36] Lopez-Gonzalez J, Moreno-Castilla C, Guerrero-Ruiz A, Rodriguez-Reinoso F. Effect of carbon-oxygen and carbon-sulphur surface complexed on the adsorption of mercuric chloride in aqueous solutions by activated carbons. J Chem Tech Biotechnol 1982; 32: 575-579.

[37] Krishnan KA, Anirudhan TS. Removal of mercury(II) from aqueous solutions and chlor-alkali industry effluent by steam activated and sulphurised activated carbons prepared from bagasse pith: Kinetics and equilibrium studies. J Hazard Mater 2002; 92(2): 161-183.

[38] Manchester S, Wang X, Kulaots I, Gao Y, Hurt RH. High capacity mercury adsorption on freshly ozone-treated carbon surfaces. Carbon 2008; 46(3): 518-524.

[39] Tong S, Fan M, Mao L, Jia CQ. Sequential extraction study of stability of adsorbed mercury in chemically modified activated carbons. Environ Sci Technol 2011; 45(17): 7416-7421.

[40] US Environmental Protection Agency, Office of Superfund Remediation and Technology Innovation. Treatment technologies for mercury removal from soil, waste, and water. Washington DC, EPA-542-R-07-003, 2007.

[41] Boehm HP. Surface oxides on carbon and their analysis: A critical assessment. Carbon 2002; 40(2): 145-149.

[42] Yang RT. Adsorbents: Fundamentals and applications. Hoboken NJ. Wiley; 2003.

[43] Yin CY, Aroua MK, Daud WMAW. Review of modifications of activated carbon for enhancing contaminant uptakes from aqueous solutions. Sep Purif Technol 2007; 52(3): 403-415.

[44] Puri BR. Surface complexes on carbons. Chem Phys Carbon 1970; 6: 191-282.

[45] Zhao NQ, Wei N, Li JJ, Qiao ZJ, Cui J, He F. Surface properties of chemically modified activated carbons for adsorption rate of cr(VI). Chem. Eng. J. 2005; 115(1-2): 133-138.

[46] Saha B, Tai MH, Streat M. Metal sorption performance of an activated carbon after oxidation and subsequent treatment. Process Saf. Environ. Prot. 2001; 79(B6): 345-351.

[47] Biniak S, Szymanski G, Siedlewski J, Swiatkowski A. The characterization of activated carbons with oxygen and nitrogen surface groups. Carbon 1997; 35(12): 1799-1810.

[48] Shim JW, Park SJ, Ryu SK. Effect of modification with HNO3 and NaOH on metal adsorption by pitch-based activated carbon fibers. Carbon 2001; 39(11): 1635-1642.

[49] Biniak S, Pakula M, Szymanski GS, Swiatkowski A. Effect of activated carbon surface oxygen- and/or nitrogen-containing groups on adsorption of copper(II) ions from aqueous solution. Langmuir 1999; 15(18): 6117-6122.

[50] Shen W, Li Z, Liu Y. Surface chemical functional groups modification of porous carbon. Recent Patents on Chemical Engineering 2008; 1: 27-40.

[51] Santiago M, Stuber F, Fortuny A, Fabregat A, Font J. Modified activated carbons for catalytic wet air oxidation of phenol. Carbon 2005; 43(10): 2134-2145.

[52] Figueiredo JL, Pereira MFR, Freitas MMA, Orfao JJM. Modification of the surface chemistry of activated carbons. Carbon 1999; 37(9): 1379-1389.

[53] Maroto-Valer MM, Dranca I, Lupascu T, Nastas R. Effect of adsorbate polarity on thermodesorption profiles from oxidized and metal-impregnated activated carbons. Carbon 2004; 42(12-13): 2655-2659.

[54] Rios RRVA, Alves DE, Dalmazio I, Fernando S, Bento V, Donnici CL, et al. Tailoring activated carbon by surface chemical modification with O, S, and N containing molecules. Mat Res 2001; 6(2): 129-135.

[55] Moreno-Castilla C, Carrasco-Marin F, Maldonado-Hodar FJ, Rivera-Utrilla J. Effects of non-oxidant and oxidant acid treatments on the surface properties of an activated carbon with very low ash content. Carbon 1998; 36(1-2): 145-151.

[56] Li YH, Lee CW, Gullett BK. Importance of activated carbon's oxygen surface functional groups on elemental mercury adsorption. Fuel 2003; 82(4): 451-457.

[57] Moreno-Castilla C, Ferrogarcia MA, Joly JP, Bautistatoledo I, Carrascomarin F, Riverautrilla J. Activated carbon surface modifications by nitric-acid, hydrogen-peroxide, and ammonium peroxydisulfate treatments. Langmuir 1995; 11(11): 4386-4392.

[58] Salame II, Bandosz TJ. Study of water adsorption on activated carbons with different degrees of surface oxidation. J Colloid Interface Sci 1999; 210(2): 367-374.

[59] Salame II, Bandosz TJ. Surface chemistry of activated carbons: Combining the results of temperature-programmed desorption, boehm, and potentiometric titrations. J Colloid Interface Sci 2001; 240(1): 252-258.

[60] Oliveira LCA, Rios RVRA, Fabris JD, Garg V, Sapag K, Lago RM. Activated carbon/iron oxide magnetic composites for the adsorption of contaminants in water. Carbon 2002; 40(12): 2177-2183.

[61] Oliveira LCA, Petkowicz DI, Smaniotto A, Pergher SBC. Magnetic zeolites: A new adsorbent for removal of metallic contaminants from water. Water Res 2004; 38(17): 3699-3704.

[62] Gorria P, Sevilla M, Blanco JA, Fuertes AB. Synthesis of magnetically separable adsorbents through the incorporation of protected nickel nanoparticles in an activated carbon. Carbon 2006; 44(10): 1954-1957.

[63] Cornell R, Schwertmann U. The iron oxides. Weinheim: VCH; 1996.

[64] Okamoto S. Iron hydroxides as magnetic scavengers. IEEE Trans Magn 1974; MA10(3): 923-926.

[65] Masel RI. Principles of adsorption and reaction on solid surfaces. New York: Wiley; 1996.

[66] Faust S, Aly O. Adsorption processes for water treatment. Boston: Butterworth Publishers; 1987.

[67] Stumm W, Morgan J. Aquatic chemistry : Chemical equilibria and rates in natural waters 3rd ed. ed. New York: Wiley; 1996.

[68] International Union of Pure and Applied Chemistry. Manual of Symbols and Terminology, Part 1, Colloid and Surface Chemistry. 2002; Available at: http://www.iupac.org/reports/2001/colloid_2001/manual_of_s_and_t/. Accessed February, 2009.

[69] Calgon Carbon Corporation. Laboratory evaluation of granular activated carbons for liquid phase applications. Pittsburg PA, IB-1002-0907, 2007; .

[70] Coolidge AS. The adsorption of mercury vapor by charcoal. J Am Chem Soc 1927; 49: 1949-1952.

[71] Shiels DO. The adsorption of mercury vapor by activated charcoal. J Phys Chem 1929; 33: 1398-1402.

[72] Krishnan SV, Gullett BK, Jozewicz W. Sorption of elemental mercury by activated carbons. Environ Sci Technol 1994; 28(8): 1506-1512.

[73] Liu J, Cheney MA, Wu F, Li M. Effects of chemical functional groups on elemental mercury adsorption on carbonaceous surfaces. J Hazard Mater 2011; 186(1): 108-113.

[74] Goel J, Kadirvelu K, Rajagopal C, Garg VK. Removal of mercury(II) from aqueous solution by adsorption on carbon aerogel: Response surface methodological approach. Carbon 2005; 43(1): 197-200.

[75] Kadirvelu K, Kavipriya M, Karthika C, Vennilamani N, Pattabhi S. Mercury(II) adsorption by activated carbon made from sago waste. Carbon 2004; 42(4): 745-752.

[76] Carrott PJM, Carrott MMLR, Nabais JMV. Influence of surface ionization on the adsorption of aqueous mercury chlorocomplexes by activated carbons. Carbon 1998; 36(1-2): 11-17.

[77] Sato S, Yoshihara K, Moriyama K, Machida M, Tatsumoto H. Influence of activated carbon surface acidity on adsorption of heavy metal ions and aromatics from aqueous solution. Appl Surf Sci 2007; 253(20): 8554-8559.

[78] Xiao B, Thomas KM. Competitive adsorption of aqueous metal ions on an oxidized nanoporous activated carbon. Langmuir 2004; 20(11): 4566-4578.

[79] SenGupta A. Environmental separation of heavy metals: Engineering processes. Boca Raton: CRC Press; 2002.

[80] Radovic LR, Moreno-Castilla C, Rivera-Utrilla J. Carbon materials as adsorbents in aqueous solutions. Chem Phys Carbon 2001; 27: 227-405.

[81] Cox M, El-Shafey E, Pichugin AA, Appleton Q. Removal of mercury(II) from aqueous solution on a carbonaceous sorbent prepared from flax shive. J Chem Technol Biotechnol 2000; 75(6): 427-435.

[82] Wiatrowski HA, Das S, Kukkadapu R, Ilton E, Barkay T, Yee N. Reduction of hg(II) to hg(0) by magnetite. Environ Sci Technol 2009; 73(14): 5307-5313.

[83] Newton DW, Ellis R, Paulsen GM. Effect of ph and complex-formation on mercury (II) adsorption by bentonite. J Environ Qual 1976; 5(3): 251-254.

[84] Sarkar D. Preliminary studies on mercury solubility in the presence of iron oxide phases using static headspace analysis. Environ Geo 2003; 10(4): 151-155.

[85] Tiffreau C, Lutzenkirchen J, Behra P. Modeling the adsorption of mercury (II) on (hydr)oxides. J Colloid Interf Sci 1995; 172: 82-93.

[86] Fauconnier N, Bee A, Roger J, Pons JN. Synthesis of aqueous magnetic liquids by surface complexation of maghemite nanoparticles. J Mol Liq 1999; 83(1-3): 233-242.

[87] O'Loughlin EJ, Kelly SD, Kemner KM, Csencsits R, Cook RE. Reduction of Ag-I, Au-III, Cu-II, and Hg-II by Fe-II/Fe-III hydroxysulfate green rust. Chemosphere 2003; 53(5): 437-446.

[88] Charlet L, Bosbach D, Peretyashko T. Natural attenuation of TCE, as, Hg linked to the heterogeneous oxidation of Fe(II): An AFM study. Chem Geol 2002; 190(1-4): 303-319.

[89] Scheinost AC, Charlet L. Selenite reduction by mackinawite, magnetite and siderite: XAS characterization of nanosized redox products. Environ Sci Technol 2008; 42(6): 1984-1989.

[90] White AF, Peterson ML. Reduction of aqueous transition metal species on the surfaces of fe(II)-containing oxides. Geochim Cosmochim Acta 1996; 60(20): 3799-3814.

[91] Senior C, editor. Behavior of mercury in air pollution control devices on coal-fired utility boilers. Engineering Foundation Conference; 2001; Salt Lake City, UT.

[92] Lighty, Silcox and Fry. Fundamentals of mercury oxidation in flue gas. Pittsburg PA, DE-FG26-03NT41797, 2004.

[93] Dunham GE, DeWall RA, Senior CL. Fixed-bed studies of the interactions between mercury and coal combustion fly ash. Fuel Process Technol 2003; 82(2-3): 197-213.

[94] Snoeyink V, Jenkins D. Water chemistry. New York: John Wiley & Sons; 1980.

[95] Elliot P, Hartenstein H, editors. Selective Separation of Mercury and Other Heavy Metals During FGD Wastewater Treatment. APC Round Table and Expo; July 8-10, 2007; Chattanooga, TN; 2007.

[96] Hahne HCH, Kroontje W. Simultaneous effect of ph and chloride concentrations upon mercury (ii) as a pollutant. Soil Sci Soc Am J 1973; 37(6): 838-843.

[97] Sing K, Everett D, Haul R, Moscou L, Pierotti R, Rouquerol J, et al. Reporting physisorption data for gas solid systems with special reference to the determination of surface-area and porosity. Pure Appl Chem 1985; 57(4): 603-619.

[98] Sanemasa I. Solubility of elemental mercury-vapor in water. Bull Chem Soc Jpn 1975; 48(6): 1795-1798.

[99] Bloom NS, Preus E, Katon J, Hiltner M. Selective extractions to assess the biogeochemically relevant fractionation of inorganic mercury in sediments and soils. Anal Chim Acta 2003; 479(2): 233-248.

[100] Perez OP, Umetsu Y, Sasaki H. Precipitation and densification of magnetic iron compounds from aqueous solutions at room temperature. Hydrometallurgy 1998; 50(3): 223-242.

[101] Menendez JA, Phillips J, Xia B, Radovic LR. On the modification and characterization of chemical surface properties of activated carbon: In the search of carbons with stable basic properties. Langmuir 1996; 12(18): 4404-4410.

[102] Laine NR, Vastola FJ, Walker PL. Importance of active surface area in carbon-oxygen reaction. J Phys Chem 1963; 67(10): 2030-&.

[103] Aggarwal D, Goyal M, Bansal RC. Adsorption of chromium by activated carbon from aqueous solution. Carbon 1999; 37(12): 1989-1997.

[104] Menendez JA, Xia B, Phillips J, Radovic LR. On the modification and characterization of chemical surface properties of activated carbon: Microcalorimetric, electrochemical, and thermal desorption probes. Langmuir 1997; 13(13): 3414-3421.

[105] Dastgheib SA, Karanfil T. Adsorption of oxygen by heat-treated granular and fibrous activated carbons. J Colloid Interface Sci 2004; 274(1): 1-8.

[106] Li YH, Lee CW, Gullett BK. The effect of activated carbon surface moisture on low temperature mercury adsorption. Carbon 2002; 40(1): 65-72.

[107] Chingombe P, Saha B, Wakeman RJ. Surface modification and characterisation of a coal-based activated carbon. Carbon 2005; 43(15): 3132-3143.

[108] Quantachrome Instruments. Nova *e* series: High speed surface area and pore size analyzers. 2008; Available at: http://www.quantachrome.com/pdf_brochures/07122.pdf. Accessed 08/07, 2009.

[109] Brunauer S, Emmett PH, Teller E. Adsorption of gases in multimolecular layers. J Am Chem Soc 1938; 60: 309-319.

[110] Barrett EP, Joyner LG, Halenda PP. The determination of pore volume and area distributions in porous substances .1. computations from nitrogen isotherms. J Am Chem Soc 1951; 73(1): 373-380.

[111] Cho D, Chon C, Kim Y, Jeon B, Schwartz FW, Lee E, et al. Adsorption of nitrate and cr(VI) by cationic polymer-modified granular activated carbon. Chem Eng J 2011; 175: 298-305.

[112] Al-Rashdi B, Somerfield C, Hilal N. Heavy metals removal using adsorption and nanofiltration techniques. Sep Purif Rev 2011; 40(3): 209-259.

[113] Laszlo K, Josepovits K, Tombacz E. Analysis of active sites on synthetic carbon surfaces by various methods. Anal Sci 2001; 17: i1741-i1744.

[114] Moskowitz B. Hitchhikers guide to magnetism. 1991; Available at: http://www.irm.umn.edu/hg2m/hg2m_index.html. Accessed 9/18, 2009.

[115] Looney BB, Denham ME, Vangelas KM, Bloom NS. Removal of mercury from low-concentration aqueous streams using chemical reduction and air stripping. J Environ Eng-ASCE 2003; 129(9): 819-825.

[116] Balogh SJ, Nollet YH. Mercury mass balance at a wastewater treatment plant employing sludge incineration with offgas mercury control. Sci Total Environ 2008; 389(1): 125-131.

[117] Rauret G, Lopez-Sanchez JF, Sahuquillo A, Barahona E, Lachica M, Ure AM, et al. Application of a modified BCR sequential extraction (three-step) procedure for the determination of extractable trace metal contents in a sewage sludge amended soil reference material (CRM 483), complemented by a three-year stability study of acetic acid and EDTA extractable metal content. J Environ Monit 2000; 2(3): 228-233.

[118] Filgueiras AV, Lavilla I, Bendicho C. Chemical sequential extraction for metal partitioning in environmental solid samples. J Environ Monit 2002; 4(6): 823-857.

[119] Hall G, Gauthier G, Pelchat J, Pelchat P, Vaive J. Application of a sequential extraction scheme to ten geological certified reference materials for the determination of 20 elements. J Anal At Spectrom 1996; 11(9): 787-796.

[120] Kim CS, Bloom NS, Rytuba JJ, Brown GE. Mercury speciation by X-ray absorption fine structure spectroscopy and sequential chemical extractions: A comparison of speciation methods. Environ Sci Technol 2003; 37(22): 5102-5108.

[121] Fergusson J. The heavy elements: Chemistry, environmental impacts, and health effects. Oxford: Pergamon Press; 1990.

[122] Tessier A, Campbell PGC, Bisson M. Sequential extraction procedure for the speciation of particulate trace-metals. Anal Chem 1979; 51(7): 844-851.

[123] Gubbins D, Herrero Bervera E, SpringerLink (Online service). Encyclopedia of geomagnetism and paleomagnetism [electronic resource]. Dordrecht: Springer; 2007.

[124] Zhang F, Itoh H. Adsorbents made from waste ashes and post-consumer PET and their potential utilization in wastewater treatment. J Hazard Mater 2003; 101(3): 323-337.

[125] Annadurai G, Juang R, Lee D. Use of cellulose-based wastes for adsorption of dyes from aqueous solutions. J Hazard Mater 2002; 92(3): 263-274.

[126] Ho Y, McKay G. The sorption of lead(II) ions on peat RID C-8624-2009. Water Res 1999; 33(2): 578-584.

[127] Ho Y, McKay G. Pseudo-second order model for sorption processes RID C-8624-2009. Process Biochem 1999; 34(5): 451-465.

[128] Ho Y. Review of second-order models for adsorption systems RID C-8624-2009. J Hazard Mater 2006; 136(3): 681-689.

[129] Nan Q, LeVan M. Adsorption equilibrium modeling for water on activated carbons. Carbon 2005; 43(11): 2258-2263.

[130] Li L, Quinlivan P, Knappe D. Effects of activated carbon surface chemistry and pore structure on the adsorption of organic contaminants from aqueous solution. Carbon 2002; 40(8): 2085-2100.

[131] Mahajan O, Moreno-Castilla C, Walker P. Surface-treated activated carbon for removal of phenol from water. Sep Sci Technol 1980; 15(10): 1733-1752.

[132] Lee W, Reucroft P. Vapor adsorption on coal- and wood-based chemically activated carbons: surface oxidation states and adsorption of H_2O. Carbon 1999; 37(1): 7-14.

[133] Ranganathan K. Adsorption of hg(II) ions from aqueous chloride solutions using powdered activated carbons. Carbon 2003; 41(5): 1087-1092.

[134] Goel J, Kadirvelu K, Rajagopal C. Mercury (II) removal from water by coconut shell based activated carbon: Batch and column studies. Environ Technol 2004; 25(2): 141-153.

[135] Khalkhali RA, Omidvari R. Adsorption of mercuric ion from aqueous solutions using activated carbon. Polish J Environ Studies 2005; 14(2): 185-188.

[136] Uchimiya M, Chang S, Klasson KT. Screening biochars for heavy metal retention in soil: Role of oxygen functional groups. J Hazard Mater 2011; 190(1-3): 432-441.

BIOGRAPHICAL SKETCH

Emily Kaye Faulconer is the daughter of Charles and Susan Faulconer born in Galax, VA in 1982. The family relocated to Lynchburg, VA in 1984. Following the footsteps of both her mother and her uncle, Jim Davis, Emily graduated from Shenandoah Valley Academy in 1999. Emily achieved her associate's degree from Central Virginia Community College in 2002 and continued on to Virginia Commonwealth University, graduating cum laude with her bachelor's degree in Forensic Science in 2004. After working as a certifying scientist at a forensic drug testing facility and teaching high school sciences for three years, Emily began her pursuit of an Environmental Engineering Sciences graduate degree at the University of Florida in 2008, under the guidance of David Mazyck, Ph.D. She received her Ph.D. in Environmental Engineering Sciences in the spring of 2012.